PETROGENESIS OF NEPHELINE- AND SCAPOLITE-BEARING METACARBONATES FROM SOUTHWESTERN BAFFIN ISLAND, NUNAVUT, CANADA

Jared P. Butler

Submitted in Partial Fulfilment of the Requirements
for the Degree of Bachelor of Sciences, Honours
Department of Earth Sciences
Dalhousie University, Halifax, Nova Scotia
April 2007

ABSTRACT

The petrography and mineral chemistry of granulite-facies metacarbonates from the Paleoproterozoic Lake Harbour Group (LHG), southwestern Baffin Island, reflect the combined effects of regional metamorphism and subsequent fluid infiltration. In the study area the LHG comprises polydeformed metacarbonates and quartzofeldspathic metasediments, intruded by syntectonic foliated monzogranites and post-deformation pegmatitic syenogranites. Impure marbles from the study area comprise two assemblages corresponding to variations in the proportion of carbonate versus silicate minerals: forsterite + spinel + calcite + dolomite, and forsterite + diopside + phlogopite + calcite; both consistent with relatively high X_{CO2}, and a minimum temperature of ca. 750 °C at 8.0 kbar. In the silicate-rich impure marbles, the earliest phase of metamorphism (M_{1a}) involved the sequential formation of calcite, phlogopite, diopside, and forsterite by the following reactions: *3 Dol + Kfs + H_2O = Phl + 3 Cal + 3 CO_2*, *Dol + Qtz = Di + 2 CO_2*, and *3 Dol + Di = 4 Cal + 2 Fo + 2 CO_2*. The subsequent formation of vermicular K-feldspar and nepheline intergrowths is consistent with the reaction: *3 Ab + 3 Cal + Phl = Kfs + 3 Ne + 3 Di + 3CO_2*, and implies decreasing X_{CO2}, possibly reflecting to late- to post-M_{1a} fluid infiltration. Scapolite, varying in composition from Me_{31} – Me_{77}, is locally present in calc-silicates, clinopyroxenites, and monzogranites associated with the LHG, and suggests the infiltration of Cl-rich fluids possibly derived to post-deformation pegmatitic syenogranite emplacement. In Kimmirut, southern Baffin Island, intense alteration of nepheline and scapolite has been linked to sapphire formation in calc-silicate lenses within stratigraphically correlative marbles. The scapolite + nepheline association described here may represent a precursor assemblage, implying that LHG metacarbonates from southwestern Baffin Island may be good targets for gemstone exploration.

TABLE OF CONTENTS

TABLE OF TABLES

TABLE OF FIGURES

TABLE OF MINERAL ABBREVIATIONS

Mineral	Abbreviation
Albite	Ab
Annite	Ann
Anorthite	Ann
Augite	Aug
Biotite	Bt
Calcite	Cal
Clinopyroxene	Cpx
Clinozoisite	Czo
Diopside	Di
Dolomite	Dol
Fayalite	Fa
Forsterite	Fo
Hedenbergite	Hd
Hercynite	Hc
Hornblende	Hb
Kalsilite	Kal
Marialite	Ma
Meionite	Me
Nepheline	Ne
Orthoclase	Or
Pargasite	Prg
Phlogopite	Phl
Spinel	Spl
Titanite	Ttn
Winchite	Wn

ACKNOWLEDGEMENTS

I wish to express my sincerest gratitude to my supervisors, Dr. Rebecca Jamieson and Dr. Marc St-Onge (GSC Ottawa) for their support in the completion of this thesis; to Dr. Joe Whalen (GSC Ottawa) for organizing whole-rock geochemical analyses; to the entire crew of the 2006 SWBIG project for providing such an excellent field season; and to the Geological Survey of Canada for their generous support.

CHAPTER 1: INTRODUCTION

The utility of metacarbonates as indicators of the temperature conditions and equilibrium fluid-phase compositions of their formation is well established in the literature (Spear, 1995; Yardley, 1995; and references therein). Numerous studies have shown that prograde metamorphism of impure marbles, rocks in which carbonate minerals predominate, typically involves the sequential formation of talc, tremolite, diopside, and forsterite (Winter, 2001; Yardley, 1995; and references therein). The regional metamorphism of calc-silicates, rocks in which Ca-silicate minerals predominate, is complicated by their compositional variability. Classical studies by Ferry (1976, 1983) showed that the progressive metamorphism of calc-silicates may involve the sequential formation of ankerite, biotite, amphibole, zoisite, and diopside; and furthermore that this sequence is commonly affected by chemical mass-transfer resulting from the infiltration of externally derived fluids. Fluid infiltration is probably common in high-grade metacarbonates, particularly in contact metamorphic environments (Spear, 1995). Interpreting the petrological significance of mineral assemblages in metacarbonates thus requires the recognition and distinction of features resulting from increasing temperature from those resulting from fluid-rock interaction.

In southwestern Baffin Island, metacarbonates comprise a significant proportion (ca. 15%) of the Paleoproterozoic metasedimentary Lake Harbour Group (LHG). The LHG was regionally metamorphosed to granulite- and subsequently amphibolite-facies conditions during the Paleoproterozoic formation of the Trans-Hudson Orogen (THO) (St-Onge et al., 2006b). Syntectonic granitoid metaplutonic rocks pervasively intruded the LHG during the earliest granulite-facies metamorphic event, followed by the emplacement of post-deformation syenogranite dykes and plutons. This study investigates the mineralogical and textural effects of this high-grade regional metamorphism in the LHG metacarbonates. The specific objectives of this study were to:

1. document the geochemistry, mineralogy, and texture of representative metacarbonates and intruded monzogranites;
2. determine the sequence of metamorphic reactions in the metacarbonates, and estimate the *P-T* conditions, and fluid-phase compositions of their formation;
3. distinguish the mineralogical and textural effects resulting from regional metamorphism from those resulting from localized fluid infiltration and/or metasomatic alteration.

To achieve these objectives a detailed petrographic study of representative samples of the LHG marbles, associated calc-silicates, and intruded monzogranites was completed. Electron microprobe (EMP) and X-ray fluorescence (XRF) analyses were used to determine the mineral chemistry, and whole-rock major and trace element compositions respectively, of selected lithologies. Petrographic observations were used to infer the likely sequence of mineral-forming reactions, and relevant phase diagrams (*P-T* and T-X_{CO2}) were calculated using the internally consistent dataset and reaction calculation software of Berman, 1991.

The study is organized as follows: Chapter 2 presents the regional geology of the Quebec-Baffin segment of the THO, followed by descriptions and field relations of lithologies as they appear within the study area. Chapter 3 presents the whole-rock geochemistry of selected lithologies. Chapter 4 presents the petrography and mineral chemistry of these lithologies. Chapter 5 presents the inferred sequence of metamorphic reactions in the LHG impure marbles, and addresses specific reactions of interest in associated calc-silicates and monzogranites. Chapter 6 discusses the petrology of the impure marbles in the context of the THO, and addresses similarities between the mineralogy of calc-silicates from the study area and sapphire-bearing LHG calc-silicates from Kimmirut, Baffin Island.

The field component of this study was conducted from June to August 2006 under the auspices of the Southwestern Baffin Island Integrated Geoscience Project (SWBIG),

co-led by Dr. Marc St-Onge of the Geological Survey of Canada (GSC Ottawa) and, Dan Utting of the Canada-Nunavut Geoscience Office (C-NGO).

CHAPTER 2: REGIONAL GEOLOGY AND STUDY AREA

2.1 Trans-Hudson Orogen

The geology of southwestern Baffin Island reflects a complex evolution involving polyphase deformation and metamorphism during the Paleoproterozoic formation of the Trans-Hudson Orogen (THO). The orogen juxtaposes the Archean Superior craton to the south with an assemblage of Archean crustal components that includes the Wyoming craton to the west, the Hearne domain and Rae craton to the north, and the Nain craton to the east (St-Onge et al., 2006). The orogen extends ca. 4,600 km along strike from the central United States to northern Quebec, Baffin Island, and Labrador where it is truncated by the Meso- to Neoproterozoic Grenville Orogen (St-Onge et al., 2006).

A comprehensive review of the tectonostratigraphic framework of the THO is provided by St-Onge et al. (2000, 2002, 2006). In the Quebec-Baffin segment of the THO, major south-verging sutures separate the northern Archean Rae craton and two assemblages of allochthonous Paleoproterozoic crustal elements, the Meta-Incognita microcontinent, and the Narsajuaq island-arc terrane and associated Watts Group ophiolite, from the Archean basement and Paleoproterozoic cover sequences of the Superior craton (Fig. 2.1). The Meta-Incognita microcontinent encompasses central to southern Baffin Island and comprises Archean basement and Paleoproterozoic cover sequences intruded by the Paleoproterozoic Andean margin-type Cumberland Batholith. Whether the Meta-Incognita microcontinent was rifted from the Superior craton or the Rae craton, or whether it is exotic with respect to both, has yet to be determined.

2.2 Geology of southwestern Baffin Island

Situated within the Foxe Peninsula in southwestern Baffin Island, the SWBIG project area provides nearly full exposure of the Paleoproterozoic metasedimentary Lake Harbour Group (LHG) and metaplutonic rocks of the Meta-Incognita microcontinent (Fig. 2.1) (Appendix D). These and associated lithologies are briefly described below

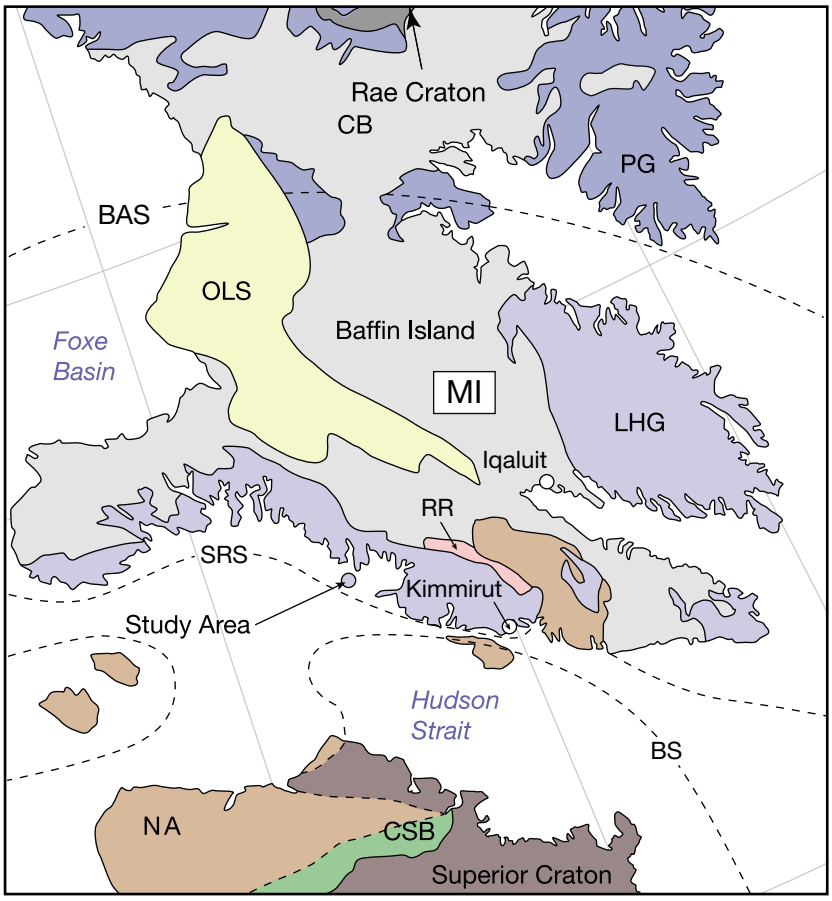

Phanerozoic

- Ordovician limestone (OLS)

Paleoproterozoic

- Narsajuaq Island Arc (NA): arc plutonic rocks (1863 ± 2 to 1840 +4/-3 Ma)
- Cumberland batholith (CB) (1865 +4/-2 to 1848 ± 2 Ma)
- Cape Smith Belt (CSB): mafic volcanic rocks (1918 +9/-7 to 1870 ± 4 Ma)
- Lake Harbour Group (LHG): carbonate and clastic rocks (1934 ± 2 to 1865 +4/-2 Ma)

Archean

- Ramsay River orthogneiss (RR) (3019 ± 5 to 2784 ± 9 Ma)
- Rae Craton
- Superior Craton (3220 +32/-23 to 2740 ± 10 Ma)

Figure 2.1: Geology of the Quebec-Baffin segment of the Trans-Hudson Orogen. Dashed lines represent south-verging crustal sutures separating structural domains. BS: Bergeron suture; SRS: Soper River suture; BAS: Baffin suture; MI: Meta-Incognita microcontinent. The northern and southern edges of the Meta-Incognita microcontinent are defined by the Baffin suture and Soper River sututes respectively. Modified from St-Onge et al. (2000). Ages for units from St-Onge et al. (2001) and references therein.

from oldest to youngest.

The LHG comprises minor quartzites, stratigraphically overlain by impure marbles and a dominant sequence of sulphidic psammites and pelites, together interpreted as a northeast-facing continental margin shelf succession (St-Onge et al., 2006). Metacarbonates comprise ca. 15 % of the LHG and are exposed within the southern extent of the SWBIG project area where they form laterally extensive (several kilometer) layers up to ca. 100 m thick. Basaltic to komatiitic metavolcanics of the Schooner Bay Formation (SBF) are locally juxtaposed with the lower LHG along south-verging thrust-faults at the western end of the Foxe Peninsula. Numerous ultramafic (peridotite to pyroxenite) to mafic (diorite) sills intrude the LHG and predate the emplacement of local metaplutonic (dominantly granitoid) rocks. Several phases of granitoid metaplutonic rocks, interpreted as representing the southern margin of the Cumberland Batholith, pervasively intruded the LHG, including dominant foliated monzogranites and late syenogranite plutons and pegmatitic dykes. All of the aforementioned lithologies are locally intruded by white garnet – biotite (S-type) monzogranites attributed to partial melting of the LHG pelites. The age of the LHG is bracketed, by U-Pb ages of detrital zircons and cross-cutting intrusions, between 1934 ± 2 and ca. 1880 Ma (Scott, 1997), and that of the Cumberland Batholith between 1865 +4/-2 and 1848 ± 2 Ma (Jackson et al., 1990; Wodicka & Scott, 1997; Scott & Wodicka, 1998; Scott, 1999). The stratigraphic basement of the LHG exposed in southern Baffin Island has yielded ages between 3019 ± 5 and 1950 +6/-4 Ma (St-Onge et al., 2006). This project focuses on a small, but representative, study area comprising impure marbles, calc-silicates and quartzofeldspathic metasediments of the LHG, and intruded monzogranites correlated with the Cumberland Batholith. The geology of the study area is described below.

2.3 Geology of Aliguq Island

The numerous wave-washed islands located along the southern coast of southwestern Baffin Island provide superb geological exposure of the LHG and associated

metaplutonic rocks.

Situated among these islands at 63°42’31 N and 72°33’13 W, just north of MacDonald Island is *Aliguq* Island. The name, which translates from Inuktitut to *Crystal Island*, was suggested by prominent ethno-geographer Normand Hallendy in the absence of a known traditional place name. The island comprises four broadly grouped lithological units characteristic of the lower LHG in southwestern Baffin Island, including (in stratigraphic sequence): variably impure marbles and minor calc-silicates; a mixed sedimentary succession comprising intercalated impure quartzites and quartzo-feldspathic (Qfs) metasediments; a second, stratigraphically overlying, sequence of impure marbles and calc-silicates; and, several phases of intruded metaplutonic rocks ranging from monzogranites to syenogranites, including minor ultramafic (clinopyroxenite) xenoliths (Fig. 2.2).

The impure marbles are concentrated along the northwestern shore of Aliguq island, and are separated from structurally higher impure marbles by intruded foliated monzogranites (Fig. 2.2). In general, they define a spectrum of bulk-compositions from carbonate-rich to silicate-rich impure marbles. They are characteristically white to greenish-gray, medium- to coarse-grained, and well foliated to nodular. The dominant S_1 foliation, where present, is characterized by ca. 2-5 cm thick boudinaged diopside (and locally nepheline)-dominated calc-silicate layers contained within calcite and forsterite-dominated impure marbles (Fig. 2.3). The calc-silicate layers typically exhibit forsterite mantles. Thin, ca. 5-10 cm thick boudinaged monzogranite veins also exhibit forsterite mantles and locally trend parallel to S_1 (Fig. 2.4). The proportion of calc-silicate layers versus impure marble layers decreases stratigraphically upward, grading into relatively massive, carbonate-rich marbles. In general, the S_1 foliation parallels primary structures in stratigraphically underlying quartzites, and may represent primary (depositional) variations in bulk composition. Mineralogically, the impure marbles comprise variable proportions of forsterite, diopside, pargasite, phlogopite, nepheline, K-feldspar, spinel,

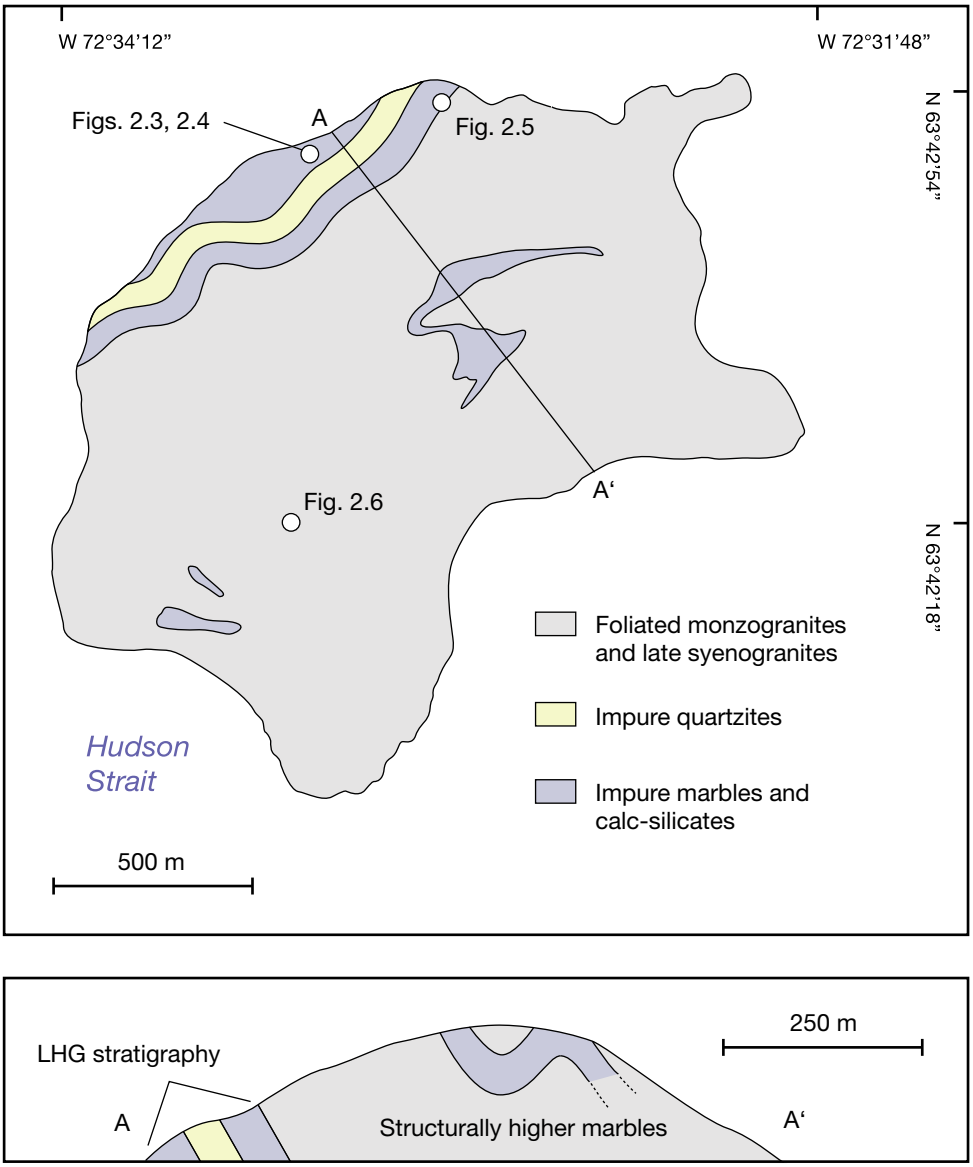

Figure 2.2: Geology of Aliguq Island. Top: The island comprises three main lithologies (from northwest to southeast): impure marbles are stratigraphically overlain by impure quartzites and quartzofeldspathic metasediments, stratigraphically overlain by a second sequence of impure marbles. The sequence is intruded by the volumetrically dominant foliated monzogranites. Bottom: Schematic cross-section illustrating approximate attitudes of the LHG units.

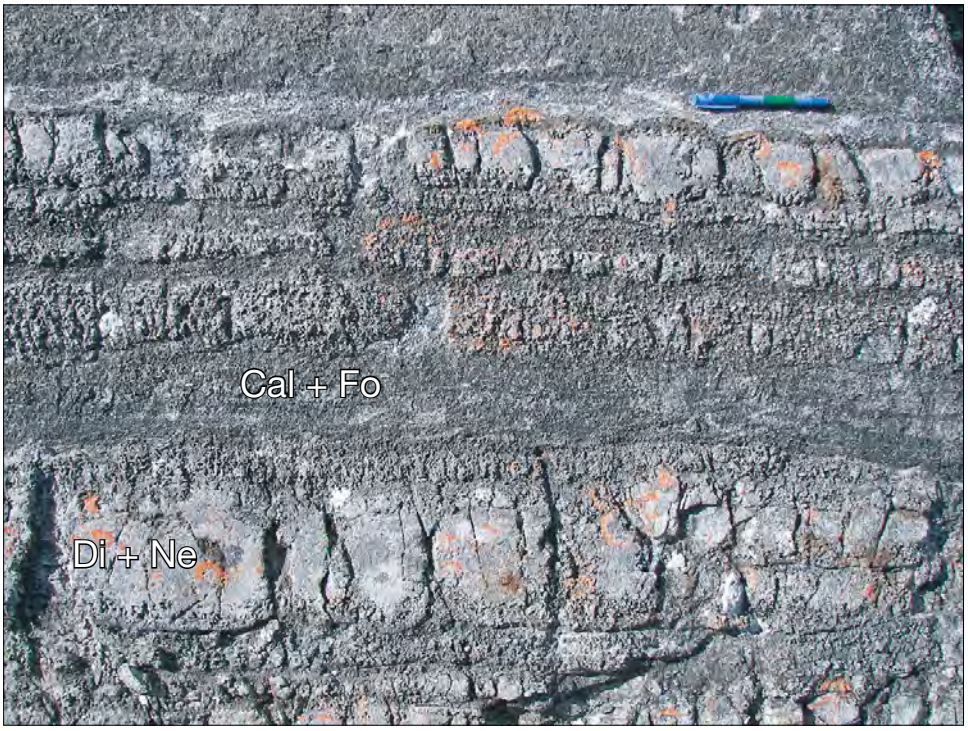

Figure 2.3: Photograph of foliated impure marbles. Diopside and nepheline (Di + Ne)-dominated, locally boudinaged calc-silicate layers define the dominant S_1 foliation in the impure marbles. The calc-silicate layers are separated from the calcite and forsterite-dominated (Cal + Fo) impure marbles by mantles of forsterite. Pen for scale. Photograph by Marc St-Onge.

Figure 2.4: Photograph of boudinaged monzogranite veins in impure marbles. Boudinaged monzogranite veins (a) in the impure marbles (b) exhibit forsterite (Fo) mantles (c). Are these veisn the pre-metasomatized equivalents of the calc-silicate layers? Pen for scale. Photograph by Marc St-Onge.

calcite, and dolomite. A complete description of their mineral chemistry, mineral assemblages, and associated textures is presented in Chapter 3.

The calc-silicates form ca. 1-2 meter thick tabular sheets within the interlayered impure marbles and quartzofeldspathic metasediments adjacent to the intruded monzogranites (Fig. 2.5). They are greenish-grey to dark green, coarse-grained, and weakly foliated to massive. The dominant S_1 foliation, where present, is characterized by alternating, essentially monomineralic diopside and pargasite, and minor calcite-dominated layers or zones. A subtle, secondary ca. 1 cm spaced cleavage defined by ca. < 0.5 mm thick, calcite-filled brittle fractures is present locally in the calc-silicates, and is interpreted as an axial planar fabric with respect to the SE-plunging folds. Fractures truncating S_1 and containing scapolite crystals up to ca. 20 cm long are localized within the structurally higher calc-silicates and may reflect late-stage fluid infiltration (Ch. 4). Mineralogically, the calc-silicates comprise diopside, pargasite, phlogopite, calcite, scapolite, and minor clinozoisite and titanite. The meso-scale textural heterogeneity of the calc-silicates implies formation involving diffusion metasomatism between adjacent layers of highly contrasting compositions. Their protolith is not recognizable from field relations alone.

Granitoid metaplutonic rocks comprise the volumetrically dominant lithologies on Aliguq Island and throughout southwestern Baffin Island (Fig. 2.1). On Aliguq island, at least three phases are present, including: foliated beige clinopyroxene – hornblende – biotite monzogranites (*A*); relatively massive, pinkish-grey, clinopyroxene – titanite (± scapolite ± calcite) monzogranites (*B*); and massive pink syenogranite plutons and pegmatitic dykes. The dominant foliation (S_1) is defined by compositional layering characterized by alternating clinopyroxene, hornblende or biotite-rich layers and quartzo-feldspathic layers (Fig. 2.6). Along the northwestern edge of the island, the structurally lower impure marbles are in contact with the *A* monzogranites and syenogranites. The distribution of the *B* monzogranites is less well constrained, but they appear to be

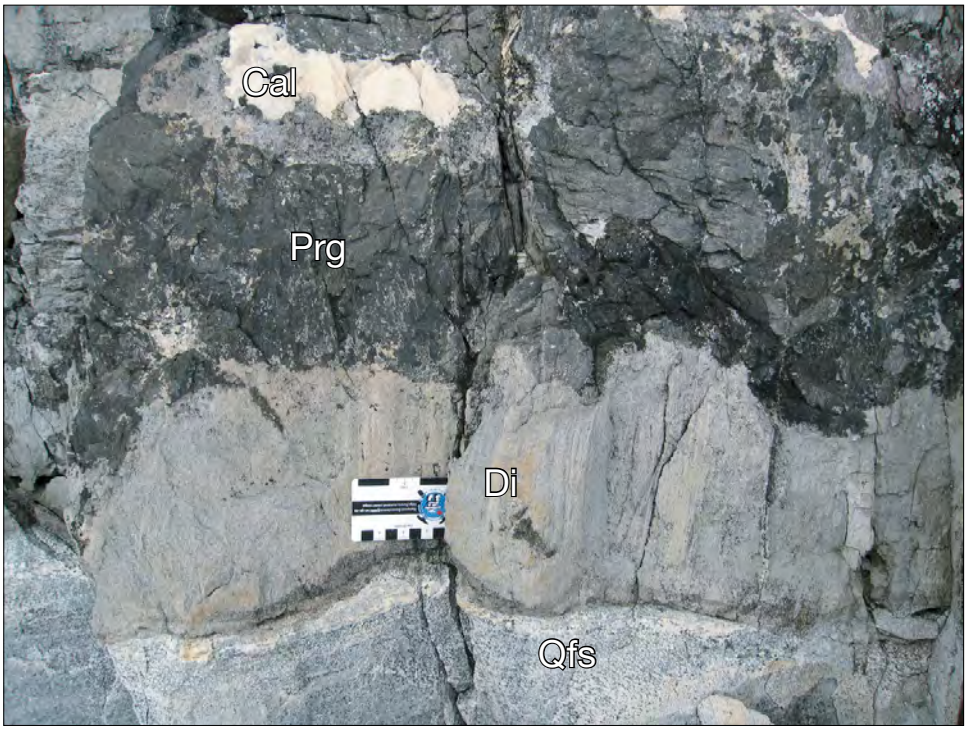

Figure 2.5: Photograph of calc-silicates. The calc-silicates are highly zoned, and characterized by essentially monominerallic diopside (Di), pargasite (Prg), and calcite (Cal)-dominated zones. These zones may have formed by diffusion metasomatism between impure marbles and adjacent quartzofeldspathic metasediments (Qfs).

Figure 2.6: Photograph of foliated *A* monzogranites. Foliated monzogranites represent the volumetrically dominant lithology in the study area. The dominant S_1 foliation is defined by alternating clinopyroxene and/or hornblende-rich and quartzofeldspathic domains, and a parallel biotite-schistosity.

concentrated in the southeastern extent of the island. Within the calc-silicates, scapolite mineralization appears to be concentrated at contacts between the *B* monozgranites and the structurally higher impure marbles. Adjacent to these contacts, scapolite and calcite are present within the *B* monzogranites. The massive syenogranites cross-cut the multiply deformed *A* monzogranites throughout the island, indicating post-deformation (D_2) emplacement. The foliated monzogranites are, in general, concordant with the intruded impure marbles. Clinopyroxenite xenoliths containing scapolite are concentrated within the monzogranites at the southeastern end of the island and are intruded by late syenogranite dykes and veins.

Structurally, Aliguq Island appears to comprise the northwestern limb of a regional-scale, northeast-trending F_2 synform or synformal basin. Throughout the island the dominant S_1 foliation is SE-dipping and folded by both smaller, ca. 100-m scale, shallowly NE-plunging F_2 folds, and by moderately SE-plunging F_3 folds (Fig. 2.7). Within the impure marbles F_2 and F_3 deformation significantly reorient the S_1 fabric resulting in complicated fold interference patterns defined by the thin calc-silicate boudins. Evidence of polyphase deformation is much less apparent within the monzogranites, and is in general limited to the localized, ca. 1 cm scale, crenulation of the S_1 fabric. The distribution of the *B* monzogranites coincides with the intersection of F_2 and F_3 synforms, i.e., with the highest structural levels exposed on the island.

2.4 Regional metamorphism

In southern Baffin Island, south of Iqaluit, the LHG underwent prograde M_{1a} metamorphism characterized by *P-T* conditions ranging from 790 °C and 6.9 kbar to 845 °C and 8.4 kbar. Metamorphic monazite associated with the S_1 compositional foliation yeilded ages between ca. 1849 and 1835 Ma, indicating that M_{1a} metamorpic conditions were maintained for at least ca. 14 Myr. Dating of anatectic garnet-leucogranites brackets partial melting of the LHG pelites between ca. 1841 and 1837 Ma. The age range determined for M_{1a} metamorphism coincides with the late stages of the 1865 +4/-2 – 1848

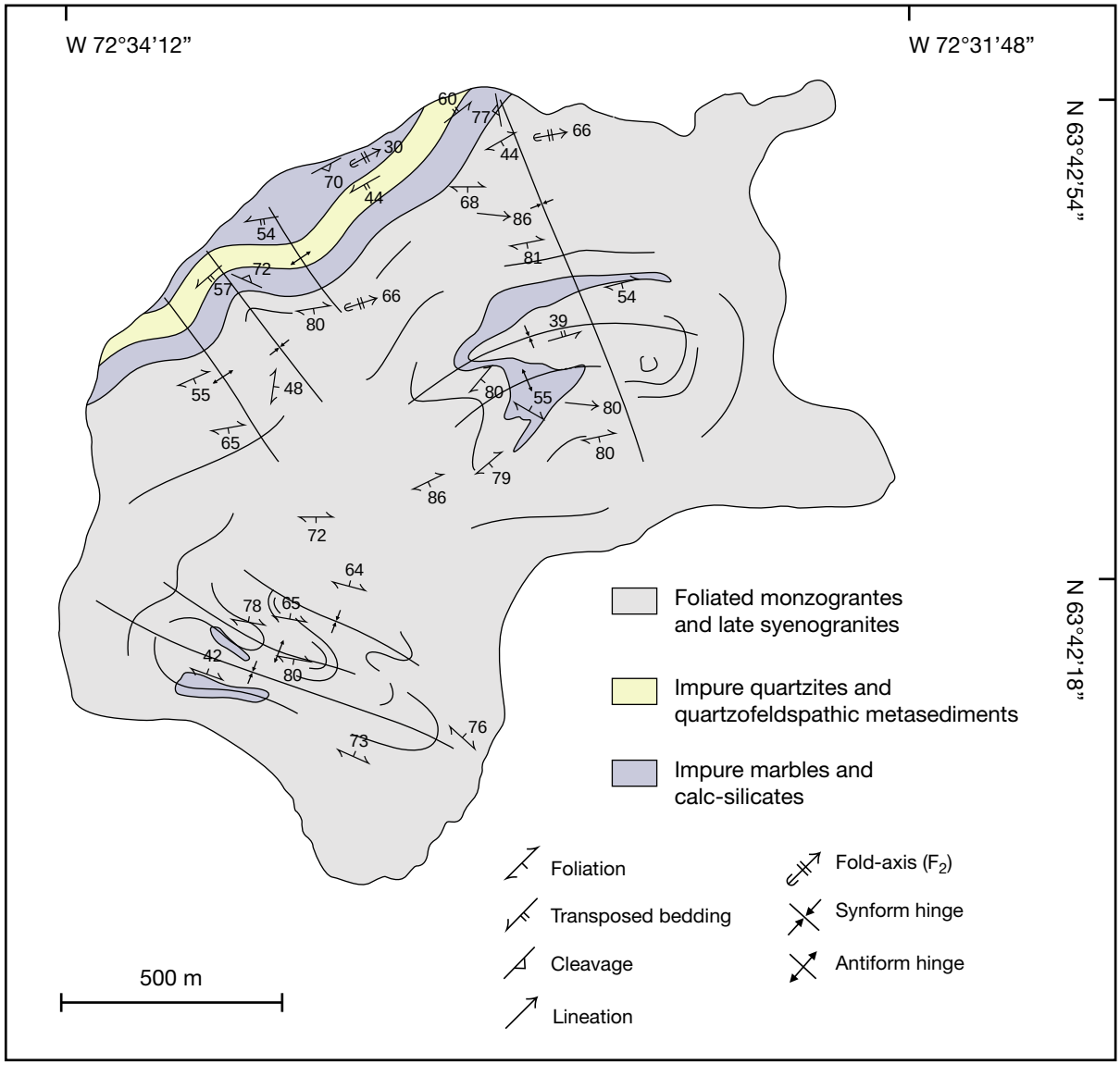

Figure 2.7: Structural geology of Aliguq Island. On the northwestern side of the island, the dominant S_1 foliation is primarily NE-trending. ENE-trending F_2, and SSE-trending F_3 folds reorient the dominant S_1 foliation throughout the study area.

± 2 Ma emplacement of the CB, and post-dates the D_1 accretion of the Narsajuaq island-arc terrane to the upper Churchill plate (St-Onge et al., 2006b). Subsequent M_2 retrograde metamorphism, bracketed by monazite ages between ca. 1820 ± 1 and 1808 ± 3 Ma, was characterized by *P-T* conditions ranging from 665 °C and 5.0 kbar to 765 °C and 7.7 kbar, and is attributed to the underthrusting and dehydration of orogenic lower-plate supracrustal units (St-Onge et al., 2000). Titanite from metacarbonates from southern Baffin Island yeilded an age of 1790 ± 1 Ma. This age is interpreted as resulting from post-M_2 fluid infiltration associated with the emplacement of the ca. 1795 – 1784 Ma syenogranites (St-Onge et al., 2006b).

CHAPTER 3: WHOLE-ROCK GEOCHEMISTRY

Whole-rock geochemical analyses were obtained for selected lithologies from the study area, the results of which are summarized below. The analyses were funded by the GSC and completed at Geoscience Laboratories, Sudbury ON. The lithologies were selected to represent a spectrum of bulk compositions, from carbonate-rich marbles, through calc-silicates, to monzogranites. In general, the analyses were obtained in order to determine the extent to which variations in mineral assemblage reflect whole-rock composition. Table 3.1 lists the whole-rock major element compositions, and Figure 3.1 illustrates variations in the ratios of selected components versus SiO_2 (both in wt. % oxides). Table 3.2 lists the whole-rock trace element compositions. Sample locations are provided in Appendix C. The number of analyses (one sample per lithology) precludes a rigorous statistical analysis, and the following discussion should be not be treated as such.

Table 3.1: Whole-rock major element compositions of selected lithologies

Sample	B133	B142	B103	B119	B137	B159
Lithology	Marble	Calc-silicate	Qfs metasediments	*A* monzogranite	Scp + Cal *B* monzogranite	*B* monzogranite
wt. %						
SiO_2	4.75	49.18	73.44	59.79	66.34	64.21
TiO_2	0.03	0.34	0.31	0.54	0.32	0.55
Al_2O_3	0.87	5.02	11.79	17.79	12.60	13.15
Fe_2O_3	1.60	1.79	0.76	6.66	4.44	5.56
MnO	0.17	0.05	N.D.	0.05	0.05	0.08
MgO	11.55	16.06	3.10	1.87	1.37	1.77
CaO	42.25	24.05	2.94	2.28	9.07	6.74
Na_2O	N.D.	0.56	6.72	3.15	4.17	3.74
K_2O	0.01	0.79	0.56	8.46	1.91	5.03
P_2O_5	N.D.	N.D.	0.07	0.10	0.10	0.12
LOI	39.28	3.28	0.63	0.26	0.49	0.20
Total	100.47	101.14	100.34	100.95	100.86	101.15

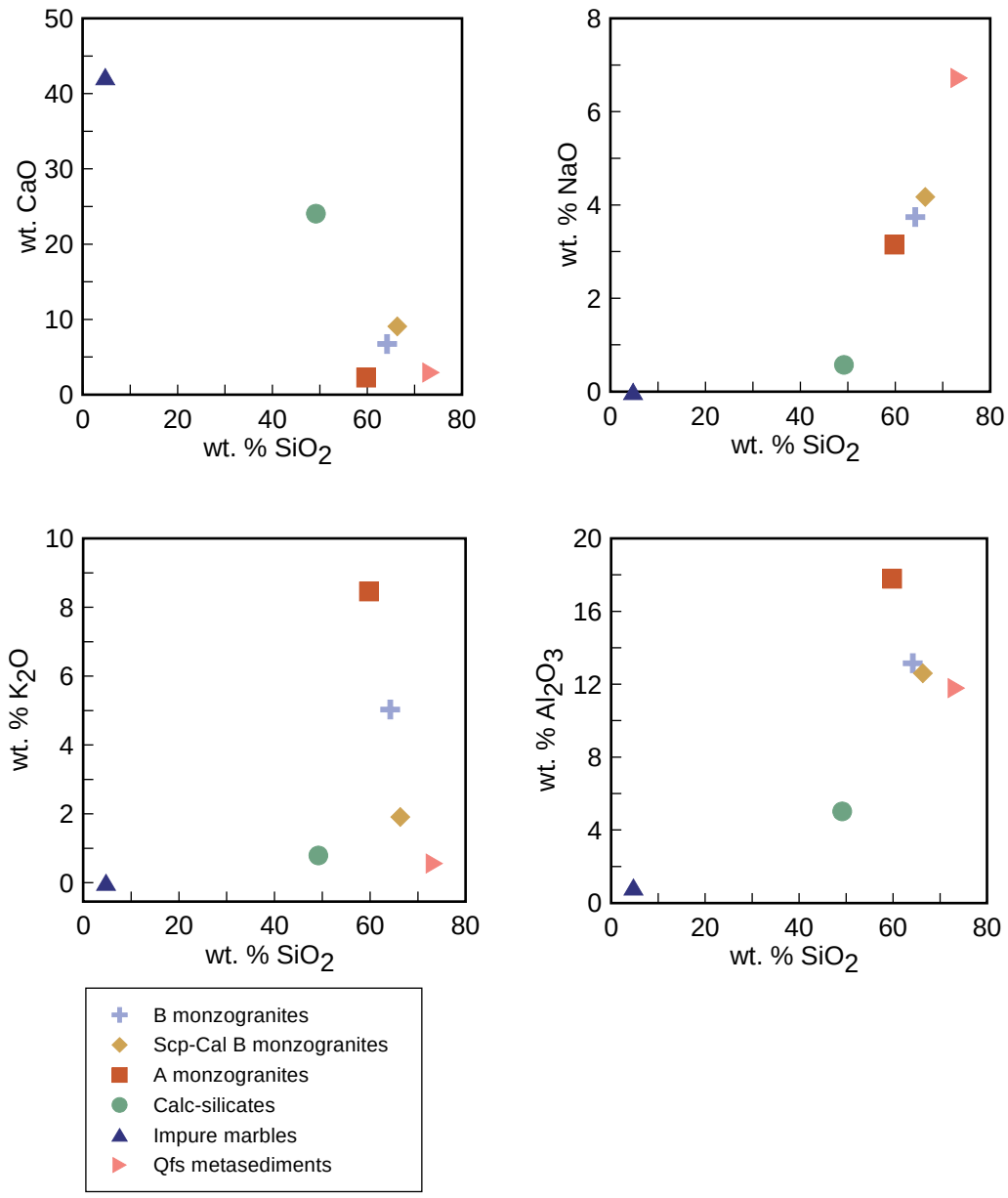

Figure 3.1: Compositional variations in selected major elements (in wt. % oxides) in representative lithologies from the study area.

Table 3.2: Whole-rock trace element compositions of selected lithologies (in order of increasing atomic radius)

Sample	B133	B142	B103	B119A	B137	B159
Lithology	Marble	Calc-silicates	Qfs metasediments	*A* monzogranite	Scp + Cal *B* monzogranite	*B* monzogranite
ppm						
U	0.05	0.85	1.88	1.51	2.28	3.99
Ta	N.D.	1.04	0.98	1.08	1.67	1.56
Nb	0.4	6.4	7.5	11.7	9.9	13.3
Hf	1.1	3.8	3.5	3.3	2.8	8.1
Zr	41.9	129.9	121.5	116	92.9	302.2
Yb	0.24	2.52	1.1	1.72	1.76	2.42
Lu	0.03	0.37	0.17	0.26	0.30	0.40
Tm	0.04	0.38	0.17	0.27	0.25	0.34
Er	0.30	2.50	1.11	1.90	1.67	2.26
Yb	3.37	23.3	10.33	17.24	15.38	20.4
Ho	0.12	0.81	0.37	0.68	0.60	0.77
Dy	0.68	3.93	1.94	3.6	3.15	3.97
Tb	0.12	0.62	0.33	0.60	0.55	0.66
Gd	0.90	3.87	2.24	4.07	3.82	4.54
Eu	0.38	0.56	0.38	1.22	0.66	0.96
Sm	0.97	4.35	2.87	5.33	5.08	5.91
Th	N.D.	1.38	8.12	17.83	8.62	13.86
Nd	4.62	22.09	15.1	31.79	28.75	32.92
Pr	1.15	5.74	3.90	8.84	7.59	8.82
Ce	9.17	49.8	30.56	78	62.31	71.24
La	4.07	24.12	11.4	40.56	26.66	27.23
Sr	124.9	22.1	14.8	135.3	96.9	148
Rb	0.54	119.2	6.44	>150.00	62.88	>150.00
Cs	0.03	3.23	0.12	5.42	1.15	0.41

3.1 Impure marbles

The carbonate-rich impure marbles comprise CaO, MgO, and subordinate SiO_2 and Fe_2O_3, reflecting the abundant calcite and dolomite and subordinate forsterite and spinel. With respect to trace elements, the impure marbles contain abundant Sr, again reflecting the presence of abundant calcite. The silicate-rich impure marbles were not analyzed.

3.2 Calc-silicates

The calc-silicates comprise SiO_2 (ca. 50 wt. %), CaO, and MgO, and subordinate Al_2O_3 and Fe_2O_3, reflecting the abundant diopside. Relative to the monzogranites, they

are depleted in SiO_2, Al_2O_3, Fe_2O_3, K_2O, and Na_2O (K_2O and Na_2O in particular), and enriched in CaO, and MgO. In general, the major element compositions of the calc-silicates are intermediate between those of the impure marbles and quartzofeldpathic metasediments or monzogranites (Fig. 3.1). With respect to trace elements, the calc-silicates contain abundant Ce, La, Nd, Rb, Sr, Y, and Zr. In general, their trace element compositions differ significantly from those of the impure marbles. The bulk compositions of the calc-silicates may have resulted from chemical interactions (e.g. assimilation, and/or diffusion metasomatism) between the impure marbles and the quartzofeldspathic metasediments or monzogranites. The former is consistent with the distrubtion of the calc-silicates as meter-scale sheets within the quartzofeldspathic metasediments. Interpretation of the calc-silicates is complicated by their meso-scale textural (and thus compositional) heterogeneity, and further sampling and analysis is required to constrain their paragenesis.

3.3 Quartzo-feldspathic metasediments

The quartzo-feldspathic metasediments comprise SiO_2 (ca. 73 wt. %), significant Al_2O_3 and Na_2O, and subordinate CaO and Fe_2O_3. Relative to the other lithologies they are notably depleted in Ce, La, Rb, and Sr, (Rb and Sr in particular). Despite their compositional similarities to the monzogranites, their fine-grained texture and spatial association with the impure marbles imply a metasedimentary protolith. The high Na_2O content (ca. 7 wt. %) corresponds to the presence of winchite, a sodic-calcic amphibole, and abundant albite. The abundant Na_2O may reflect primary evaporates, or alternatively, metasomatic alteration involving the infiltration of Na-rich fluids.

3.4 Monzogranites

Two phases of geochemically distinct monzogranites (*A* and *B*) were identified within the study area. The presence of calcite and scapolite in the *B* monzogranites is reflected in increased CaO (from ca. 7 – 9 wt. %), corresponding to decreased K_2O (from ca. 5 – 2 wt. %), Rb (from > 150 – ca. 63 ppm), and Sr (from ca. 148 – ca. 97 ppm) contents. The

decrease in highly fluid-mobile elements such as K_2O, Rb, and Sr implies metasomatic alteration of the calcite and scapolite-bearing *B* monzogranites.

Figure 3.2 illustrates the composition of the monzogranites in terms of wt. % SiO_2 versus total alkalis, defined as wt. % $NaO + K_2O$. The *A* monzogranites are alkaline, and the *B* monzogranites exhibit minor variation, from very near alkaline to subalkaline, corresponding to the absence or presence of calcite and scapolite respectively. Figure 3.3 illustrates the composition of the monzogranites in terms of alumina saturation, defined as the mol. Al_2O_3 / ($Na_2O + K_2O + CaO$) versus mol. ($Na_2O + K_2O$) / Al_2O_3. The *A* monzogranites are peraluminous, and the *B* monzogranites are metaluminous but again exhibit some variation, from 0.62 – 0.80 mol. ($Na_2O + K_2O$) / Al_2O_3 in scapolite-bearing and scapolite-free varieties respectively. The compositional variations between the *A* and *B* monzogranites are clearly defined, and are interpreted as reflecting primary igneous processes. Conversely, the compositional variations within the *B* monzogranites, corresponding to the presence or absence of calcite and scapolite, appear to reflect local chemical interactions involving either assimilation and/or metasomatism, both of which may be related to adjacent metacarbonates.

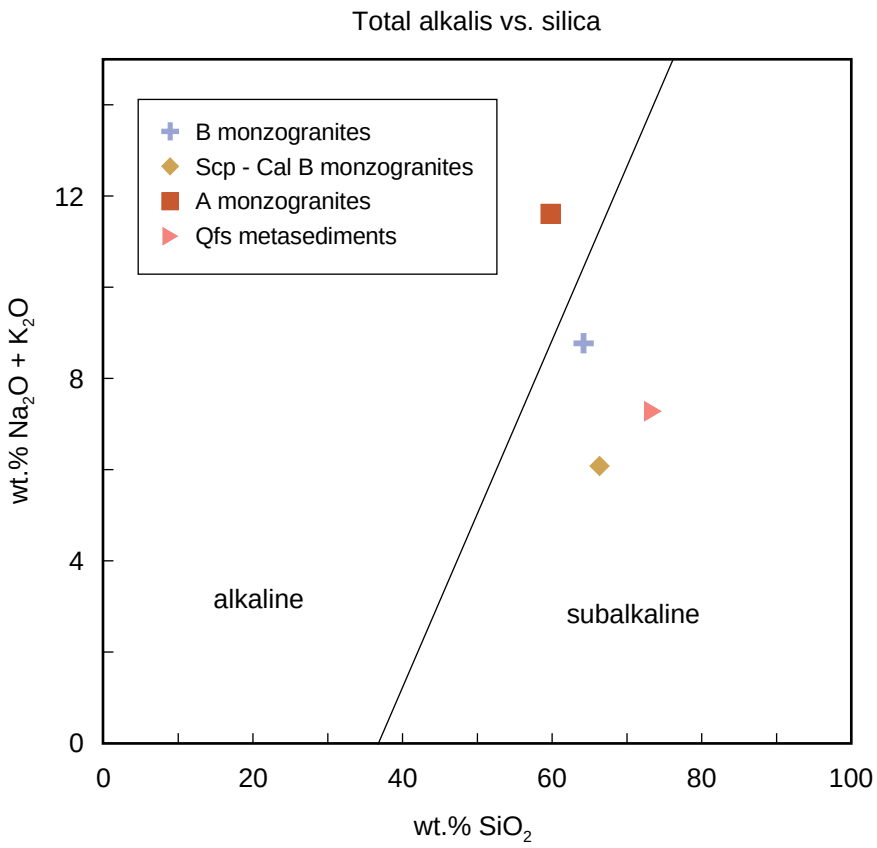

Figure 3.2: Total alkalis ($Na_2O + K_2O$) versus silica in the monzogranites and quartzofeldspathic metasediments. The *A* monzogranites are alkaline, and the *B* monzogranites vary from nearly alkaline to subalkaline, corresponding to the lack or presence of calcite and scapolite respectively. The variation in the *B* monzogranites may be attributed to metasomatic alteration.

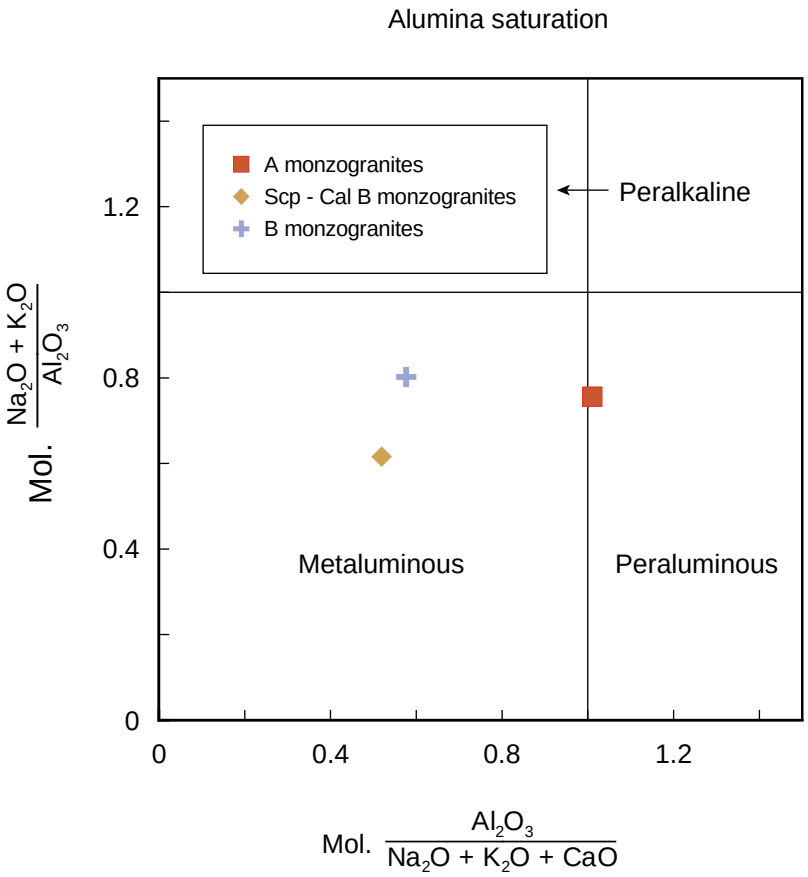

Figure 3.3: Compositional variations in alumina saturation in the monzogranites. The *A* monzogranites are peraluminous, and the *B* monzogranites are metaluminous. Variation in the *B* monzogranites corresponds to the presence of calcite and scapolite and may reflect metasomatic alteration related to nearby metacarbonates.

CHAPTER 4: PETROGRAPHY AND MINERAL CHEMISTRY

A detailed petrographic study was completed in order to constrain the relative timing and sequence of mineral formation, mineral assemblages, and correlated deformation fabrics in representative samples from the study area. Electron microprobe (EMP) analyses were used to determine the major element compositions of significant phases. Details of the EMP analytical parameters, and the complete set of analyses are provided in Appendix A. Calculated structural formulas for significant phases are presented below (Tables 4.1 – 4.10).

4.1 Lake Harbour Group marbles

Impure marbles, by definition, comprise less than 95% and greater than 50% carbonate minerals. Metacarbonates containing greater than 50% and less than 95% silicate minerals are termed carbonate calc-silicates (hereafter *calc-silicates*) or carbonate silicates, corresponding to a majority of Ca-silicate versus silicate minerals respectively (Rosen et al., 2004). In this study, the distinction between impure marbles and calc-silicates is largely a matter of scale. The term *impure marbles* is herein applied to both carbonate-rich, texturally equilibrated impure marbles, and finely interlayered silicate-rich impure marbles and calc-silicates. The term *calc-silicates* is applied to the distinct diopside and pargasite-rich tabular bodies distributed at intrusive contacts in the impure marbles.

4.1.1 Carbonate-rich marbles

The volumetrically dominant carbonate-rich marbles comprise variable proportions of compositionally uniform forsterite (Fo_{93}) (Table 4.1), spinel (Spl_{77}) (Table 4.2), calcite, and dolomite. Calcite contains a very minor magnesite component, from 0.032 – 0.059 Mg cations per formula unit (*cpfu*), and exhibits extensive exsolution of fine-grained dolomite lamellae.

Table 4.1: Olivine compositions

Lithology	Mineral	Structural formula (Deer et al., 1992)	End-members
		$(Mg,Fe)_2Si_2O_4$	Fo: $Mg_2Si_2O_4$; Fa: Fo: $Fe_2Si_2O_4$
Carbonate-rich marbles	Fo	$(Fe_{0.14}Mg_{1.87})Si_{0.99}O_4$	Fo_{93}; Fa_7
Silicate-rich marbles	Fo	$(Fe_{0.11}Mg_{1.90})Si_{0.99}O_4$	Fo_{95}; Fa_5

Table 4.2: Spinel compositions

Lithology	Mineral	Structural formula (Deer et al., 1992)	Substitutions
	Spl	Spinel: $MgAl_2O_4$; Hercynite: $Fe^{2+}Al_2O_4$	
Carbonate-rich marbles	Spl	$(Fe_{0.24}Mg_{0.80})Al_{1.97}O_4$	Spl_{77}; Hc_{23}

Figure 4.1 illustrates the well equilibrated texture of the carbonate-rich marbles. The texture is characterized by the random distribution of highly xenoblastic, fine- to medium-grained silicate minerals within a matrix of coarse-grained, granoblastic calcite and minor, somewhat xenoblastic dolomite. Forsterite contains inclusions of calcite and spinel, and is locally altered to serpentine. Dolomite is typically distributed adjacent to, and commonly encloses, forsterite. Each of the phases is in mutual contact with no obvious reaction textures, implying an equilibrated assemblage.

4.1.2 Silicate-rich marbles

In contrast with the carbonate-rich marbles, the silicate-rich marbles exhibit a high degree of mineralogical and textural complexity. They comprise variable proportions of forsterite (Fo_{95}), diopside (Di_{93}) (Table 4.3), phlogopite (Phl_{87}) (Table 4.4), nepheline (Ne_{71}) (Table 4.5), K-feldspar (Or_{92}) (Table 4.6), and calcite but not dolomite. Observed variations in the chemical compositions of these phases are described below.

Table 4.3: Clinopyroxene compositions

Lithology	Mineral	Structural formula (Deer et al., 1992)	End-members
		Diopside – Hedenbergite: $Ca(Mg,Fe)[Si_2O_6]$; Augite: $(Ca,Mg,Fe,Ti,Al)_2[(Si, Al)_2O_6$	Di: $CaMgSi_2O_6$; Hd: $CaFeSi_2O_6$
Silicate-rich marbles	Di	$(Ca_{0.97}Na_{0.03})(Mg_{0.94}Al_{0.04}Fe_{0.03})(Si_{1.96}Al_{0.04})O_6$	Di_{93}; Hd_3
Calc-silicates	Di	$(Ca_{0.97}Na_{0.02})(Mg_{0.90}Fe_{0.05}Al_{0.05})(Si_{1.94}Al_{0.06})O_6$	Di_{90}; Hd_5
A monzogranites	Aug	$(Ca_{0.90}Na_{0.04})(Mg_{0.76}Fe_{0.28})(Si_{1.97}Al_{0.03})O_6$	Di_{73}; Hd_{27}
B monzogranites	Hd	$(Ca_{0.97}Na_{0.04})(Mg_{0.38}Fe_{0.60})(Si_{1.98}Al_{0.02})O_6$	Di_{39}; Hd_{61}
Clinopyroxenite	Di	$(Ca_{0.93}Na_{0.02})(Mg_{0.85}Fe_{0.14}Al_{0.03})(Si_{2.02})O_6$	Di_{83}; Hd_{14}
Qfs metasediments	Di	$(Ca_{0.88}Na_{0.05})(Mg_{0.91}Fe_{0.10}Al_{0.04})(Si_{2.02})O_6$	Di_{86}; Hd_9

Table 4.4: Mica compositions

Lithology	Mineral	Structural formula (Deer et al., 1992)	End-members
		Phlogopite – Biotite: $K_2(Mg,Fe^{2+})_{6-4}(Fe_{3+},Al,Ti)_{0-2}[Si_{6-5}Al_{2-3}O_{20}](OH,F)_4$	Ann: $K_2Fe_6[Si_6Al_2O_{20}](OH_4)$; Phl: $K_2Mg_6[Si_6Al_2O_{20}](OH_4)$
Silicate-rich marbles	Phl	$(K_{0.87})(Mg_{2.61}Al_{0.17}Fe_{0.12}Ti_{0.09})(Si_{2.79}Al_{1.21})O_{10}(OH_{1.67}F_{0.33})$	Phl_{87}; Ann_{13}
Calc-silicates	Phl	$(K_{0.85})(Mg_{2.70}Fe_{0.17}Al_{0.08}Ti_{0.05})(Si_{2.92}Al_{1.08})O_{10}(OH_{1.10}F_{0.89})$	$Phl_{90;}Ann_6$
A monzogranites	Bt	$(K_{0.81})(Mg_{1.88}Fe_{0.80}Ti_{0.22})(Si_{2.86}Al_{1.14})O_{10}(OH_{1.41}F_{0.55}Cl_{0.05})$	Phl_{65}; Ann_{28}

Table 4.5: Nepheline compositions

Lithology	Mineral	Structural formula (Deer et al., 1992)	End-members
		Nepheline: $Na_3(Na,K)[Al_4Si_4O_{16}]$	Ne: $Na[Al_4Si_4O_{16}]$; Kal: $K[Al_4Si_4O_{16}]$
Silicate-rich marbles	Ne	$Na_{2.41}K_{0.97}\square_{0.58}Ca_{0.05}Al_{4.09}Si_{4.06}O_{16}$	Ne_{69-78}; Kal_{22-31}

Table 4.6: Feldspar compositions

Lithology	Mineral	Structural formula (Deer et al., 1992)	End-members
		Alkali Feldspars: $(K,Na)[AlSi_2O_8]$; Plagioclase $Na[AlSi_3O_8] – Ca[Al_2Si_2O_8]$	Or: $KAlSi_2O_8$; Ab: $NaAlSi_3O_8$; An: $CaAl_2Si_2O_8$
Silicate-rich marbles	K-feldspar	$K_{0.92}Al_{1.08}Si_{2.95}O_8$	Or_{100}
A monzogranites	K-feldspar	$K_{0.69}Na_{0.12}Al_{1.00}Si_{3.04}O_8$	Or_{85}; Ab_{15}
	Plagioclase	$Na_{0.53}Ca_{0.27}Al_{1.26}Si_{2.78}O_8$	Ab_{66}; An_{44}
B monzogranites	K-feldspar	$K_{0.89}Na_{0.04}Al_{1.02}Si_{2.99}O_8$	Or_{96}; Ab_4
	Plagioclase (cores)	$Na_{0.72}Ca_{0.15}Al_{1.19}Si_{2.85}O_8$	Ab_{83}; An_{17}
	Plagioclase (rims)	$Na_{0.81}Ca_{0.01}Al_{1.04}Si_{3.00}O_8$	Ab_{99}; An_1
Clinopyroxenite	K-feldspar	$K_{0.93}Al_{1.08}Si_{2.95}O_8$	Or_{100}
	Plagioclase	$Na_{0.64}Ca_{0.07}Al_{1.10}Si_{2.98}O_8$	Ab_{90}; Ab_{10}
Qfs metasediments	K-feldspar	$K_{0.85}Al_{1.02}Si_{3.01}O_8$	Or_{100}
	Plagioclase	$Na_{0.73}Al_{1.03}Si_{3.04}O_8$	An_{100}

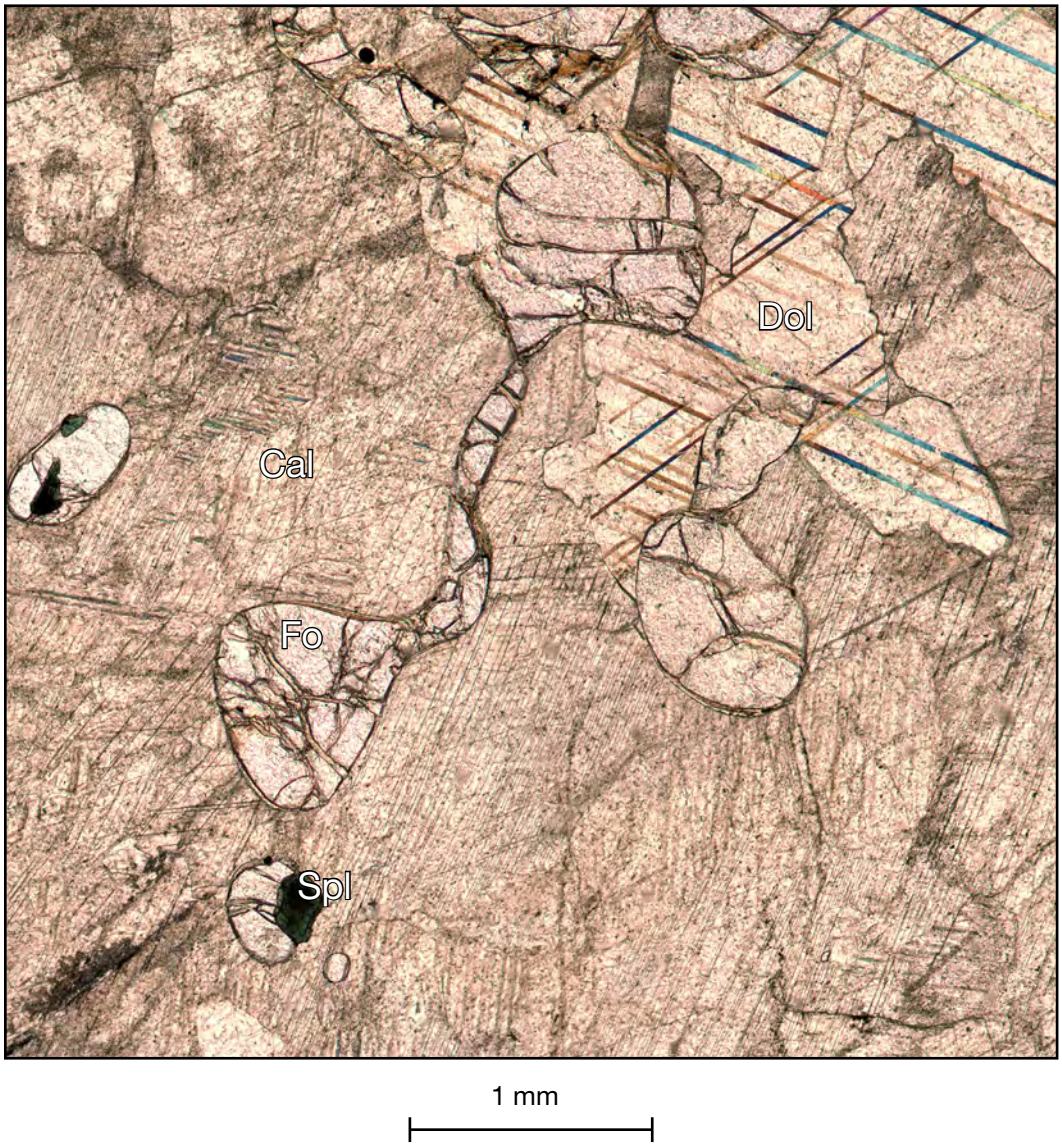

Figure 4.1: Photomicrograph of forsterite in carbonate-rich marble. The sample comprises highly xenoblastic forsterite (Fo), and spinel (Spl) radomly distributed within a matrix of coarse-grained calcite (Cal) and dolomite (Dol) (Sample B133).

Diopside locally exhibits compositional zoning characterized by increasing Al from core to rim, from 0.083 – 0.010 *cpfu*. Phlogopite varies in composition with increasing proximity to the intruded monzogranites, from 0.06 – 0.012 Ti *cpfu*, corresponding to increasing X_{Mg} (Mg/Mg+Fe in *cpfu*) (Fig. 4.2). In general, the Ti content of phlogopite typically increases with increasing temperature, but decreases with increasing pressure (Henry et al., 2005). Nepheline varies in composition from 0.763 – 1.07 K *cpfu* (from Ne_{69} – Ne_{78}), corresponding to the presence or absence of coexisting K-feldspar respectively.

Texturally, the silicate-rich marbles vary stratigraphically on the scale of 5 – 10 m, from well foliated to nodular, corresponding to a decreased abundance of boudinaged calc-silicate layers in the latter. Figure 4.3 illustrates the foliated texture of the silicate-rich marbles on the hand-specimen scale. The most silicate-rich marbles are characterized by a several-centimeter-scale compositional foliation (S_1), defined by alternating calcite and forsterite-dominated (impure marble) layers, diopside (and locally nepheline)-dominated (calc-silicate) layers, and phlogopite-dominated layers (silicate layers).

The calcite and forsterite-dominated layers comprise medium-grained xenoblastic forsterite, diopside, phlogopite (hypidioblastic), nepheline and K-feldspar randomly distributed within a matrix of calcite (Fig. 4.4). Diopside is locally present as coarse-grained poikiloblasts containing fine-grained inclusions of calcite and phlogopite, and exhibits partial mantles of forsterite (Fig. 4.5). Nepheline contains inclusions of diopside, phlogopite and forsterite, implying relatively late formation. Forsterite and nepheline are separated by thin reaction zones of phlogopite. Adjacent to calcite nepheline exhibits radiating fibrous reaction rims of a hydrous Ca-Na-Al-silicate mineral, possibly mesolite. K-feldspar is present exclusively in fine-grained vermicular intergrowths with nepheline. With the exception of nepheline and K-feldspar, each of the phases is in mutual contact with no obvious reaction textures, implying an equilibrated assemblage. The observed

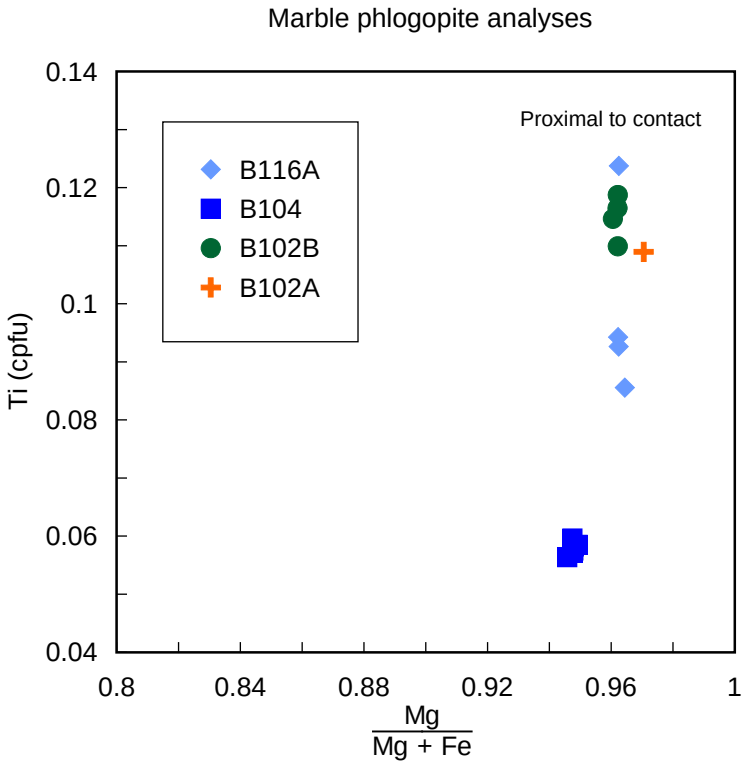

Figure 4.2: Compositional variations in the Ti contents of phlogopite in the impure marbles. Ti content increases with increasing proximity to the contact with the monzogranites, and may be related to increasing metamorphic temperatures.

Figure 4.3: Photograph of foliated, silicate-rich marble hand specimen. The dominant S_1 foliation is compositional. Three mineralogical zones are pictured, including calcite (Cal) and forsterite (Fo)-rich (impure marble); forsterite, diopside (Di), and calcite-rich; phlogopite-dominated; and, diopside and nepheline-rich layers (Sample B116A).

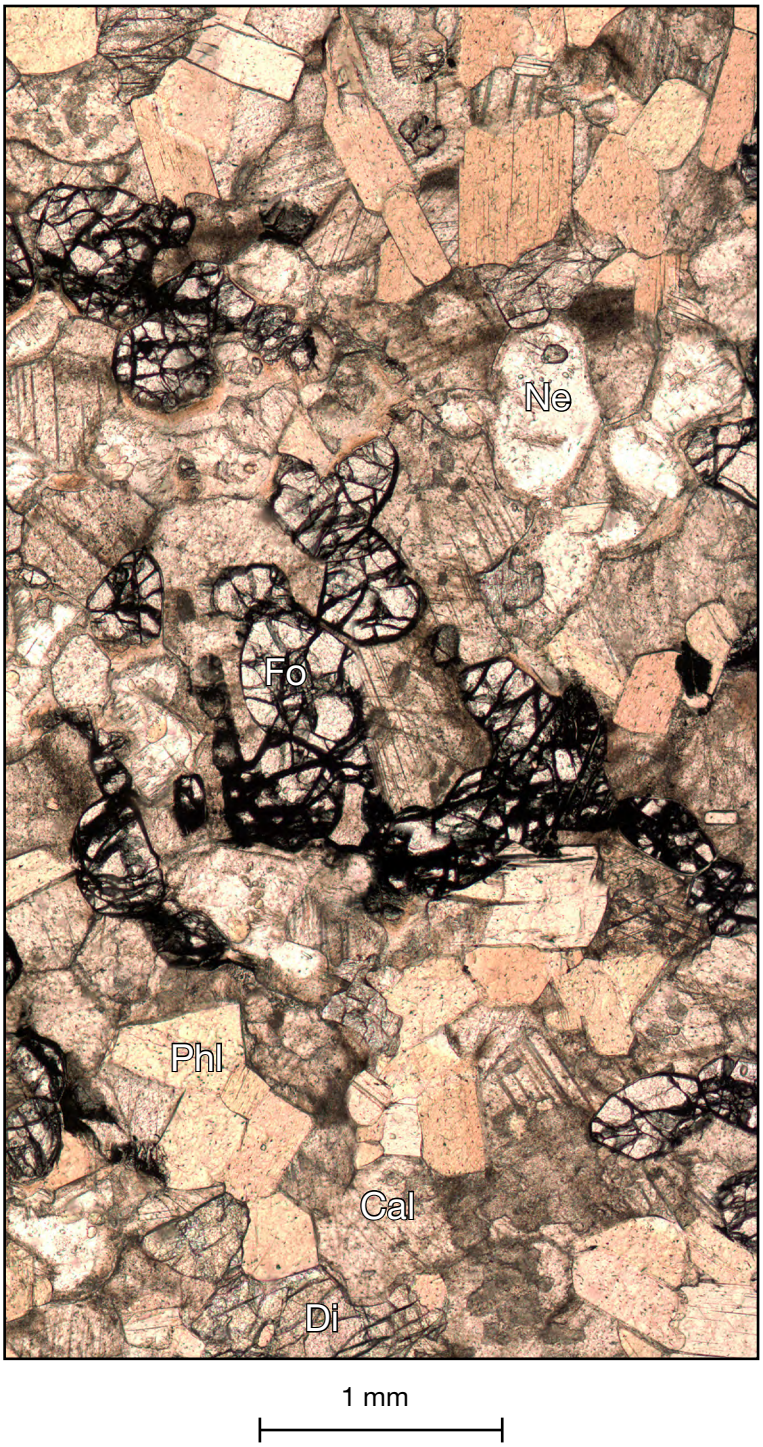

Figure 4.4: Photomicrograph of calcite and forsterite-rich impure marble layer. These layers comprise randomly distributed, equigranular forsterite (Fo), diopside (Di), phlogopite (Phl), nepheline (Ne), and calcite (Cal) (Sample B116A).

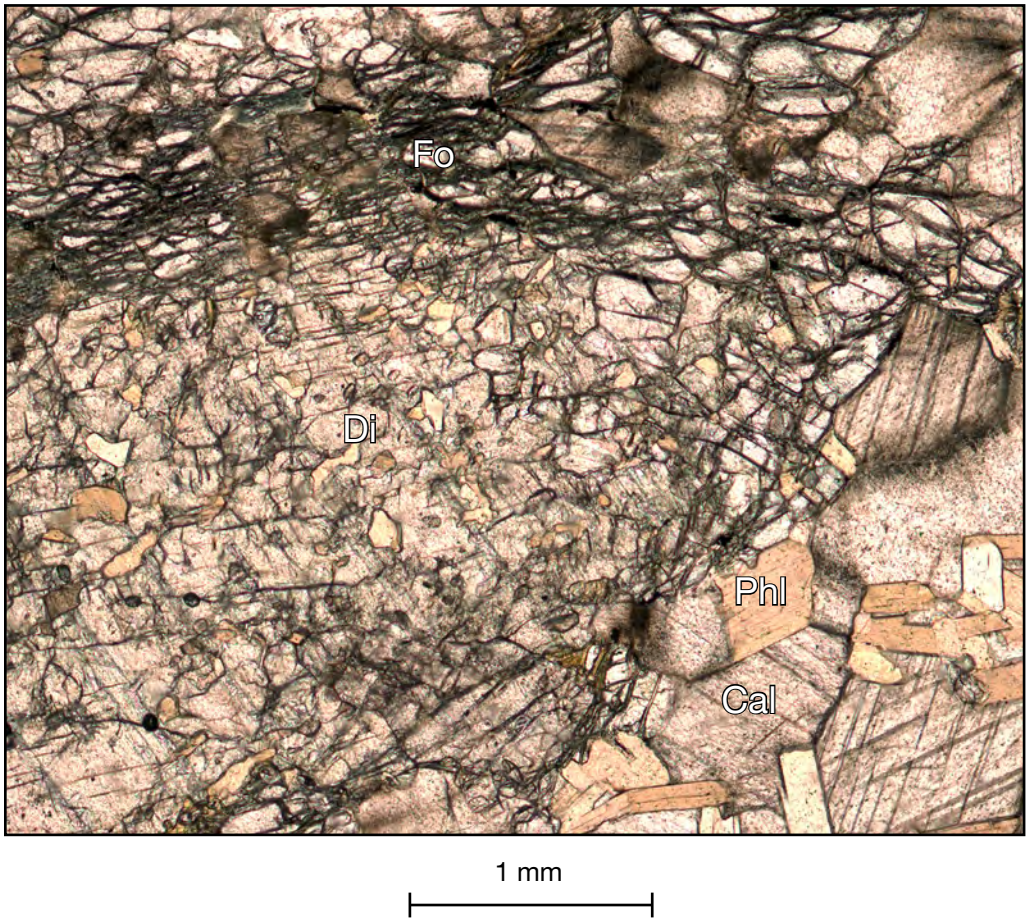

Figure 4.5: Photomicrograph of diopside poikiloblast in silicate-rich marble. A diopside (Di), poikiloblast containing inclusions of phlogopite (Phl) and calcite (Cal) is partially mantled by forsterite (Fo). The poikiloblast is situated within a forsterite-bearing layer with phlogopite and granoblastic calcite (Sample B104A).

inclusion relationships, intergrowths, and core-mantle textures indicate the following sequence of mineral growth: phlogopite and calcite, diopside, forsterite, secondary calcite and phlogopite, and nepheline and K-feldspar.

The diopside-dominated calc-silicate layers vary significantly in thickness from ca. 1-10 cm. At outcrop scale they form calc-silicate boudins characterized by diopside-dominated cores and well defined forsterite mantles which separate them from adjacent calcite and forsterite-dominated impure marbles. They comprise coarse-grained, xenoblastic diopside poikiloblasts, calcite together with nepheline, phlogopite, and locally minor apatite (Fig. 4.6). Where present in significant proportions, calcite separates diopside and nepheline, the latter typically containing inclusions of diopside. The ratio of nepheline to diopside increases with proximity to adjacent phlogopite-rich layers.

The phlogopite-dominated layers are ca. 0.5 cm thick, and comprise fine-grained, randomly oriented hypidioblastic phlogopite and minor, fine-grained xenoblastic diopside (Fig. 4.6). They are concentrated adjacent to the diopside-dominated layers with significant proportions of nepheline.

Figure 4.7 illustrates the nodular texture of the silicate-rich marbles on the hand-specimen scale. The nodular texture is characterized by ovoid aggregates of xenoblastic forsterite, and locally diopside, randomly distributed within a matrix of coarse-grained, granoblastic calcite. A discontinuous, spaced, compositional foliation (S_1), defined by concentrations of fine-grained, randomly oriented phlogopite is also present.

The lack of shape preferred orientation of any phase, in particular phlogopite, implies that the observed compositional layers reflect either primary stratigraphic variations in bulk composition, or alternatively, locally metasomatized monzogranite veins. The pervasive compositional foliation in many of the silicate-rich marbles indicates that chemical equilibrium has probably not been attained beyond individual 2 – 5 cm scale compositional layers. A secondary, spaced cleavage was observed in hand specimen but

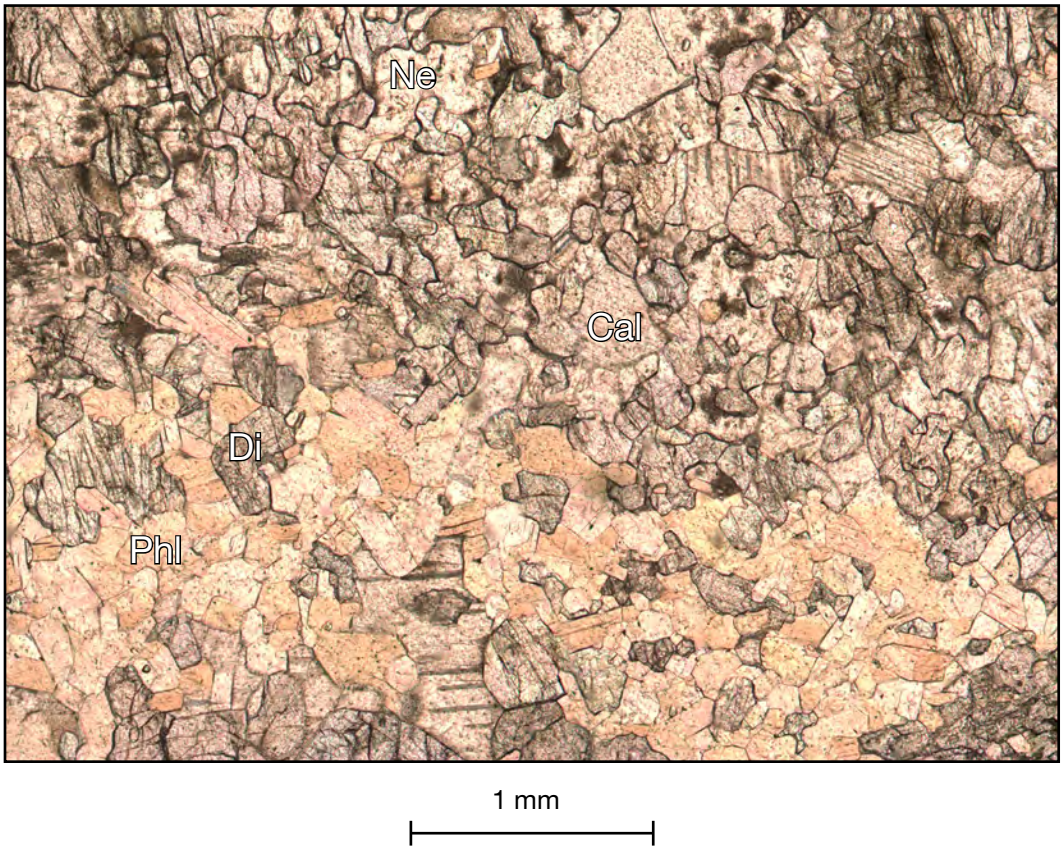

Figure 4.6: Photomicrograph of diopside-dominated layer in silicate-rich impure marble. The (upper) diopside-dominated layer comprises diopside (Di), nepheline (Ne), and calcite (Cal). Nepheline appears to be overgrowing diopside. The adjacent (lower) phlogopite-rich layer comprises phlogopite, diopside, and minor calcite (Sample B116A).

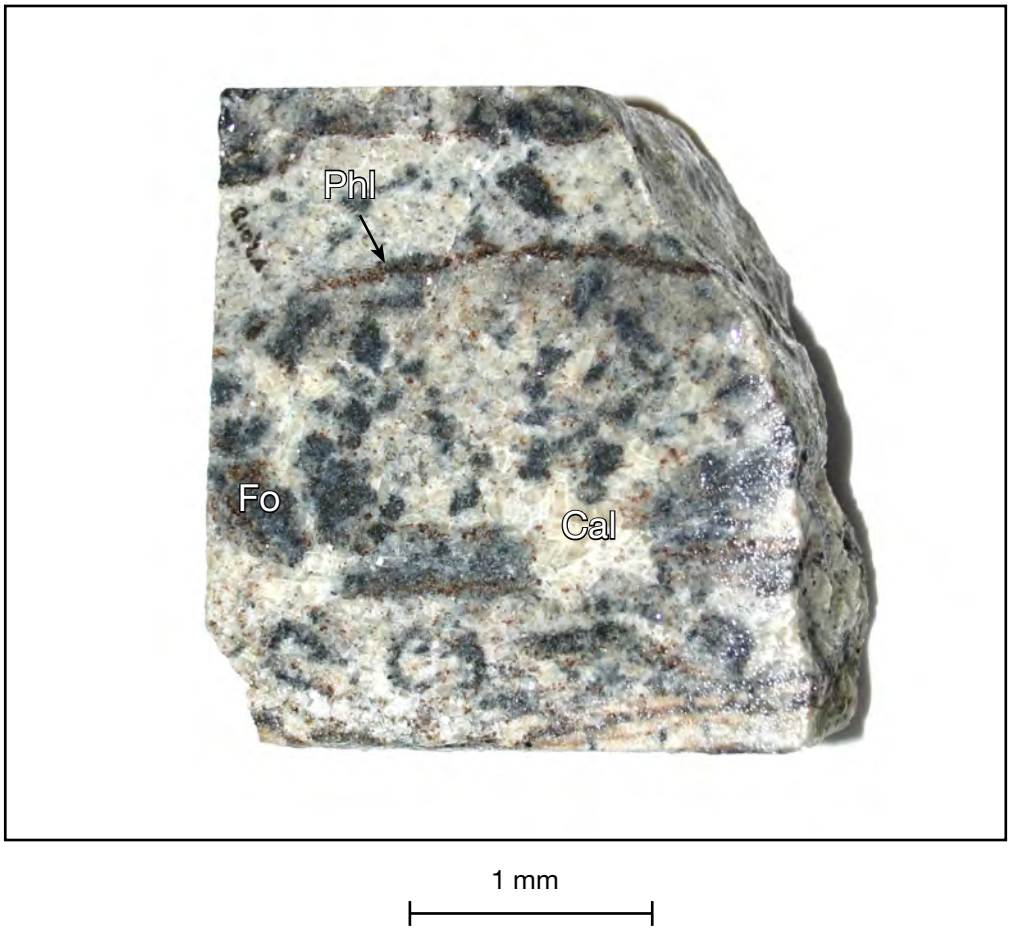

Figure 4.7: Photograph of nodular textured impure marble in hand specimen. The nodular texture is defined by the random distribution of ovoid forsterite (Fo) aggregates, locally cored by relict diopside in thin section (not pictured), within a matrix of coarse-grained, granoblastic calcite (Cal). Discontinuous phlogopite (Phl)-rich layers define a subtle foliation (Sample B102A).

not in thin section.

4.2 Calc-silicates

The calc-silicate zones that characterize the contact between the LHG marbles and the intruded monzogranites comprise diopside (Di_{90}), pargasite (Table 4.7), phlogopite, scapolite (Me_{48-77} and $X_{Cl} = 0.034 – 0.063$) (Table 4.8), and calcite, with minor clinozoisite (Table 4.9), titanite (Table 4.10), plagioclase, and quartz. Observed variations in the chemical compositions of these phases are described below.

Table 4.7: Amphibole compositions

Lithology	Mineral	Structural formula (Deer et al., 1992)
	Hornblende	$(Na,K)_{0-1}Ca_2(Mg, Fe^{2+},Fe^{3+},Al)_5Si_{6-7.5}Al_{2-0.5}O_{22}(OH)_2$
Calc-silicates	Pargasite	$(Na_{0.60}K_{0.26})Ca_{2.04}(Mg_{3.81}Al_{0.54}Fe_{0.33}Ti_{0.07})\ (Si_{6.02}Al_{1.98})O_{22}(OH_{1.04}F_{0.93}Cl_{0.03})$
A monzogranites	Magnesio-hastingsite	$(K_{0.71}Na_{0.27})Ca_{1.83}(Mg_{2.93}Fe_{1.67}Ti_{0.21}Al_{0.11})\ (Si_{6.45}Al_{1.55})O_{22}(OH_{1.40}F_{0.50}Cl_{0.10})$
Qfs metasediments	Winchite	$(Na_{0.20}K_{0.14})(Ca_{1.33}Na_{0.67})(Mg_{4.47}Fe_{0.40}Ti_{0.19})\ (Si_{7.82}Al_{0.18})O_{22}(OH_{1.64}F_{0.35})$

Table 4.8: Scapolite compositions

Lithology	Mineral	Structural formula (Deer et al., 1992)	End-members
	Scapolite	$(Na,Ca,K)_4[Al_3(Al,Si)_3Si_6O_{24}](Cl,CO_3,SO_4)$	Ma: $Na_4[Al_3Si_9O_{24}]Cl$; Me: $Ca_4[Al_6Si_6O_{24}]CO_3$
Calc-silicates	Meionite	$(Na_{1.19}Ca_{1.92}K_{0.10})Al_3(Al_{1.33}Si_{1.18})Si_6O_{24}(Cl_{0.48}CO_{3\text{-}0.51})$	$Ma_{33\text{-}52}$; $Me_{48\text{-}77}$
B monzogranites	Marialite	$(Na_{1.78}Ca_{1.22}K_{0.10})Al_3(Al_{0.80}Si_{1.73})Si_6O_{24}(Cl_{0.63}CO_{3\text{-}0.36})$	Ma_{60}; Me_{40}
Clinopyroxenite	Marialite	$(Na_{1.35}Ca_{0.65}K_{0.16})Al_3(Al_{0.45}Si_{2.27})Si_6O_{24}(Cl_{0.84}CO_{3\text{-}0.65})$	Ma_{69}; Me_{31}

Table 4.9: Clinozoisite compositions

Lithology	Mineral name	Structural formula (Deer et al., 1992)
	Clinozoisite	$Ca_2Al_2O{\cdot}AlOH[Si_2O_7][SiO_4]$
Calc-silicates		$Ca_{2.11}Fe^{3+}{}_{0.15}Al_{2.95}Si_{3.13}O_{12}OH$

Table 4.10: Titanite compositions

Lithology	Mineral	Structural formula (Deer et al., 1992)
	Titanite	$CaTi[SiO_4](O,OH,F)$
Calc-silicates		$Ca_{1.06}(Ti_{0.81}Al_{0.14})(Si_{1.06})O_4(O_{0.91}F_{0.09})$
Clinopyroxenite		$Ca_{1.03}(Ti_{0.89}Al_{0.09})(Si_{0.99})O_4(O_{0.90}F_{0.10})$
B monzogranites		$Ca_{1.00}(Ti_{0.91}Al_{0.08}Fe_{0.03})(Si_{0.99})O_4(O_{0.92}F_{0.08})$

Figure 4.8 illustrates the composition of the phlogopite and biotite from all lithologies in terms of X_{Mg} versus wt. % F + Cl. Phlogopite in the calc-silicates is relatively enriched in F, containing from 0.76 – 0.95 F anions per formula unit (*apfu*). In general, F is typically incorporated into phlogopite with high Mg/Fe (Faryad, 2002). Figure 4.9 illustrates the compositional variation of scapolite from the calc-silicates in terms of equivalent anorthite (EqAn), defined as 100(Al-3/3) (in *cpfu*), versus X_{Cl}, defined as Cl/(CO3+SO3+Cl) (in *apfu*). Scapolite in the calc-silicates varies significantly from Me_{48} – Me_{77}, and from 0.35 – 0.64 Cl *apfu*, increasing with proximity to phlogopite.

Texturally, the calc-silicates are characterized by an irregular, meso-scale compositional foliation defined by alternating, ca. > 5 cm, essentially monominerallic granoblastic diopside, pargasite, and minor calcite layers, truncated by highly irregular and texturally complex phlogopite-rich zones comprising phlogopite, scapolite, titanite, and clinozoisite (Figs. 4.10, 4.11). Diopside and pargasite are coarse-grained and hypidio- to idioblastic. Pargasite contains hypidioblastic inclusions of diopside, and locally xenoblastic inclusions of plagioclase. Scapolite is present within phlogopite-rich zones as medium-grained skeletal inclusions adjacent to calcite, and as fine-grained intergrowths in phlogopite which appear to radiate outward from diopside and pargasite (Fig. 4.11). The latter are locally intergrown with diopside. Scapolite is also present within the diopside-dominated zones as relatively complete, hypidioblastic grains, typically spatially associated with calcite. In outcrop, scapolite crystals up to 20 cm long are present within brittle fractures. Immediately adjacent to these fractures scapolite appears to be overgrowing embayed diopside, suggesting replacement (Fig. 4.12). The observed inclusion relationships, intergrowths, and inferred replacement textures indicate

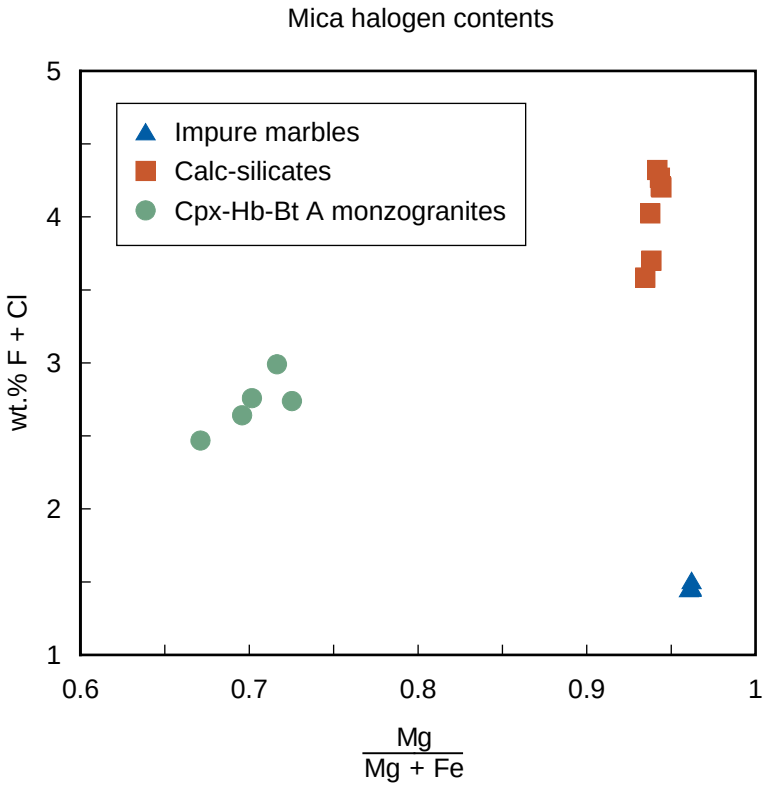

Figure 4.8: Compositional variations in the halogen contents of biotite and phlogopite from selected lithologies. The phlogopite in the calc-silicates shows relative enrichment in F. The biotite in the monzogranites is Cl-bearing, with negligable F.

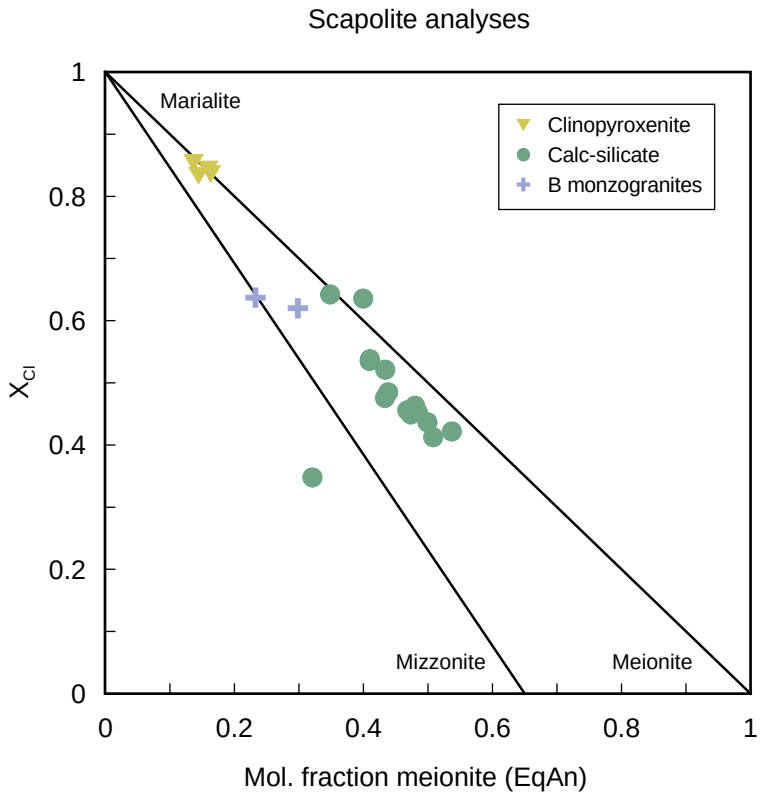

Figure 4.9: Compositional variations in scapolite from selected lithologies. Equivalent anorthite (EqAn) is defined as 100(Al - 3)/3. Solid lines represent solid-solution between end-members marialite, meionite, and mizzonite. Scapolite in the calc-silicates varies considerably in composition. Scapolite in the monzogranites is realtively uniform in composition and somewhat more marialitic. In the clinopyroxenites, scapolite exhibits a significant Cl-rich (marialitic) component.

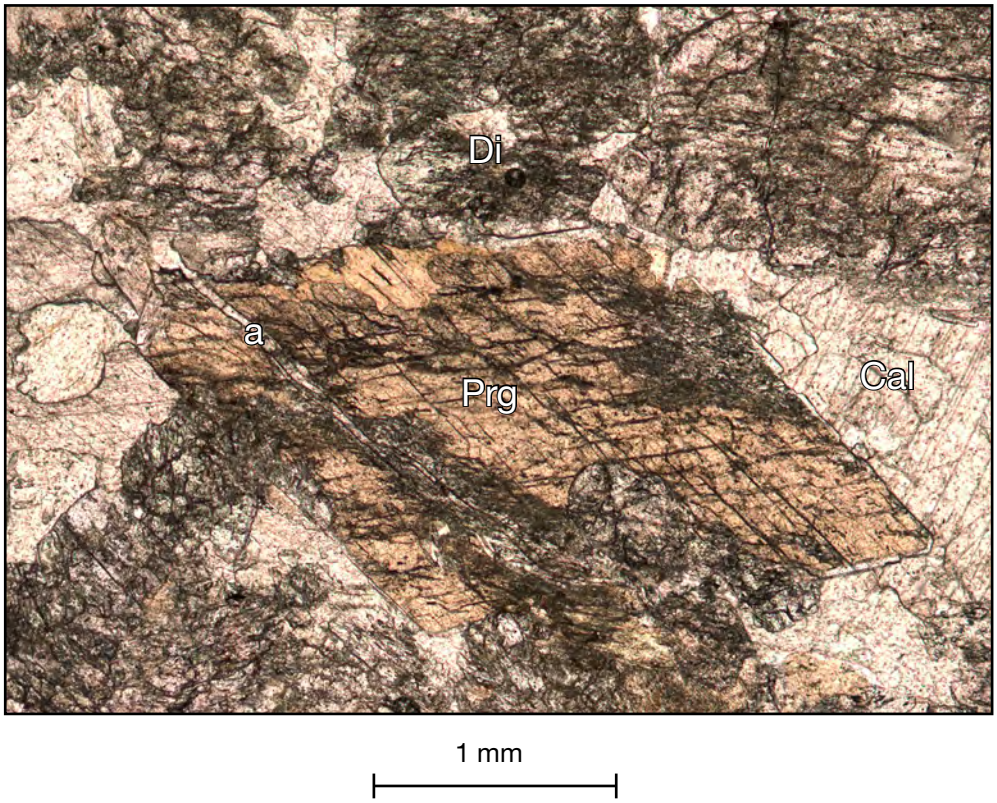

Figure 4.10: Photomicrograph of diopside and pargasite in calc-silicate. Idioblastic pargasite (Prg) sits within a calcite (Cal)-rich zone within a diopside (Di)-dominated calc-silicate. The pargasite is cross-cut by a calcite-filled vein (a).

Figure 4.11: Photomicrograph of phlogopite-rich zone in calc-silicate. The phlogopite-rich zones comprise relict diopside (Di) and pargasite (Prg), in addition to phlogopite (Phl), calcite (Cal), and scapolite (Scp). The calcite is rimmed by phlogopite (a). Phlogopite appears to be replacing pargasite adjacent to calcite (b). Scapolite is present both as individual grains within or adjacent to calcite, and as complex, fine-grained intergrowths with phlogopite that extend between pargasite and diopside.

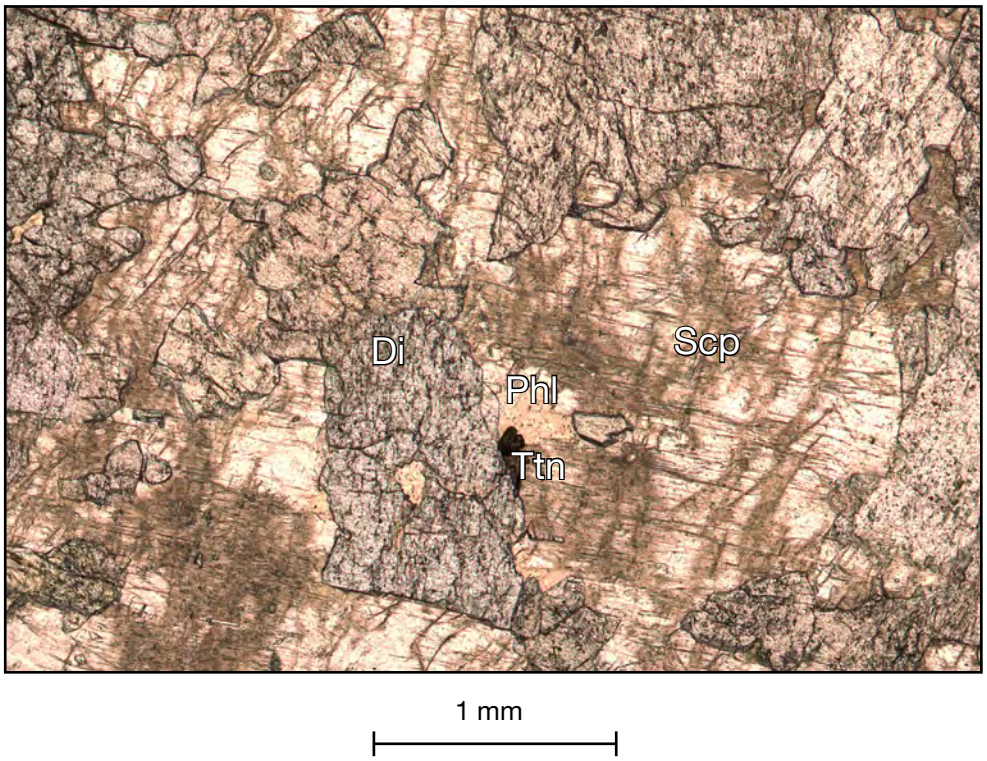

Figure 4.12: Photomicrograph of scapolite-rich zone in calc-silicate. Scapolite (Scp) appears to be overgrowing diopside (Di), and minor phlogopite (Phl) and titanite (Ttn). The scapolite exhibits unidentified, fine-grained alteration. The distribution of scapolite in the calc-silicates appears to be fracture-controlled (Sample BSCP).

the following sequence of mineral growth: quartz and plagioclase, diopside, pargasite, calcite, clinozoisite, secondary diopside and scapolite, and phlogopite.

A subtle, secondary 1 cm spaced cleavage defined by < 0.5 mm thick, calcite-filled brittle fractures is present locally in the calc-silicates, and is interpreted as an axial planar fabric with respect to the SE-plunging F_2 folds. This fabric is best developed in areas in calc-silicates in which scapolite is absent.

4.3 Monzogranites

Two phases of monzogranites intruded the LHG marble, each exhibiting a distinct bulk composition, mineralogy, and texture. Their mineral chemistry and petrography are described below.

4.3.1 Clinopyroxene – hornblende – biotite A monzogranites

The *A* monzogranites are silica-saturated, slightly alkaline, and peraluminous. They comprise augite (Di_{73}), magnesio-hastingsite, biotite (Ann_{28}), perthitic K-feldspar (Or_{85}), plagioclase (An_{44}), and quartz.

Texturally, the *A* monzogranites are characterized by a pervasive compositional foliation (S_1) defined by alternating augite-rich; hornblende-rich; and dominantly quartzo-feldspathic layers. Biotite is present throughout and defines a subtle spaced cleavage parallel to the dominant compositional foliation (Fig. 4.13). A subtle secondary foliation is defined by alignment of biotite oblique to S_1 (Fig. 4.14). Biotite partially included in augite exhibits highly irregular, embayed morphologies, and thin mantles of quartz and plagioclase interpreted as textural evidence of dehydration-melting (Fig. 4.13). Each of the phases is in mutual contact, implying an equilibrated assemblage.

4.3.2 Clinopyroxene – titanite ± scapolite ± calcite B monzogranites

The *B* monzogranites are silica over-saturated, subalkaline, and metaluminous. They comprise hedenbergite (Di_{39}), titanite, scapolite (Ma_{60} and $X_{Cl} = 0.63$), perthitic K-feldspar (Or_{96}) with sub-microscopic plagioclase lamellae, zoned plagioclase ($An_{17} – An_1$, from core to rim), calcite, and quartz. The scapolite and calcite are present exclusively in

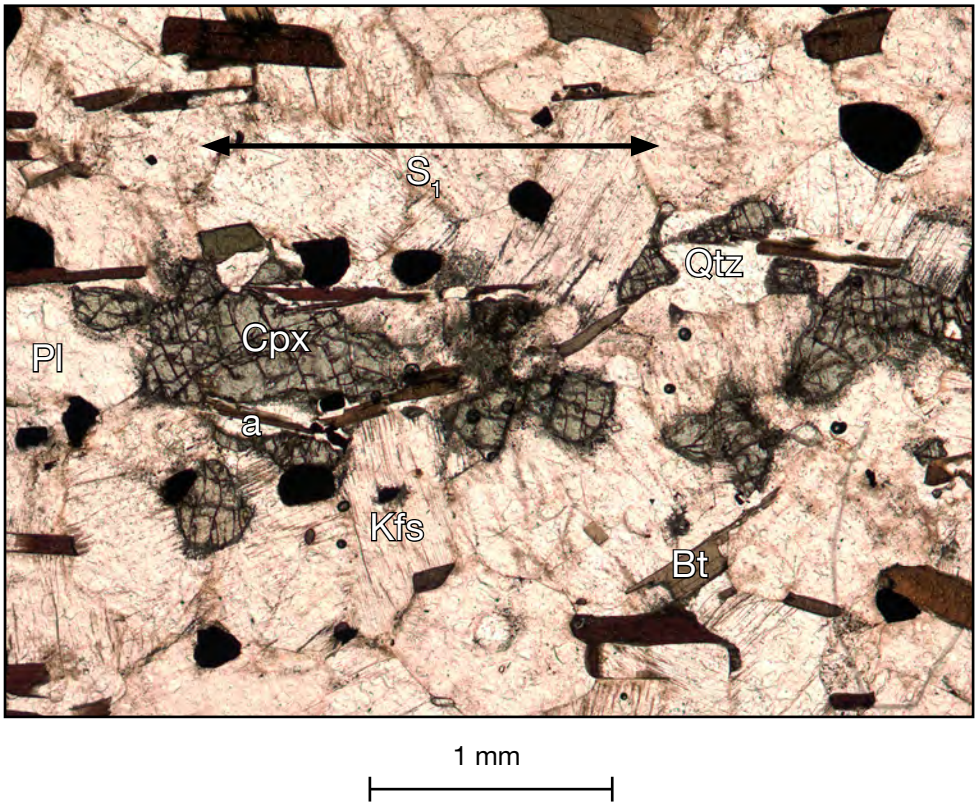

Figure 4.13: Photomicrograph of clinopyroxene in *A* monzogranite. The sample comprises clinopyroxene (Cpx), hornblende (not pictured), biotite (Bt), K-feldspar (Kfs), plagioclase (Pl), quartz (Qtz), and opaques. The distribution of clinopyroxene and hornblende defines a compositional foliation (S_1). Biotite impinging upon clinopyroxene grains is highly embayed and rimmed by quartz, implying dehydration (a) (Sample B119A).

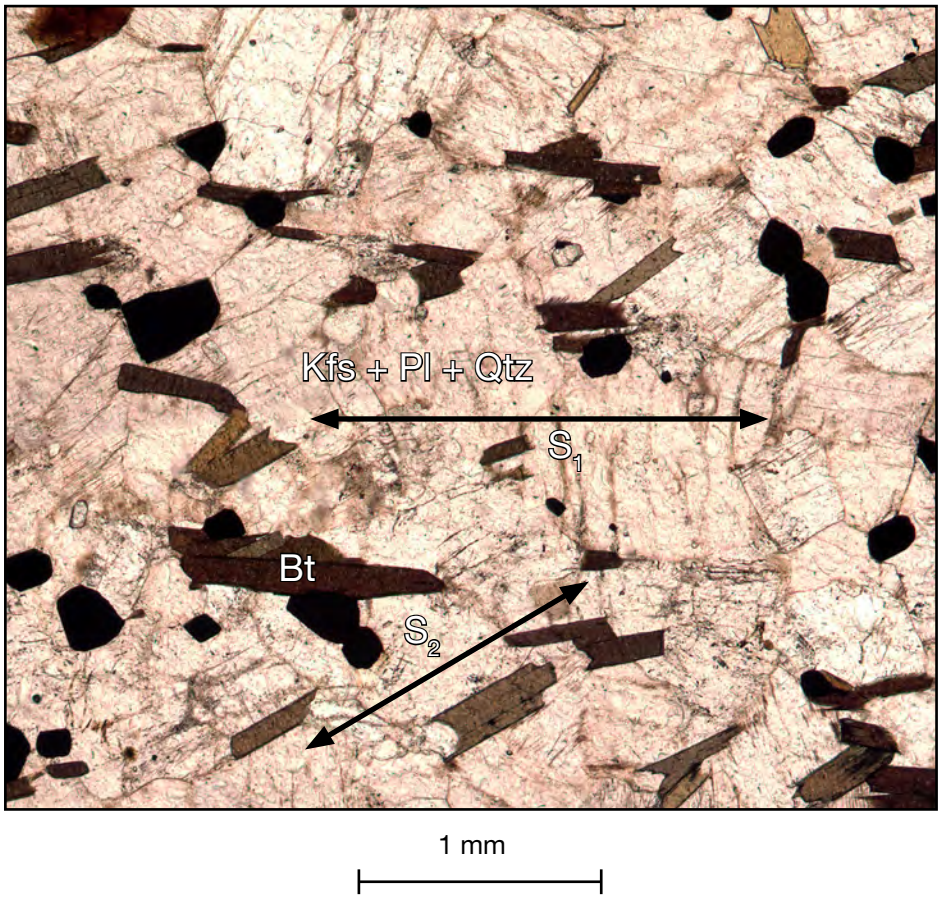

Figure 4.14: Photomicrograph of biotite-defined schistosity in *A* monzogranite. Biotite (Bt) defines a weak, spaced schistosity (S_1), and and an even weaker, oblique schistosity (S_2) (Sample B119).

B monzogranites directly adjacent to the calc-silicates.

Texturally the *B* monzogranites are characterized by a cm-scale moderately developed foliation defined by a grain-size variation from medium- to coarse-grained, and by alternating hedenbergite-rich and dominantly quartzo-feldspathic layers. Where present scapolite and calcite are typically distributed in coarse-grained moderately granoblastic, hedenbergite-rich layers. The straight grain-boundaries and random distribution of both scapolite and calcite indicates that they represent part of an equilibrated assemblage (Fig. 4.15). K-feldspar locally exhibits a core-and-mantle texture characterized by the mantling of coarse-grained K-feldspar by finer-grained aggregates of recrystallized K-feldspar. Directly adjacent to the contact with the calc-silicates, the *B* monzogranite contains what is interpreted, based upon modal mineralogy and mineral chemistry, to be a xenolith of the *A* monzogranite.

4.4 Clinopyroxenites

The clinopyroxenite xenoliths within the monzogranites comprise diopside (Di_{83}), scapolite (Ma_{69} and $X_{Cl} = 0.85$), plagioclase (An_{10}) with coarse anti-perthitic K-feldspar lamellae (Or_{100}), and titanite.

Figure 4.9 illustrates the composition of scapolite in the clinopyroxenites in terms of EqAn versus X_{Cl}, and reveals relative enrichment of Cl when compared with scapolite in the calc-silicates.

Texturally, the clinopyroxenites are massive, and characterized by randomly oriented medium- to coarse-grained diopside with minor titanite inclusions, and minor interstitial antiperthite and scapolite.

4.5 Quartzo-feldspathic metasediments

The quartzo-feldspathic metasediments locally intercalated with the marbles comprise diopside (Di_{86}), winchite, plagioclase (An_{100}), minor K-feldspar (Or_{100}), quartz, and retrograde epidote and actinolite.

Winchite varies in composition between samples from 0.123 – 0.224 Al *cpfu*, from

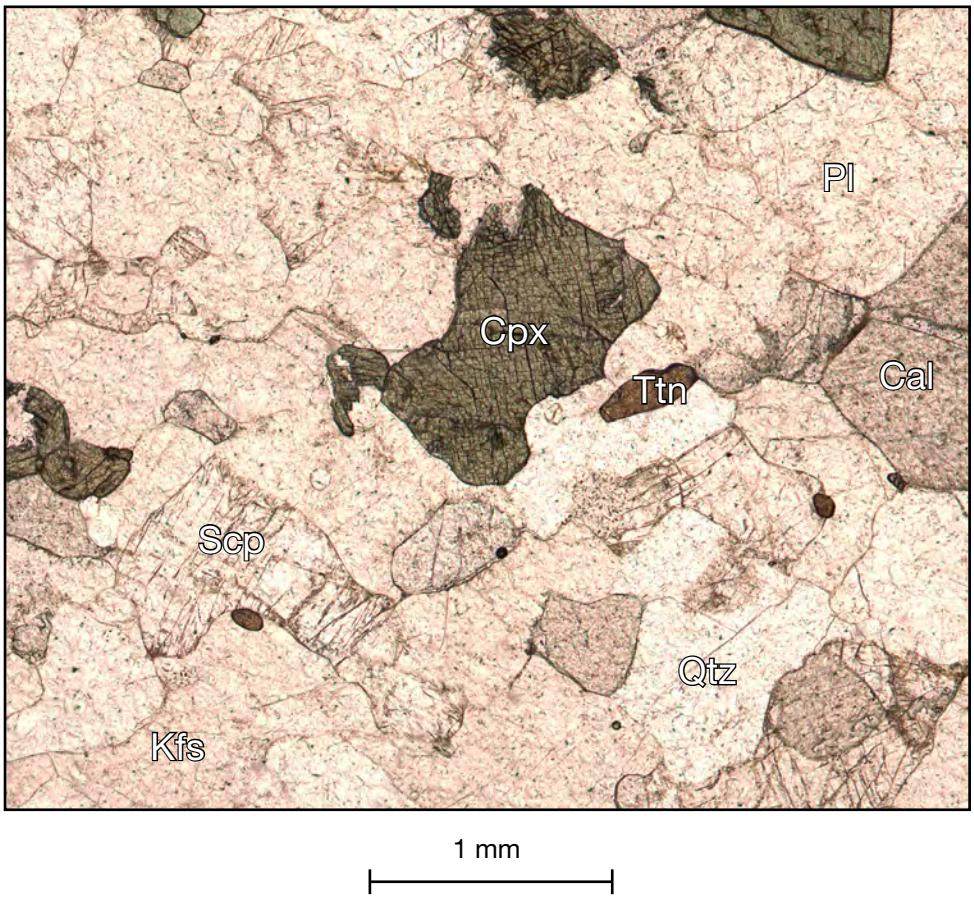

Figure 4.15: Photomicrograph of calcite and scapolite-bearing *B* monzogranite. The sample comprises clinopyroxene (Cpx), titanite (Ttn), scapolite (Scp), calcite (Cal), K-feldspar (Kfs), plagioclase (Pl), and quartz (Qtz). The distribution of clinopyroxene defines a compositional foliation (not pictured). Calcite and scapolite exhibit straight grain boundaries implying that they are in equilibrium with surrounding minerals (Sample B137).

0.085 – 0.180 K *cpfu*, and from 0.038 – 1.08 Na *cpfu*. Of these, K and Na increase, while Al decreases with proximity to the contact with the Type II monzogranites.

Texturally, the quartzo-feldspathic metasediments are characterized by a weak compositional foliation defined by alternating, ca. 3 – 5 cm thick diopside- and winchite-bearing layers. Diopside and winchite are medium-grained and are distributed within a fine- to medium-grained matrix of granoblastic plagioclase, quartz, and very minor K-feldspar. Winchite exhibits partial replacement by fine-grained actinolite.

4.6 Scapolite chemistry

Scapolite is a common constituent of sapphire-bearing rocks from southern Baffin Island, where its replacement by plagioclase and phlogopite locally produces Al_2O_3. Accordingly its distribution and chemistry within the study area warrant particular attention. Scapolite comprises two ideal anhydrous end-members: marialite (Ma) $Na_4Al_3Si_9O_{24}Cl$, and meionite (Me), $Ca_4Al_6Si_6O_{24}CO_3$. The latter may exhibit $CO_3 – SO_4$ solid solution, particularly at extreme depths. The term mizzonite is commonly applied to scapolite of intermediate composition (EqAn = 67) (Moecher & Essene, 1991).

The composition of scapolite is a function of two factors: the *P–T* conditions and the activity of fluid components at the time of its formation. In general, the meionite (CO_3-rich) content increases in calc-silicates with increasing metamorphic grade (Moecher & Essene, 1991). Figure 4.9 illustrates the compositional variation of scapolite from the study area. The compositions of scapolite define an approximately linear trend from intermediate compositions ($Me_{48} – Me_{77}$), to more Cl-rich compositions (Ma_{69}), in the calc-silicates and clinopyroxenites respectively, consistent with compositions from other high-grade metamorphic terranes (Moecher & Essene, 1991). EMP analyses revealed no $CO_3 – SO_4$ solid solution. In general, the presence of Cl-rich scapolite implies the presence of a high NaCl activity during scapolite formation (Mora & Valley, 1989).

Figure 4.16 illustrates the compositions of coexisting plagioclase and scapolite in the *B* monzogranites and clinopyroxenites in terms of X_{Cl} and EqAn. Plagioclase was

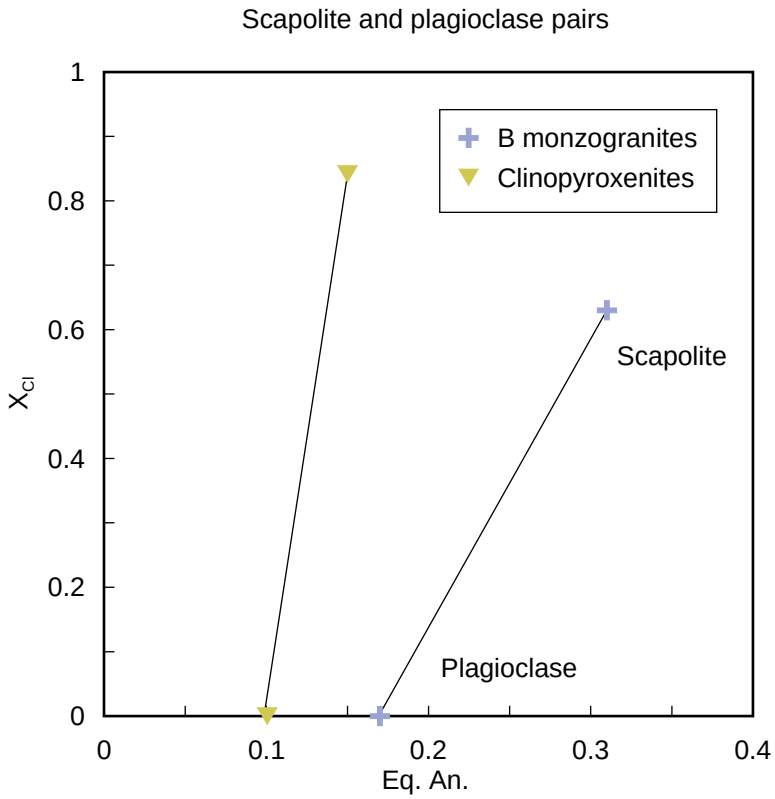

Figure 4.16: Compositions of coexisting plagioclase and scapolite in the clinopyroxenites and *B* monzogranites. A positive slope indicates relative Ca-enrichment in scapolite versus plagioclase, and is consistent with the two having formed in equilibrium with each other.

observed in the calc-silicates, but not analyzed, and is therefore not included in this assessment. In general, for equilibrated plagioclase-scapolite pairs, scapolite is relatively Ca-rich, corresponding to a positive slope in Figure 4.16 (Kullerud & Erambert, 1999). Thus, in both the *B* monzogranites and the clinopyroxenites, plagioclase and scapolite are inferred to have equilibrated. This further implies that the compositions of plagioclase and scapolite in these lithologies reflect the composition of the grain-boundary fluid during their formation.

The compositions of coexisting phlogopite and scapolite should exhibit similar trends of Cl-enrichment or depletion (Mora & Valley, 1989). Phlogopite from the calc-silicates contains little to no Cl. This implies that either phlogopite did not equilibrate with scapolite; that it contained no initial Cl; or that any initially present Cl was partitioned into infiltrating fluids by exchange of Cl with OH. In contrast, F is strongly partitioned into hydrous phases as devolatilization proceeds with prograde metamorphism (Mora & Valley, 1989).

4.7 Summary

The earliest identifiable tectonometamorphic event (M_{1a}) in the study area is the development of a pervasive compositional foliation and associated high-temperature, probably granulite-facies mineral assemblages that vary with bulk composition. In the impure marbles, this metamorphism involved the sequential formation of calcite, phlogopite, diopside, forsterite, and K-feldspar and nepheline. Chapter 5 interprets this sequence in the context of regional metamorphism.

CHAPTER 5: METAMORPHISM AND P-T ESTIMATES

5.1 Metamorphism of metacarbonate rocks

Mineral assemblages in metacarbonates are a function of temperature, pressure, bulk-composition, and fluid-phase composition. The latter, often expressed in terms of mol. fraction CO_2, is highly influenced by the presence (or lack thereof) of infiltrating fluids. In the presence of infiltrating fluids, volatilization and devolatilization reactions are externally buffered, and the fluid composition may remain constant with progressive metamorphism. Infiltration-driven metamorphism is considered relatively common in contact metamorphic environments, where H_2O-rich fluids released from crystallizing hydrous melts infiltrate surrounding metacarbonate rocks (Spear, 1995). In the absence of external fluid infiltration, the fluids generated during devolatilization reactions remain within the grain boundary network of a rock, and the composition of the fluid-phase, buffered internally, evolves (usually) to more CO_2-rich values, with progressive metamorphism. The composition of the fluid-phase directly influences the temperature of decarbonation reactions. Therefore, whether a metacarbonate rock is subjected to infiltrating fluids has a profound effect on the reactions encountered, and resulting mineral assemblages formed during prograde metamorphism (Spear, 1995).

5.2 Metasomatism and metasomatic processes

Metasomatism is defined as metamorphism accompanied by changes in whole-rock composition (Winter, 2001). Diffusion metasomatism involves the transfer of components down chemical potential gradients through another medium, including solids or stationary fluids. Conversely, infiltration metasomatism involves the passive mass transfer of dissolved species in an infiltrating fluid.

5.3 Lake Harbour Group marbles

The mineral assemblages in the impure marbles provide approximate constraints on the temperature conditions and fluid-phase compositions of their formation. Phase

diagrams illustrating the stability of relevant phases with respect to temperature and fluid-phase composition ($T\text{-}X_{CO2}$) at a given pressure were constructed using the internally consistent database and reaction calculation software of Berman (1991). The default solution models were used for phlogopite, clinopyroxene, olivine, and amphibole. In general, the temperature effects of solid-solution in clinopyroxene and olivine should be minimal because both are very near their respective Mg-rich end-members. Independent estimates of metamorphic conditions of 800 °C and ca. 8.0 kbar for M_{1a} were provided by St-Onge et al. (2006b).

5.3.1 Carbonate-rich marbles

The carbonate-rich, dolomitic marbles comprise the assemblage forsterite + spinel + calcite + dolomite. Insufficient textural evidence is available to constrain the sequence of mineral-forming reactions. However, similar assemblages have been reported from other high-grade metamorphic terranes (Letargo & Lamb., 1995; Tropper et al., 2003). In general, the presence of coexisting forsterite and calcite implies high-temperature, probably granulite-facies conditions (see reaction 5.3; Fig.5.1).

5.3.2 Silicate-rich marbles

The sequential formation of dolomite, calcite, diopside, and forsterite during high-temperature, prograde metamorphism of metacarbonates is well documented in the literature (Spear, 1995; Yardley, 1995; and references therein). However, the presence in the study area of phases including K-feldspar, nepheline, pargasite, and phlogopite adds considerable complexity to interpreting the metamorphism of the impure marbles.

The silicate-rich impure marbles comprise the assemblage forsterite + diopside ± pargasite + phlogopite + calcite. K-feldspar and nepheline are interpreted as late phases. Figure 5.1 illustrates the calculated isobaric $T–X_{CO2}$ diagram for these phases calculated at 8.0 kbar.

Fine-grained inclusions of calcite and phlogopite are present within diopside, and represent the earliest identifiable phases in the impure marbles. If one assumes a

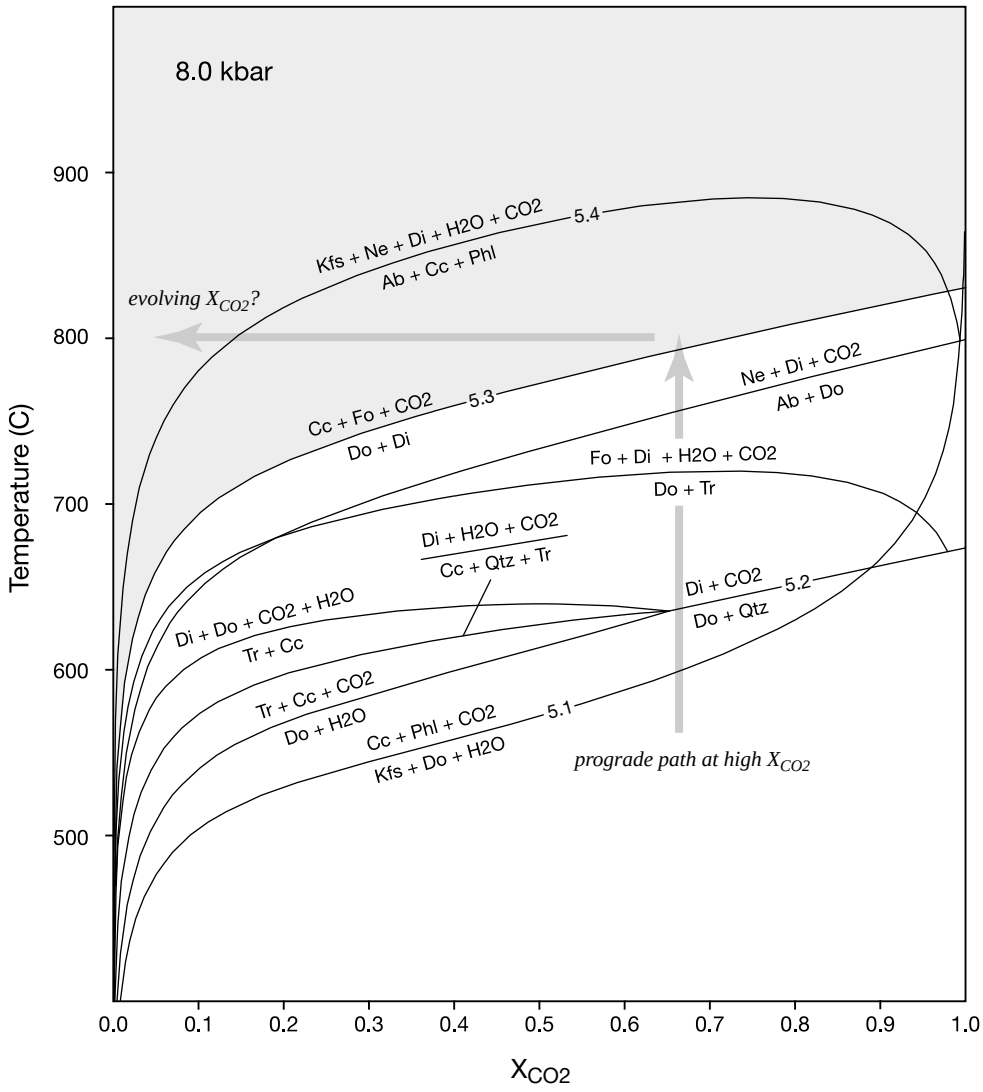

Figure 5.1: Temperature versus fluid-phase composition (T-X_{CO2}) diagram for impure marbles. The diagram was calculated using the "thermobarometry with estimation of equilibration state" (TWEEQU) program of Berman, 1991. The shaded area represents the stability of the assemblage calcite + forsterite. The vertical arrow illustrates the inferred prograde T-X_{CO2} path. The horizontal arrow illustrates how intergrown K-feldspar and nepheline may have formed by reaction 5.4 if X_{CO2} was lowered by the infiltration of H_2O-rich fluids.

sedimentary protolith comprising calcite, dolomite, and minor K-feldspar and quartz, the early formation of calcite and phlogopite is consistent with the reaction:

$$3\ Dol + Kfs + H_2O = Phl + 3\ Cal + 3\ CO_2 \quad (5.1)$$

At 8.0 kbar, and intermediate values of X_{CO2} (ca. 0.5), reaction 5.1 takes place at ca. 550 °C (Fig. 5.1).

Diopside is ubiquitous in the silicate-rich impure marbles. Figure 5.1 reveals that several reactions may explain the formation of diopside, and which reaction first forms diopside is primarily determined by the fluid-phase composition. Given an appropriate bulk-composition, in the presence of $X_{CO2} < 0.65$ tremolite is formed first. No textural evidence of relict tremolite was observed. Its complete absence from the impure marbles may indicate $X_{CO2} > 0.65$ during prograde metamorphism. The formation of diopside at $X_{CO2} > 0.65$ is consistent with the reaction:

$$Dol + Qtz = Di + 2\ CO_2 \quad (5.2)$$

At 8.0 kbar, and $X_{CO2} = 0.65$, reaction 5.2 takes place at a minimum temperature of ca. 620 °C (Fig. 5.1). Reaction 5.2 may account for the absence of quartz in the impure marbles, if one assumes it went to completion. The presence of essentially monominerallic diopside-rich calc-silicate layers may therefore reflect originally dolomite + quartz-rich sedimentary layers. Alternatively, they may represent monominerallic zones formed during diffusion metasomatism.

Forsterite is present as mantles on diopside poikiloblasts and diopside-rich calc-silicate boudins, and as individual, inclusion-free grains commonly formed adjacent to diopside within forsterite and calcite-rich layers. If one assumes that the impure marbles were initially closed to infiltrating fluids, the introduction of forsterite after diopside implies increasing temperatures, consistent with the reaction:

$$3\ Dol + Di = 4\ Cal + 2\ Fo + 2\ CO_2 \quad (5.3)$$

At 8.0 kbar, and again assuming relatively high X_{CO2} (ca. 0.65), reaction 5.3 takes place at ca. 800 °C. This temperature represents lower limit for peak M_{1a} metamorphism of the

impure marbles. The persistence of diopside in samples containing coexisting forsterite and calcite is interpreted to reflect the complete consumption of dolomite by reaction 5.3.

Pargasite is present locally in textural equilibrium with forsterite and phlogopite in more carbonate-rich impure marbles, and with diopside and calcite in coarse-grained marble veins. Insufficient textural evidence is available to constrain the sequence of mineral-forming reactions.

Nepheline is present both with and without coexisting K-feldspar, and in either case inclusions of forsterite, diopside, and phlogopite imply relatively late formation. Vermicular K-feldspar – nepheline intergrowths further imply simultaneous formation of K-feldspar and nepheline, but do not preclude the possibility of separate nepheline and nepheline + K-feldspar-forming reactions. Interpreting the introduction of nepheline is complicated by the absence of a coexisting Na-bearing phase from which a reaction may be inferred. However, if one assumes that albite was initially present (as in adjacent calc-silicates), or alternatively, that appropriate Na and Si concentrations were present as dissolved species in infiltrating fluids, the formation of coexisting K-feldspar and nepheline may be accounted for by the reaction:

$$3\,Ab + 3\,Cal + Phl = Kfs + 3\,Ne + 3\,Di + 3\,CO_2 \qquad (5.4)$$

At 8.0 kbar, and $XCO_2 = 0.5$, reaction 5.4 takes place at ca. 875 °C, well above the estimated regional temperatures. However, the temperature of reaction 5.4 decreases significantly at near end-member values of X_{CO2}, and at $X_{CO2} = 0.15$ is encountered at 800 °C. Thus, a shift in the composition of the fluid-phase to a value below $X_{CO2} = 0.15$ would result in the introduction of K-feldspar and nepheline. For reaction 5.4 to progress as a result of variations in temperature and/or pressure would require isothermal decompression, and is inconsistent with clockwise P-T-t paths estimated for M_1 metamorphism (St-Onge et al., 2006b). The decrease in X_{CO2} necessary to initiate reaction 5.4 would imply a fundamental shift to open-system behavior in which the fluid-composition was controlled by infiltrating fluids. The necessary decrease in X_{CO2}

may have been accomplished by the infiltration of H_2O-rich fluids derived from the monzogranites, or late syenogranite pegmatites.

5.4 Calc-silicates

The calc-silicates comprise the assemblage diopside + pargasite + scapolite + phlogopite + calcite + clinozoisite ± plagioclase ± quartz. Similar assemblages are documented in LHG associated calc-silicates (some sapphire-bearing) from Kimmirut, southern Baffin Island (Dzikowski, 2006; Tait & Hawthorne, 2001; Herd & Peterson, 2000).

Diopside, phlogopite, and quartz represent the earliest phase in the calc-silicates, followed by pargasite, calcite, scapolite, and secondary phlogopite. Scapolite is distributed within late fractures and appears to be replacing pargasite and early diopside. The formation of scapolite after pargasite is consistent with the reaction:

$$3\,Prg + 21\,Qtz + 10\,Cal = 3\,Ab + 12\,Di + Me + CO_2 + 3\,H_2O \qquad (5.5)$$

At 8.0 kbar, and $X_{CO2} = 0.5$, reaction 5.5 takes place at ca. 675 °C (Berman, 1991). The temperature of reaction 5.5 depends on the activity of meionite in scapolite, and if ideality is assumed ($a_{Me} = 0.5$) reaction 5.5 takes place at ca. 600 °C.

Clinozoisite is present only in very minor proportions, and was not observed in contact with plagioclase or scapolite. In general, the presence of clinozoisite at high-temperatures in equilibrium with either of these phases implies a relatively H_2O-rich fluid-phase. For example, at 8.0 kbar and a temperature of ca. 800 °C, clinozoisite is limited to X_{CO2} < ca. 0.05 by the reaction (Berman, 1991):

$$Me + H_2O = 2\,Czo + CO_2 \qquad (5.6)$$

The low values of X_{CO2} implied by reaction 5.6 are consistent with the infiltration of H_2O-rich fluids. Moreover, the meso-scale compositional heterogeneity (alternating diopside and pargasite-dominanted domains) of the calc-silicates implies localized diffusion metasomatism may have played a role in their formation.

5.5 Monzogranites

The mineral assemblages in the monzogranites are typical of quartzofeldspathic rocks at upper-amphibolite- to granulite-facies conditions. However, the absence of orthopyroxene severely limits their utility for quantitatively estimating the *P–T* conditions of their formation. Therefore, only specific points of interest will be discussed.

5.5.1 Clinopyroxene – hornblende – biotite A monzogranites

The *A* monzogranites comprise the assemblage clinopyroxene + hornblende + biotite + K-feldspar + plagioclase + quartz. In metabasites, at high pressures (ca. 8.0 kbar) clinopyroxene and plagioclase are typically introduced at ca. 800 °C by the continuous breakdown of hornblende to clinopyroxene and plagioclase (Spear, 1995). The observed dehydration of biotite to plagioclase and quartz also implies high-temperature, approximately granulite-facies conditions.

5.5.2 Clinopyroxene – titanite ± scapolite ± calcite B monzogranites

The *B* monzogranites comprise the assemblage clinopyroxene + titanite ± scapolite ± calcite + K-feldspar + plagioclase + quartz. The presence of coexisting scapolite and calcite is problematic insofar as neither are typical primary igneous phases in granitoid rocks. Their presence appears to be spatially associated with the adjacent calc-silicates, and corresponds to increasing CaO, and decreasing K_2O and Rb contents relative to the (presumably) unaltered *B* monzogranites. These features imply that scapolite and calcite formed from the metasomatic alteration of the *B* monzogranites by infiltrating CO_2-rich (and Cl-rich) fluids derived from the adjacent metacarbonates. The formation of scapolite in the monzogranites is consistent with the reaction:

$$Cal + 3\,An = 3\,Me \qquad (5.7)$$

At 8.0 kbar, and a given X_{CO2}, reaction 5.7 takes place at ca. 850 °C (Berman, 1991). The temperature of reaction 5.7 depends on the activity of meionite in scapolite, and if ideality is assumed ($a_{Me} = 0.4$) reaction 5.7 takes place at ca. 700 °C. This represents a lower temperature limit for reaction 5.7.

Reaction 5.7 also accounts for the presence of interstitial scapolite in the clinopyroxenite xenoliths. The close spatial association between the clinopyroxenites and the intruded syenogranites implies that the latter may have provided the Cl-rich fluids required to form scapolite.

5.6 Calcite – dolomite thermometry

The activity of $MgCO_3$ (magnesite) in calcite coexisting in equilibrium with dolomite varies systematically with temperature according to the following function (Rice, 1977):

$$\mathrm{Log}_{10}\, X_{MgCO3\,(Cal)} = -\,(\,1690 / T\,(°K)\,) + 0.795$$

An average temperature of ca. 530 ± 40 °C was calculated for the dolomitic marbles. The large discrepancy between the calculated temperatures and those inferred from mineral assemblages is attributed to exsolution of dolomite from calcite during cooling, as observed in some samples. The reintegration of fine-scale dolomite lamellae in calcite to yield pre-exsolution calcite compositions was not attempted because of the high concentration of unidentified sub-micro-scale inclusions in calcite.

5.7 Summary

The mineral assemblages in the impure marbles, calc-silicates, and monzogranites, are consistent with granulite-facies metamorphic conditions of ca. 800 °C and 8.0 kbar for M_{1a} estimated by St-Onge et al. (2006b). The sequential formation of calcite, phlogopite, diopside, and forsterite in the impure marbles may be attributed to increasing temperture. The presence of vermicular K-feldspar and nepheline intergrowths in the silicate-rich impure marbles implies relatively low X_{CO2}, and may be attributed to the infiltration of H_2O and possibly Na-rich fluids.

CHAPTER 6: DISCUSSION

Previous investigations of LHG marbles from southern Baffin Island focused primarily on their association with gemstone-bearing calc-silicates (LeCheminant, 2005; Dzikowski, 2006; Rohtert, 2006). This study represents the first detailed petrological investigation of the LHG marbles from southwestern Baffin Island in a purely metamorphic context.

6.1 Regional deformation and metamorphism

The earliest identified (M_{1a}) mineral assemblages and associated S_1 fabrics in the impure marbles, calc-silicates, and monzogranites, are consistent with granulite-facies metamorphic conditions of ca. 800 °C and 8.0 kbar for M_{1a} estimated by St-Onge et al. (2006b). In general, evidence for subsequent M_2 retrogression is minimal. In the impure marbles and calc-silicates, S_2 comprises a locally developed ca. 1-2 cm spaced, axial planar (to F_2), cleavage defined by < 0.5 mm calcite-filled fractures. In the *A* monzogranites, S_2 locally comprises a weak biotite-defined schistosity and local, centimeter-scale crenulations of S_1. Field relations and textural relationships imply that nepheline and scapolite are late phases. However, their distribution is spatially restricted, and exhibits no correlation with the S_2 fabrics. Therefore, although late-forming, neither nepheline nor scapolite can unequivocally be attributed to M_2 retrogression. As discussed below, scapolite formation may be attributed to Cl-rich fluid infiltration related to post-deformation syenogranite intrusion. Relatively late, localized, greenschist-facies retrogression is indicated by the presence of actinolite and epidote in the quartzofeldspathic metasediments.

6.2 Localized fluid infiltration and metasomatism

To quantify the effects of metasomatic alteration typically requires a degree of observational detail and compositional analysis beyond the scope of this study (Ague, 2003). Nevertheless, certain features described above are best explained by localized

chemical interactions and/or infiltration-driven metasomatic alteration, rather than closed-system, isochemical metamorphism.

6.2.1 K-feldspar and nepheline intergrowths

The presence of vermicular K-feldspar and nepheline intergrowths in the silicate-rich impure marbles implies relatively low X_{CO2}, and may be attributed to the infiltration of H_2O and possibly Na-rich fluids (Ch. 5; Fig. 5.1) originating from the intruded monzogranites or syenogranites, or an as of yet unidentified source.

6.2.2 Scapolite formation

The compositional variations in the *B* monzogranites (increased wt. % CaO, and decreased wt. % K_2O and Rb) corresponding to the presence of scapolite and calcite imply metasomatic alteration, probably involving the loss of mobile elements during the infiltration of CO_2 and possibly Cl-rich fluids. In the calc-silicates and clinopyroxenites, scapolite is either fracture-controlled or interstitial, and is attributed to the late-stage infiltration of Cl-rich fluids possibly derived from the late pegmatitic syenogranites. clinopyroxenites were injected by late

6.3 Implications for regional sapphire exploration

Sapphires are present in calc-silicates within the LHG marbles near Kimmirut in southern Baffin Island. The sapphire-bearing calc-silicates comprise diopside, phlogopite, muscovite, plagioclase, scapolite, nepheline, and corundum (LeCheminant, 2005). Sapphire-bearing calc-silicates typically contain highly altered nepheline and scapolite, and both appear to be prerequisite for sapphire mineralization. Mineral assemblages in the sapphire-bearing calc-silicates are interpreted as retrograde (LeCheminant, 2006), with the formation of scapolite attributed to the infiltration of saline fluids. The subsequent loss of scapolite to plagioclase and phlogopite symplectites may have yielded excess Al, producing corundum (Dzikowski, 2006)

In general, the nepheline and scapolite associations in the metacarbonates in the study area resemble those from Kimmirut. The absence of retrograde plagioclase and

muscovite, and the persistence of pargasite and scapolite, imply that the nepheline + scapolite association described here represents a precursor assemblage, or unaltered equivalent, to the sapphire-bearing calc-silicates from Kimmirut.

CHAPTER 7: CONCLUSIONS

7.1 Conclusions

1. In southwestern Baffin Island, metacarbonates (impure marbles and calc-silicates) comprise ca. 15% of the Paleoproterozoic metasedimentary Lake Harbour Group. In the study area, polydeformed metacarbonates and quartzofeldspathic metasediments of the LHG are intruded by dominant syntectonic (D_1) foliated monzogranites with minor clinopyroxenite xenoliths, and post-deformation pegmatitic syenogranites (Ch. 2).

2. Two phases of monzogranites, the alkaline *A* monzogranites and subalkaline *B* monzogranites, intruded the LHG marbles in the study area (Ch.3). The localized presence of scapolite and calcite in the *B* monzogranites corresponds to increasing wt. % CaO, and decreased wt. % K_2O and Rb (both mobile elements), attributable to metasomatic alteration involving the infiltration of CO_2 and possibly halogen-rich fluids. In general, the compositions and textures of the calc-silicates imply formation involving the intense diffusion metasomatism of an impure marble protolith (Ch. 3).

3. The earliest tectonometamorphic event in the study area is the development of a pervasive compositional foliation and associated granulite-facies mineral assemblages (Ch. 4). The impure marbles comprise two assemblages corresponding to primary variations in bulk composition, including forsterite + spinel + calcite + dolomite, and forsterite + diopside ± pargasite + phlogopite + calcite + nepheline + K-feldspar in the carbonate-rich, and silicate-rich marbles respectively. The *A* monzogranites comprise the assemblage clinopyroxene + hornblende + biotite + K-feldspar + plagioclase + quartz. The *B* monzogranites comprise the assemblage clinopyroxene + titanite ± scapolite ± calcite + K-feldspar + plagioclase + quartz. Evidence of subsequent deformation or metamorphism is poorly defined or absent. Scapolite in the calc-silicates and

clinopyroxenites probably reflects late-stage fluid infiltration possibly related to pegmatite emplacement.

4. The mineral assemblages and textures in the impure marbles primarily reflect prograde M_{1a} metamorphism, at a temperature range consistent with estimated conditions of ca. 800 °C and 8.0 kbar (St-Onge et al., 2006) (Ch. 5). The sequential formation of calcite, phlogopite, diopside, and forsterite in the impure marbles is consistent with the following reactions: *3 Dol + Kfs + H_2O = Phl + 3 Cal + 3 CO_2* (5.1), *Dol + Qtz = Di + 2 CO_2* (5.2), *3 Dol + Di = 4 Cal + 2 Fo + 2 CO_2* (5.3). The presence of late K-feldspar and nepheline is consistent with the reaction
3 Ab + 3 Cal + Phl = Kfs + 3 Ne + 3 Di + 3 CO_2 (5.4), and implies a decrease in X_{CO2}, suggesting the infiltration of H_2O-rich and possibly Na-bearing fluids, which may have originated from the monzogranites or pegmatites. The inferred sequence of reactions is consistent with previous studies of high-grade metacarbonates (Spear, 1995; Yardley, 1995; and references therein).

7.2 Recommendations for further study

Infiltrating fluids probably played an important role in the formation of nepheline and scapolite in the LHG metacarbonates from southwestern Baffin Island. Further studies should focus on constraining the composition and source of these fluids. Fluid-phase compositions may be obtained from further study of mineral assemblages and by fluid-inclusion studies. Further petrographical study and chemical analyses are also required to constrain the role of metasomatic alteration in the formation of the calc-silicates.

REFERENCES

Berman, R.G. 1991. Thermobarometry using multiequilibrium calculations: a new technique with petrologic applications. Canadian Mineralogist, 29: 833-855.

Deer, W.A., Howie, R.A., and J. Zussman. 1996. An introduction to rock-forming minerals. Prentice Hall.

Dzikowski, T.J. 2006. Mineralogy and geochemistry of pyroxene, nepheline, mica, scapolite, and feldspar from the Kimmirut sapphire occurrence, Baffin Island. Student research project. Department of Earth and Ocean Sciences, University of British Columbia, Vancouver, BC.

Faryad, S.W. 2002. Metamorphic conditions and fluid compositions of scapolite-bearing rocks from the lapis lazuli deposit at Sare Sang, Afghanistan. Journal of Petrology, 43: 725-747.

Ferry, J.M. 1983. Mineral reactions and element migration during metamorphism of calcareous sediments from the Vassalboro Formation, south-central Maine. American Mineralogist, 68: 334-354.

Ferry, J.M. 1976. Metamorphism of calcareous sediments in the Waterville-Vassalboro area, south-central Maine: Mineral reactions and graphical analysis. American Journal of Science, 276: 841-882.

Henry, D.J., Guidotti, C.V., and J.A. Thomson. 2005. The Ti-saturation surface for low- to medium-pressure metapelitic biotites: Implications for geothermometry and Ti-substitution mechanisms. American Mineralogist, 90: 316-328.

Herd, C.D.K., and R.C. Peterson. 2000. Violet-colored diopside from southern Baffin Island, Nunavut, Canada. The Canadian Mineralogist, 38: 1193-1199.

Jackson, G. D., Hunt, P. A., Loveridge, W. D., Parrish, R. R., 1990. Reconnaissance geochronology of Baffin Island, N.W.T. Geological Survey of Canada Paper 1989-2: 123-148.

Kullerud, K., and M. Erambert. 1999. Cl-scapolite, Cl-amphibole, and plagioclase equilibria in ductile shear zones at Nusfjord Lofoten, Norway: Implications for fluid compositional evolution during fluid-mineral interaction in the deep crust. Geochimica et Cosmochimica Acta, 22: 3829-3844.

LeCheminant, A.N., Groat, L.A., Mortensen, J.K., Gertzbein, P., Rohtert, W., and G. Giuliani. 2005. Sapphires from Kimmirut, Baffin Island, Nunavut, Canada. Goldschmidt conference 2005 poster.

Letargo, C.M.R., and Lamb, W.M. 1995. Comparison of calcite + dolomite thermometry and carbonate + silicate equilibria: constraints on the conditions of metamorphism of the Llano uplift, central Texas, U.S.A. American Mineralogist, 80: 131-145.

Moecher, D.P., and E.J. Essene. 1991. Calculation of CO_2 activities using scapolite equilibria: constraints on the presence and composition of a fluid phase during high grade metamorphism. Contributions to Mineralogy and Petrology, 108: 219-240.

Mora, C.I., and J.W. Valley. 1989. Halogen-rich scapolite and biotite: Implications for metamorphic fluid-rock interaction. American Mineralogist, 74: 721-737.

Rice, J.M. 1977. Progressive metamorphism of impure dolomitic limestone in the Marysville aureole, Montana. American Journal of Science, 277: 1-24.

Rohtert, W.R. 2006. 2005 Report on field activities for the Beluga Sapphire project, Nunavut Canada. Prepared for True North Gems Inc. Available from: http://www.truenorthgems.com/i/pdf/2006-04-20_BaffinIsland_43-101.pdf

Rosen, O.M., Desmons, J. and D. Fettes. 2004. Towards a unified nomenclature of metamorphism: Metacarbonate and related rocks. A proposal on behalf of the IUGS Subcommission on the Systematics of Metamorphic Rocks. Provisional recommendations. Available from: http://www.bgs.ac.uk/SCMR/docs/scmr_carb_r.pdf

Spear, F.S. 1995. Metamorphic phase equilibria and pressure-temperature-time paths. Mineralogical Society of America Monograph, Washington, DC.

Scott, D. J. 1997. Geology, U – Pb, and Pb – Pb geochronology of the Lake Harbour Area, southern Baffin Island: implications for the Paleoproterozoic tectonic evolution of northeastern Laurentia. Canadian Journal of Earth Sciences, 34: 140-155.

Scott, D. J., and Wodicka, N. 1998. A second report on the U – Pb geochronology of southern Baffin Island, Northwest territories. Geological Survey of Canada Paper 1998-F: 47-57.

Scott, D. J. 1999. U – Pb geochronology of the eastern Hall Peninsula, southern Baffin Island, Canada: a northern link between the Archean of West Greenland and the Paleoproterozoic Torngat Orogen of northern Labrador. Precambrian Research, 93: 5-26.

St-Onge, M.R., M.P. Searle, and N. Wodicka. 2006. Trans-Hudson Orogen of North America and Himalaya-Karakoram-Tibetan Orogen of Asia: Structural and thermal characteristics of the lower and upper plates, Tectonics, 25: doi: 10.1029/2005TC001907

St-Onge, M.R., Wodicka, N., and O. Ijewliw. 2006b. Polymetamorphic evolution of the Trans-Hudson Orogen, Baffin Island, Canada: Integration of petrological, structural, and geochronological Data. Journal of Petrology, 48: 271-302.

St-Onge, M.R., Scott, D.J., and N. Wodicka. 2002. Review of crustal architecture and evolution in the Ungava Peninsula – Baffin island area: connection to the Lithoprobe ECSOOT transect. Canadian Journal of Earth Sciences, 39: 589-610.

St-Onge, M.R., Wodicka, N., and S.B. Lucas. 2000. Granulite- and amphibolite-facies metamorphism in a convergent-plate-margin setting: synthesis of the Quebec-Baffin segment of the Trans-Hudson Orogen. The Canadian Mineralogist, 38: 379-398.

Tait, K.T., and F.C. Hawthorne. 2001. Al-Mg disorder in a gem-quality pargasite from Baffin Island, Nunavut, Canada. The Canadian Mineralogist, 93: 1725-1732.

Tropper, P., Tessadri, R., and J. Konzett. 2003. Spinel-bearing carbonates as petrogenetic recorders of the Variscan P-T evolution of the Austroalpine basement of the Otztal Complex (Tyrol, Austria). Journal of the Czech Geological Society, 48: 1-2.

Winter, J.D. 2001. An introduction to igneous and metamorphic rocks. Prentice Hall. Toronto.

Wodicka, N. and Scott, D. J. 1997. A preliminary report on the U Pb geochronology of the Meta Incognita Peninsula, southern Baffin Island, Northwest Territories. Geological Survey of Canada Paper 1997-C: 167-178.

Yardley, B.W.D. 1995. Introduction to metamorphic petrology. Longman Scientific and Technical. New York.

APPENDIX A: MICROPROBE ANALYSES

Tables A.1 - A.14 present electron microprobe (EMP) analyses for amphibole, calcite, clinozoisite, feldspar, mica, nepheline, olivine, pyroxene, scapolite, spinel, and titanite. A map illustrating sample locations is provided in Appendix C. The analyses were done at the Dalhousie University Regional Electron Microprobe Laboratory using the JEOL JXA-8200 electron microprobe. The operating conditions were as follows: acceleration voltage, 15 kV; spot size, 2μm; beam current, 20 nA.

Tables A.1 – A.14 make use of the following abbreviations:

Lithology	Abbreviation
A monzogranites	A mg
B monzogranites	B mg
Calc-silicates	Cs
Clinopyroxenites	Cpxites
Marbles	Mb
Quartzofeldspathic metasediments	Qfs ms

Table A.1: Amphibole analyses

Sample	B119	B119	B119	B141	B141	B141	B141	B141	B142	B142	B142	B142
Lithology	A mzg	A mzg	A mzg	Cs	Cs	Cs	Cs	Cs	Cs	Cs	Cs	Cs
No.	233	234	235	267	271	273	274	283	341	342	352	348
Mineral	Hb	Hb	Hb	Prg	Prg	Prg	Prg	Prg	Prg	Prg	Prg	Prg
Wt. %												
SiO_2	44.42	43.62	44.32	42.73	43.74	43.45	43.30	44.06	43.09	43.68	41.73	43.64
TiO_2	1.80	1.76	2.05	0.63	0.56	0.55	0.62	0.75	0.69	0.73	0.54	0.74
Al_2O_3	9.63	9.61	9.68	15.78	15.17	16.15	16.17	15.02	14.63	14.93	15.65	14.76
FeO	13.55	14.28	13.22	2.99	2.62	2.60	2.41	2.64	2.98	2.85	2.71	3.78
MgO	13.49	13.16	13.69	18.00	18.62	18.49	18.42	18.80	18.35	18.37	18.33	17.99
MnO	0.27	0.25	0.26	0.05	0.04	0.04	0.04	0.03	0.00	0.02	0.03	0.01
CaO	11.66	11.52	11.79	13.11	13.23	13.25	13.34	13.23	13.05	13.21	13.22	13.14
Na_2O	1.89	1.89	1.79	2.88	2.62	2.70	2.73	2.68	2.49	2.45	2.60	2.28
K_2O	1.45	1.47	1.40	1.50	1.36	1.37	1.28	1.39	1.49	1.52	1.39	1.39
SO_3	0.07	0.06	0.03	0.05	0.01	0.01	0.02	0.00	0.00	0.00	0.00	0.00
F	1.02	1.09	1.11	2.11	2.09	2.13	2.27	2.16	1.98	2.15	2.25	1.90
O=F	-0.43	-0.46	-0.47	-0.89	-0.88	-0.90	-0.95	-0.91	-0.83	-0.91	-0.95	-0.80
Cl	0.43	0.40	0.39	0.26	0.10	0.10	0.09	0.08	0.08	0.09	0.07	0.26
O=Cl	-0.10	-0.09	-0.09	-0.06	-0.02	-0.02	-0.02	-0.02	-0.02	-0.02	-0.01	-0.06
Total	99.24	98.60	99.25	99.28	99.36	99.98	99.83	99.95	98.07	99.13	97.64	99.11
Cations (calculated on the basis of 23 O)												
Si	6.48	6.43	6.45	5.96	6.07	5.99	5.97	6.07	6.07	6.08	5.91	6.09
Ti	0.20	0.19	0.22	0.07	0.06	0.06	0.06	0.08	0.07	0.08	0.06	0.08
Al	1.65	1.67	1.66	2.59	2.48	2.62	2.63	2.44	2.43	2.45	2.61	2.43
Fe	1.65	1.76	1.61	0.35	0.30	0.30	0.28	0.30	0.35	0.33	0.32	0.44
Mn	0.03	0.03	0.03	0.01	0.00	0.00	0.00	0.00	0.00	0.00	0.00	0.00
Mg	2.93	2.89	2.97	3.74	3.85	3.80	3.79	3.86	3.86	3.81	3.87	3.74
Ca	1.82	1.82	1.84	1.96	1.97	1.96	1.97	1.95	1.97	1.97	2.01	1.97
Na	0.44	0.45	0.42	0.65	0.59	0.60	0.61	0.59	0.56	0.55	0.59	0.51
K	0.27	0.28	0.26	0.27	0.24	0.24	0.23	0.24	0.27	0.27	0.25	0.25
S	0.01	0.01	0.00	0.01	0.00	0.00	0.00	0.00	0.00	0.00	0.00	0.00
F	0.47	0.51	0.51	0.93	0.92	0.93	0.99	0.94	0.88	0.95	1.01	0.84
Cl	0.11	0.10	0.10	0.06	0.02	0.02	0.02	0.02	0.02	0.02	0.02	0.06
Total	16.07	16.14	16.08	16.59	16.50	16.52	16.55	16.52	16.50	16.50	16.65	16.41

Table A.1 Amphibole analyses (continued)

Sample	B103	B103	B103
Lithology	Qfs ms	Qfs ms	Qfs ms
No.	327	328	331
Mineral	Wn	Wn	Wn
Wt. %			
SiO_2	55.88	55.91	56.43
TiO_2	1.60	1.54	1.26
Al_2O_3	1.38	1.26	1.15
FeO	3.83	3.79	3.59
MgO	22.13	21.81	21.75
MnO	0.01	0.02	0.02
CaO	9.46	9.57	10.35
Na_2O	2.62	2.36	1.73
K_2O	0.55	0.54	0.48
SO_3	0.03	0.01	0.00
F	0.85	0.98	0.69
O=F	-0.36	-0.41	-0.29
Cl	0.05	0.06	0.05
O=Cl	-0.01	-0.01	-0.01
Total	98.07	97.52	97.24
Cations (calculated on the basis of 23 O)			
Si	7.70	7.73	7.81
Ti	0.17	0.16	0.13
Al	0.22	0.21	0.19
Fe	0.44	0.44	0.41
Mn	0.00	0.00	0.00
Mg	4.54	4.50	4.49
Ca	1.40	1.42	1.53
Na	0.58	0.52	0.38
K	0.10	0.09	0.09
S	0.00	0.00	0.00
F	0.37	0.43	0.30
Cl	0.01	0.01	0.01
Total	15.54	15.52	15.35

Table A.2 Amphibole analyses (no Cl, F)

Sample	B117A	B117A	B117A	B117A	B117A	B117A
Lithology	Qfs ms	Qfs ms	Qfs ms	Qfs ms	Qfs ms	Qfs ms
No.	67	68	70	71	74	77
Mineral	Wn	Act	Wn	Wn	Wn	Wn
Wt. %						
SiO_2	56.19	57.49	56.45	56.45	57.11	56.09
TiO_2	2.33	0.09	2.41	2.47	0.67	2.51
Al_2O_3	0.78	0.03	0.77	0.75	0.35	0.82
FeO	3.31	4.98	3.11	3.28	3.14	3.46
MgO	21.36	21.35	21.27	21.29	22.15	21.07
MnO	0.00	0.02	0.00	0.01	0.01	0.00
CaO	8.06	13.36	8.28	7.93	9.73	8.34
Na_2O	4.83	0.17	4.54	4.67	3.38	4.48
K_2O	0.90	0.05	1.01	0.90	0.90	1.00
Total	97.76	97.54	97.86	97.76	97.44	97.75
Cations (calculated on the basis of 23 O)						
Si	7.83	7.98	7.85	7.86	7.95	7.82
Ti	0.24	0.01	0.25	0.26	0.07	0.26
Al	0.13	0.01	0.13	0.12	0.06	0.13
Fe	0.39	0.58	0.36	0.38	0.37	0.40
Mg	4.44	4.42	4.41	4.42	4.60	4.38
Mn	0.00	0.00	0.00	0.00	0.00	0.00
Ca	1.20	1.99	1.23	1.18	1.45	1.25
Na	1.08	0.04	1.02	1.05	0.76	1.00
K	0.16	0.01	0.18	0.16	0.16	0.18
Total	15.48	15.03	15.43	15.43	15.41	15.44

Table A.3: Calcite analyses

Sample	B102A	B102A	B102A	B102A	B102A	B102A	B104	B104	B104	B104	B104	B104
Lithology	Mb	Mb	Mb	Mb	Mb	Mb	Mb	Mb	Mb	Mb	Mb	Mb
No.	153	155	160	164	165	168	35	37	41	45	48	49
Mineral	Cal	Cal	Cal	Cal	Cal	Cal	Cal	Cal	Cal	Cal	Cal	Cal
Wt. %												
SiO_2	0.00	0.00	0.00	0.00	0.00	0.00	0.00	0.24	0.00	0.00	0.25	0.19
TiO_2	0.00	0.00	0.00	0.00	0.00	0.00	0.00	0.00	0.00	0.00	0.00	0.00
Al_2O_3	0.00	0.00	0.00	0.00	0.00	0.00	0.00	0.00	0.00	0.00	0.00	0.00
Cr_2O_3	0.00	0.00	0.01	0.00	0.00	0.00	0.00	0.00	0.00	0.00	0.05	0.02
FeO	0.20	0.12	0.26	0.22	0.17	0.18	0.24	0.20	0.19	0.26	0.13	0.19
MnO	0.04	0.04	0.04	0.04	0.07	0.02	0.09	0.07	0.10	0.07	0.04	0.06
MgO	1.81	2.57	3.42	1.80	2.18	2.36	1.90	2.29	2.23	2.25	0.30	0.25
CaO	47.68	53.79	56.44	57.76	52.91	55.01	60.70	56.88	57.96	59.52	51.73	50.42
Na_2O	0.00	0.00	0.00	0.00	0.00	0.00	0.00	0.00	0.00	0.00	1.04	1.29
K_2O	0.17	0.02	0.04	0.05	0.02	0.05	0.02	0.04	0.02	0.03	0.04	0.03
Total	49.89	56.55	60.21	59.86	55.35	57.62	62.94	59.72	60.50	62.14	53.59	52.46
Cations (calculated on the basis of 1 O)												
Si	0.00	0.00	0.00	0.00	0.00	0.00	0.00	0.00	0.00	0.00	0.00	0.00
Ti	0.00	0.00	0.00	0.00	0.00	0.00	0.00	0.00	0.00	0.00	0.00	0.00
Al	0.00	0.00	0.00	0.00	0.00	0.00	0.00	0.00	0.00	0.00	0.00	0.00
Cr	0.00	0.00	0.00	0.00	0.00	0.00	0.00	0.00	0.00	0.00	0.00	0.00
Fe	0.00	0.00	0.00	0.00	0.00	0.00	0.00	0.00	0.00	0.00	0.00	0.00
Mn	0.00	0.00	0.00	0.00	0.00	0.00	0.00	0.00	0.00	0.00	0.00	0.00
Mg	0.05	0.06	0.08	0.04	0.05	0.06	0.04	0.05	0.05	0.05	0.01	0.01
Ca	0.94	0.94	0.92	0.95	0.94	0.94	0.95	0.94	0.95	0.95	0.96	0.96
Na	0.00	0.00	0.00	0.00	0.00	0.00	0.00	0.00	0.00	0.00	0.03	0.04
K	0.00	0.00	0.00	0.00	0.00	0.00	0.00	0.00	0.00	0.00	0.00	0.00
Total	1.00	1.00	1.00	1.00	1.00	1.00	1.00	1.00	1.00	1.00	1.01	1.02
Mol. % end-members												
$CaCO_3$	94.68	93.61	91.92	95.57	94.35	94.13	95.55	94.44	94.69	94.68	98.99	99.01
$MgCO_3$	5.01	6.22	7.75	4.15	5.41	5.63	4.16	5.30	5.06	4.99	0.81	0.70

Table A.3: Calcite analyses (continued)

Sample	B116A	B116A	B116A	B116A	B116A	B116A	B116A	B116A	B117A	B117A	B117A	B117A
Lithology	Mb	Mb	Mb	Mb	Mb	Mb	Mb	Mb	Qfs ms	Qfs ms	Qfs ms	Qfs ms
No.	96	97	103	109	114	119	124	125	69	73	76	78
Mineral	Cal	Cal	Cal	Cal	Cal	Cal	cal	cal	cal	cal	cal	cal
Wt. %												
SiO_2	0.00	0.00	0.00	0.00	0.00	0.00	0.00	0.00	0.00	0.00	0.17	0.00
TiO_2	0.00	0.00	0.00	0.00	0.00	0.00	0.00	0.00	0.00	0.00	0.04	0.00
Al_2O_3	0.00	0.00	0.00	0.00	0.00	0.00	0.00	0.00	0.00	0.00	0.01	0.00
Cr_2O_3	0.00	0.00	0.00	0.00	0.01	0.00	0.01	0.00	0.00	0.00	0.11	0.00
FeO	0.15	0.24	0.19	0.14	0.23	0.23	0.22	0.31	0.26	0.28	0.10	0.27
MnO	0.07	0.09	0.08	0.09	0.08	0.06	0.10	0.10	0.06	0.03	0.05	0.06
MgO	0.79	2.65	2.86	2.42	2.68	1.87	2.73	2.18	0.43	0.33	0.08	0.50
CaO	52.63	57.56	58.29	56.54	57.34	59.63	60.00	56.28	57.96	57.94	51.84	61.36
Na_2O	0.00	0.00	0.00	0.00	0.00	0.00	0.00	0.00	0.00	0.00	0.51	0.00
K_2O	0.01	0.01	0.03	0.01	0.02	0.01	0.02	0.01	0.02	0.03	0.04	0.02
Total	53.65	60.55	61.45	59.20	60.35	61.81	63.09	58.87	58.74	58.60	52.94	62.20
Cations (calculated on the basis of 1 O)												
Si	0.00	0.00	0.00	0.00	0.00	0.00	0.00	0.00	0.00	0.00	0.00	0.00
Ti	0.00	0.00	0.00	0.00	0.00	0.00	0.00	0.00	0.00	0.00	0.00	0.00
Al	0.00	0.00	0.00	0.00	0.00	0.00	0.00	0.00	0.00	0.00	0.00	0.00
Cr	0.00	0.00	0.00	0.00	0.00	0.00	0.00	0.00	0.00	0.00	0.00	0.00
Fe	0.00	0.00	0.00	0.00	0.00	0.00	0.00	0.00	0.00	0.00	0.00	0.00
Mn	0.00	0.00	0.00	0.00	0.00	0.00	0.00	0.00	0.00	0.00	0.00	0.00
Mg	0.02	0.06	0.06	0.06	0.06	0.04	0.06	0.05	0.01	0.01	0.00	0.01
Ca	0.98	0.94	0.93	0.94	0.94	0.95	0.94	0.94	0.99	0.99	0.98	0.98
Na	0.00	0.00	0.00	0.00	0.00	0.00	0.00	0.00	0.00	0.00	0.01	0.00
K	0.00	0.00	0.00	0.00	0.00	0.00	0.00	0.00	0.00	0.00	0.00	0.00
Total	1.00	1.00	1.00	1.00	1.00	1.00	1.00	1.00	1.00	1.00	1.00	1.00
Mol. % end-members												
$CaCO_3$	97.74	93.70	93.39	94.21	93.62	95.55	93.78	94.51	98.62	98.84	99.64	98.54
$MgCO_3$	2.04	5.99	6.37	5.60	6.08	4.17	5.94	5.09	1.03	0.79	0.21	1.11

Table A.3: Calcite analyses (continued)

Sample	B117A	B133	B133	B133	B133	B133	B133	B137	B137	B137	B141	B141
Lithology	Qfs ms	Mb	Mb	Mb	Mb	Mb	Mb	B mg	B mg	B mg	Cs	Cs
No.	79	11	12	13	18	22	23	132	138	140	171	81
Mineral	cal	cal	cal	cal	cal	cal	cal	cal	cal	cal	cal	cal
Wt. %												
SiO_2	0.00	0.00	0.00	0.00	0.00	0.00	0.00	0.00	0.00	0.00	0.00	0.00
TiO_2	0.00	0.00	0.00	0.00	0.00	0.00	0.00	0.00	0.00	0.00	0.00	0.01
Al_2O_3	0.00	0.00	0.00	0.00	0.00	0.00	0.00	0.00	0.00	0.00	0.00	0.00
Cr_2O_3	0.00	0.00	0.00	0.00	0.00	0.00	0.00	0.00	0.00	0.00	0.00	0.01
FeO	0.29	0.29	0.09	0.31	0.11	0.23	0.26	0.12	0.14	0.28	0.15	0.17
MnO	0.05	0.12	0.12	0.13	0.11	0.11	0.14	0.02	0.03	0.02	0.04	0.07
MgO	0.41	2.64	2.01	2.90	1.44	2.67	2.33	0.00	0.00	0.00	0.58	0.35
CaO	61.87	58.63	61.58	59.49	60.53	58.28	58.97	60.03	60.88	61.94	51.45	58.01
Na_2O	0.00	0.00	0.00	0.00	0.00	0.00	0.00	0.00	0.00	0.00	0.00	0.00
K_2O	0.02	0.03	0.03	0.03	0.02	0.03	0.02	0.02	0.02	0.02	0.02	0.04
Total	62.63	61.70	63.82	62.86	62.21	61.32	61.72	60.19	61.07	62.26	52.25	58.70
Cations (calculated on the basis of 1 O)												
Si	0.00	0.00	0.00	0.00	0.00	0.00	0.00	0.00	0.00	0.00	0.00	0.00
Ti	0.00	0.00	0.00	0.00	0.00	0.00	0.00	0.00	0.00	0.00	0.00	0.00
Al	0.00	0.00	0.00	0.00	0.00	0.00	0.00	0.00	0.00	0.00	0.00	0.00
Cr	0.00	0.00	0.00	0.00	0.00	0.00	0.00	0.00	0.00	0.00	0.00	0.00
Fe	0.00	0.00	0.00	0.00	0.00	0.00	0.00	0.00	0.00	0.00	0.00	0.00
Mn	0.00	0.00	0.00	0.00	0.00	0.00	0.00	0.00	0.00	0.00	0.00	0.00
Mg	0.01	0.06	0.04	0.06	0.03	0.06	0.05	0.00	0.00	0.00	0.02	0.01
Ca	0.99	0.94	0.95	0.93	0.97	0.94	0.94	1.00	1.00	1.00	0.98	0.99
Na	0.00	0.00	0.00	0.00	0.00	0.00	0.00	0.00	0.00	0.00	0.00	0.00
K	0.00	0.00	0.00	0.00	0.00	0.00	0.00	0.00	0.00	0.00	0.00	0.00
Total	1.00	1.00	1.00	1.00	1.00	1.00	1.00	1.00	1.00	1.00	1.00	1.00
Mol. % end-members												
$CaCO_3$	98.74	93.77	95.55	93.29	96.66	93.73	94.47	99.85	99.82	99.65	98.24	98.94
$MgCO_3$	0.90	5.88	4.34	6.33	3.20	5.97	5.20	0.00	0.00	0.00	1.54	0.83

Table A.3: Calcite analyses (continued)

Sample	B141	BB06	B115	B137	B102B	B102B	B142	B142	B142	B142	B142	B142
Lithology	Cs	B mg	Cpxite	B mg	Cs	Cs	Cs	Cs	Cs	Cs	Cs	Cs
No.	279	205	312	320	384	394	344	365	366	367	368	372
Mineral	cal	cal	cal	cal	cal	cal	cal	cal	cal	cal	cal	cal
Wt. %												
SiO_2	0.00	0.00	0.02	0.00	0.00	0.00	0.00	0.00	0.00	0.00	0.00	0.00
TiO_2	0.00	0.00	0.00	0.00	0.00	0.00	0.00	0.00	0.00	0.00	0.00	0.00
Al_2O_3	0.00	0.00	0.00	0.00	0.00	0.00	0.00	0.00	0.00	0.00	0.00	0.00
Cr_2O_3	0.03	0.00	0.04	0.02	0.00	0.00	0.00	0.00	0.00	0.00	0.00	0.00
FeO	0.02	0.03	0.31	0.15	0.19	0.15	0.01	0.03	0.03	0.17	0.11	0.01
MnO	0.02	0.90	0.08	0.02	0.04	0.06	0.04	0.04	0.02	0.04	0.04	0.00
MgO	0.19	0.00	0.07	0.00	1.83	1.72	0.22	0.00	0.02	0.67	0.49	0.00
CaO	59.93	55.60	53.98	56.88	58.16	58.89	59.89	62.50	59.68	63.12	59.93	60.59
Na_2O	0.00	0.00	0.00	0.00	0.00	0.00	0.00	0.00	0.00	0.00	0.00	0.00
K_2O	0.02	0.03	0.03	0.03	0.03	0.03	0.02	0.02	0.01	0.01	0.02	0.02
Total	60.23	56.95	54.58	57.14	60.29	60.86	60.19	62.59	59.76	64.02	60.61	60.62
Cations (calculated on the basis of 1 O)												
Si	0.00	0.00	0.00	0.00	0.00	0.00	0.00	0.00	0.00	0.00	0.00	0.00
Ti	0.00	0.00	0.00	0.00	0.00	0.00	0.00	0.00	0.00	0.00	0.00	0.00
Al	0.00	0.00	0.00	0.00	0.00	0.00	0.00	0.00	0.00	0.00	0.00	0.00
Cr	0.00	0.00	0.00	0.00	0.00	0.00	0.00	0.00	0.00	0.00	0.00	0.00
Fe	0.00	0.00	0.00	0.00	0.00	0.00	0.00	0.00	0.00	0.00	0.00	0.00
Mn	0.00	0.01	0.00	0.00	0.00	0.00	0.00	0.00	0.00	0.00	0.00	0.00
Mg	0.00	0.00	0.00	0.00	0.04	0.04	0.01	0.00	0.00	0.01	0.01	0.00
Ca	0.99	0.99	0.99	1.00	0.95	0.96	0.99	1.00	1.00	0.98	0.99	1.00
Na	0.00	0.00	0.00	0.00	0.00	0.00	0.00	0.00	0.00	0.00	0.00	0.00
K	0.00	0.00	0.00	0.00	0.00	0.00	0.00	0.00	0.00	0.00	0.00	0.00
Total	1.00	1.00	1.00	1.00	1.00	1.00	1.00	1.00	1.00	1.00	1.00	1.00
Mol. % end-members												
$CaCO_3$	99.55	99.95	99.39	99.79	95.57	95.91	99.47	99.96	99.92	98.34	98.72	99.99
$MgCO_3$	0.43	0.00	0.17	0.00	4.19	3.90	0.52	0.00	0.04	1.45	1.13	0.00

Table A.3: Calcite analyses (continued)

Sample	B133	B133	B133	B133	B133
Lithology	Mb	Mb	Mb	Mb	Mb
No.	14	15	16	17	24
Mineral	dol	dol	dol	dol	dol
Wt. %					
SiO_2	0.00	0.00	0.00	0.00	0.00
TiO_2	0.00	0.00	0.00	0.00	0.00
Al_2O_3	0.00	0.00	0.00	0.00	0.00
Cr_2O_3	0.00	0.00	0.00	0.00	0.00
FeO	0.95	0.99	0.81	0.40	1.02
MnO	0.12	0.11	0.11	0.12	0.13
MgO	22.16	22.79	22.67	22.65	22.34
CaO	33.66	34.41	33.41	33.60	34.53
Na_2O	0.00	0.00	0.00	0.00	0.00
K_2O	0.02	0.02	0.02	0.01	0.03
Total	56.91	58.31	57.02	56.79	58.05
Cations (calculated on the basis of 1 O)					
Si	0.00	0.00	0.00	0.00	0.00
Ti	0.00	0.00	0.00	0.00	0.00
Al	0.00	0.00	0.00	0.00	0.00
Cr	0.00	0.00	0.00	0.00	0.00
Fe	0.01	0.01	0.01	0.00	0.01
Mn	0.00	0.00	0.00	0.00	0.00
Mg	0.47	0.47	0.48	0.48	0.47
Ca	0.52	0.51	0.51	0.51	0.52
Na	0.00	0.00	0.00	0.00	0.00
K	0.00	0.00	0.00	0.00	0.00
Total	1.00	1.00	1.00	1.00	1.00
Mol. % end-members					
$CaCO_3$	51.60	51.44	50.95	51.35	51.99
$MgCO_3$	47.27	47.41	48.09	48.17	46.81

Table A.4: Clinozoisite analyses

Sample	B142	B142	B142
Lithology	calc-silicate	calc-silicate	calc-silicate
No.	345	346	400
Mineral	Czo	Czo	Czo
Wt. %			
SiO_2	38.08	39.27	39.76
Al_2O_3	31.24	30.48	31.69
FeO	1.84	2.46	2.54
MgO	0.16	0.50	0.04
CaO	24.39	24.20	25.17
Total	95.68	97.52	99.11
Cations (calculated on the basis of O)			
Si	3.10	3.17	3.14
Al	2.99	2.90	2.95
Fe	0.13	0.17	0.17
Mg	0.01	0.00	0.00
Ca	2.13	2.09	2.13
Total	8.37	8.37	8.39

Table A.5: Feldspar analyses

Sample	B103	B103	B103	B103	B117	B117	B117	B119	B119	B119	B119	B119
Lithology	Qfs ms	Qfs ms	Qfs ms	Qfs ms	Qfs ms	Qfs ms	Qfs ms	A mg	A mg	A mg	A mg	A mg
No.	329	330	333	334	75	82	80	225	236	237	227	228
Mineral	Pl	Pl	Kfs	Kfs	Pl	Pl	Kfs	Pl	Pl	Pl	Kfs	Kfs
Wt. %												
SiO_2	69.49	67.82	65.71	65.61	69.43	68.93	64.54	61.64	62.39	62.07	65.06	67.56
Al_2O_3	19.64	19.78	18.50	18.68	20.01	19.94	18.92	21.88	24.64	24.97	16.71	19.21
CaO	0.02	0.03	0.04	0.02	0.00	0.00	0.04	5.73	5.50	5.84	0.13	0.09
Na_2O	8.62	8.89	0.44	0.47	12.02	11.83	0.16	7.25	7.26	7.72	1.53	0.98
K2O	0.12	0.11	13.37	13.63	0.10	0.05	16.49	0.13	0.13	0.16	10.80	12.34
Total	97.92	96.66	98.09	98.40	101.56	100.75	100.16	96.63	99.94	100.77	94.23	100.20
Cations (calculated on the basis of 8 O)												
Si	3.08	3.05	3.04	3.03	3.02	3.02	2.98	2.83	2.77	2.75	3.10	3.04
Al	1.02	1.05	1.01	1.02	1.03	1.03	1.03	1.19	1.29	1.30	0.94	1.02
Ca	0.00	0.00	0.00	0.00	0.00	0.00	0.00	0.28	0.26	0.28	0.01	0.00
Na	0.61	0.64	0.03	0.03	0.84	0.83	0.01	0.54	0.52	0.55	0.12	0.07
K	0.01	0.01	0.79	0.80	0.01	0.00	0.97	0.01	0.01	0.01	0.66	0.71
Total	4.72	4.75	4.87	4.88	4.89	4.88	5.00	4.85	4.85	4.88	4.82	4.84
Mol. % end-members												
Or^{I}	1.11	0.96	95.83	95.73	0.64	0.36	98.55	0.94	0.94	1.11	84.12	90.41
Ab^{II}	98.72	98.83	3.95	4.17	99.36	99.64	1.23	64.91	65.84	65.74	15.02	9.05
An^{III}	0.17	0.21	0.21	0.09	0.00	0.00	0.21	34.16	33.22	33.15	0.85	0.53

$^{I}Or = 100K/(K+Na)$
$^{II}Ab = 100Na/(Na+Ca)$
$^{III}An = 100Ca/(Ca+Na)$

Table A.5: Feldspar analyses (continued)

Sample	B119	B119	B121	B121	B121	B121	B137	B137	B137	B137	B137	B137
Lithology	A mg	A mg	B mg	B mg	B mg	B mg	B mg	B mg	B mg	B mg	B mg	B mg
No.	238	239	252	253	250	251	130	131	133	142	144	134
Mineral	Kfs	Kfs	Pl	Pl	Kfs	Kfs	Pl	Pl	Pl	Pl	Pl	Kfs
Wt. %												
SiO_2	66.96	64.60	67.44	66.34	64.10	63.93	65.52	60.85	65.79	63.21	64.63	65.05
Al_2O_3	19.32	18.45	19.48	20.19	18.48	18.35	23.09	22.88	23.00	23.27	23.17	19.05
CaO	0.18	0.08	0.29	1.24	0.02	0.02	3.32	3.20	3.23	3.42	3.21	0.02
Na_2O	2.16	1.79	7.96	7.87	0.42	0.35	10.14	10.16	10.20	10.09	10.15	0.67
K_2O	11.12	12.75	0.08	0.10	15.73	15.57	0.14	0.27	0.26	0.19	0.21	12.79
Total	99.77	97.73	95.24	95.76	98.82	98.27	102.22	97.36	102.49	100.18	101.37	97.59
Cations (calculated on the basis of 8 O)												
Si	3.02	3.01	3.06	3.01	2.99	3.00	2.85	2.80	2.86	2.82	2.84	3.02
Al	1.03	1.01	1.04	1.08	1.02	1.01	1.19	1.24	1.18	1.22	1.20	1.04
Ca	0.01	0.00	0.01	0.06	0.00	0.00	0.16	0.16	0.15	0.16	0.15	0.00
Na	0.16	0.13	0.58	0.58	0.03	0.03	0.71	0.75	0.71	0.72	0.72	0.05
K	0.64	0.76	0.00	0.01	0.94	0.93	0.01	0.02	0.01	0.01	0.01	0.76
Total	4.86	4.93	4.71	4.74	4.98	4.97	4.91	4.96	4.92	4.94	4.92	4.87
Mol. % end-members												
Or^{I}	79.44	84.56	0.72	0.90	96.65	97.19	0.91	1.72	1.65	1.22	1.36	93.70
Ab^{II}	19.46	14.97	96.95	89.67	3.25	2.73	81.34	81.26	81.21	80.60	81.49	6.20
An^{III}	1.09	0.47	2.32	9.43	0.10	0.08	17.75	17.02	17.14	18.18	17.15	0.10

$^{I}Or = 100K/(K+Na)$
$^{II}Ab = 100Na/(Na+Ca)$
$^{III}An = 100Ca/(Ca+Na)$

Table A.5: Feldspar analyses (continued)

Sample	B159	B159	B159	B159	B159	B159	B159	B159	B159	BB06	BB06	BB06
Lithology	B mg	B mg	B mg	B mg	B mg	B mg	B mg	B mg	B mg	B mg	B mg	B mg
No.	55	60	61	62	64	65	56	63	66	193	194	195
196	Pl	Pl	Pl	Pl	Pl	Pl	Kfs	Kfs	Kfs	Kfs	Kfs	Pl
Wt. %												
SiO_2	69.18	65.24	65.19	68.73	68.92	65.64	64.50	64.87	65.11	64.64	63.96	67.43
Al_2O_3	20.21	22.64	22.50	20.12	20.44	22.51	18.74	19.00	19.06	19.09	19.25	21.06
CaO	0.14	2.84	2.90	0.19	0.45	2.62	0.02	0.01	0.00	0.00	0.00	1.11
Na_2O	11.91	10.19	10.09	11.79	11.36	10.42	0.68	0.63	0.39	0.37	0.41	11.20
K_2O	0.08	0.11	0.18	0.08	0.09	0.09	15.58	15.66	15.99	15.64	15.53	0.08
Total	101.52	101.03	100.86	100.91	101.26	101.28	99.52	100.18	100.55	99.81	99.26	100.89
Cations (calculated on the basis of 8 O)												
Si	3.01	2.87	2.87	3.01	3.00	2.88	2.99	2.99	2.99	2.98	2.97	2.96
Al	1.04	1.17	1.17	1.04	1.05	1.16	1.02	1.03	1.03	1.04	1.05	1.09
Ca	0.01	0.13	0.14	0.01	0.02	0.12	0.00	0.00	0.00	0.00	0.00	0.05
Na	0.83	0.72	0.72	0.83	0.80	0.74	0.05	0.05	0.03	0.03	0.03	0.79
K	0.00	0.01	0.01	0.00	0.01	0.01	0.92	0.92	0.94	0.92	0.92	0.00
Total	4.89	4.91	4.90	4.89	4.87	4.91	4.99	4.98	4.98	4.97	4.98	4.89
Mol. % end-members												
Or^{I}	0.50	0.74	1.15	0.51	0.63	0.59	94.66	95.11	96.98	97.07	96.75	0.55
Ab^{II}	98.74	83.70	82.99	98.45	96.83	85.16	5.25	4.84	3.02	2.93	3.25	93.28
An^{III}	0.76	15.55	15.86	1.04	2.54	14.25	0.09	0.05	0.00	0.00	0.00	6.17

$^{I}Or = 100K/(K+Na)$
$^{II}Ab = 100Na/(Na+Ca)$
$^{III}An = 100Ca/(Ca+Na)$

Table A.5: Feldspar analyses (Continued)

Sample	BB06	BB06	BB06	BB06	BB06	BB06	BB06	BB06	BB06	BB06	BB06	BB06
Lithology	B mg	B mg	B mg	B mg	B mg	B mg	B mg	B mg	B mg	B mg	B mg	B mg
No.	196	204	217	220	221	222	208	209	210	211	212	213
Mineral	Pl	Pl	Pl	Kfs	Kfs	Kfs	Kfs	Kfs	Kfs	Pl	Kfs	Pl
Wt. %												
SiO_2	67.85	66.90	67.98	66.42	67.14	66.40	66.21	67.47	64.75	66.85	64.01	67.06
Al_2O_3	20.68	21.17	18.33	16.44	17.37	17.68	18.91	19.64	18.78	19.84	18.61	19.34
CaO	0.66	1.20	0.54	0.21	0.16	0.20	0.10	0.04	0.00	0.51	0.00	0.00
Na_2O	11.43	10.96	10.98	3.38	3.30	3.42	2.30	7.54	1.74	10.15	0.28	8.54
K_2O	0.09	0.13	0.11	6.80	7.41	7.23	11.84	5.46	13.31	0.04	15.75	3.41
Total	100.71	100.37	97.95	93.25	95.41	94.96	99.42	100.15	98.64	97.39	98.69	98.36
Cations (calculated on the basis of 8 O)												
Si	2.98	2.95	3.06	3.14	3.11	3.09	3.02	3.01	3.00	3.01	2.99	3.02
Al	1.07	1.10	0.97	0.92	0.95	0.97	1.02	1.03	1.03	1.05	1.02	1.03
Ca	0.03	0.06	0.03	0.01	0.01	0.01	0.00	0.00	0.00	0.02	0.00	0.00
Na	0.81	0.78	0.79	0.26	0.25	0.26	0.17	0.54	0.13	0.74	0.02	0.62
K	0.01	0.01	0.01	0.41	0.44	0.43	0.69	0.31	0.79	0.00	0.94	0.20
Total	4.89	4.89	4.86	4.73	4.75	4.76	4.90	4.90	4.94	4.83	4.98	4.87
Mol. % end-members												
Or^{I}	0.61	0.88	0.79	60.50	63.31	61.69	79.85	36.40	85.82	0.30	97.78	24.02
Ab^{II}	95.73	92.38	96.06	37.92	35.58	36.86	19.61	63.36	14.17	96.49	2.22	75.95
An^{III}	3.66	6.74	3.15	1.58	1.12	1.44	0.54	0.24	0.01	3.21	0.00	0.02

$^{I}Or = 100K/(K+Na)$
$^{II}Ab = 100Na/(Na+Ca)$
$^{III}An = 100Ca/(Ca+Na)$

Table A.5: Feldspar analyses (Continued)

Sample	B102A	B102A	B102A	B102A	B102A	B102B	B102B	B115	B115	B115	B115
Lithology	Mb	Mb	Mb	Mb	Mb	Mb	Mb	Cpxite	Cpxite	Cpxite	Cpxite
No.	148	149	243	247	393	399	309	295	295	310	296
Mineral	Kfs	Kfs	Kfs	Kfs	Kfs	Kfs	Kfs	Kfs	Pl	Pl	Pl
Wt. %											
SiO_2	63.40	62.31	62.99	63.39	62.81	58.07	62.51	65.64	66.89	67.67	67.20
Al_2O_3	19.37	19.30	19.41	19.43	19.55	18.64	19.30	18.68	21.08	20.75	21.12
CaO	0.00	0.00	0.04	0.13	0.03	0.09	0.09	0.04	1.68	1.27	1.64
Na2O	0.04	0.04	0.12	0.15	0.26	0.05	0.04	0.47	7.87	9.75	9.38
K2O	16.11	15.52	14.70	14.97	14.87	14.80	15.38	12.64	0.15	0.08	0.10
Total	99.08	97.31	97.49	98.32	97.77	93.87	99.13	97.51	97.68	99.53	99.44
Cations (calculated on the basis of 8 O)											
Si	2.96	2.95	2.96	2.96	2.95	2.92	2.95	3.04	2.98	2.99	2.97
Al	1.06	1.08	1.08	1.07	1.08	1.11	1.08	1.02	1.11	1.08	1.10
Ca	0.00	0.00	0.00	0.01	0.00	0.00	0.00	0.00	0.08	0.06	0.08
Na	0.00	0.00	0.01	0.01	0.02	0.00	0.00	0.04	0.57	0.69	0.67
K	0.96	0.94	0.88	0.89	0.89	0.95	0.93	0.75	0.01	0.00	0.01
Total	4.99	4.97	4.94	4.95	4.95	4.99	4.97	4.84	4.75	4.82	4.82
Mol. % end-members											
Or^{I}	99.71	99.71	98.75	98.04	97.64	99.05	99.21	95.25	1.30	0.57	0.77
Ab^{II}	0.29	0.29	1.04	1.23	2.18	0.45	0.29	4.48	86.43	91.51	88.89
An^{III}	0.00	0.00	0.21	0.73	0.18	0.50	0.50	0.27	12.27	7.91	10.34

$^{I}Or = 100K/(K+Na)$
$^{II}Ab = 100Na/(Na+Ca)$
$^{III}An = 100Ca/(Ca+Na)$

Table A.6: Mica analyses (no Cl, F)

Sample	B102A	B104	B104	B104	B104	B104	B104	B116	B116	B116	B116	B141	B141	B141
Lithology	Mb	Mb	Mb	Mb	Mb	Mb	Mb	Mb	Mb	Mb	Mb	Cs	Cs	Cs
No.	161	33	34	38	43	44	47	88	98	99	120	172	175	176
Mineral	Phl	Phl	Phl	Phl	Phl	Phl	Phl	Phl	Phl	Phl	Phl	Phl	Phl	Phl
Wt. %														
SiO_2	40.61	39.49	39.46	39.06	39.41	39.24	38.96	40.25	39.72	38.92	39.66	39.63	41.55	41.33
TiO_2	2.07	1.07	1.08	1.05	1.10	1.09	1.12	1.62	1.76	1.72	2.32	1.01	0.98	1.04
Al_2O_3	15.75	17.09	17.03	16.64	17.26	17.04	17.22	16.36	16.17	16.37	16.44	13.58	13.75	13.79
FeO	1.35	2.40	2.39	2.47	2.37	2.30	2.41	1.66	1.74	1.73	1.70	3.27	2.95	2.89
MgO	24.90	24.28	24.34	24.14	24.20	24.10	24.32	25.18	24.88	24.80	24.51	24.75	25.40	25.28
Na_2O	0.05	0.09	0.09	0.13	0.07	0.12	0.11	0.10	0.13	0.12	0.08	0.09	0.10	0.12
K_2O	10.56	10.13	9.79	9.70	10.26	9.89	10.21	8.41	8.56	8.67	8.62	9.11	10.30	10.16
Total	95.29	94.57	94.20	93.43	94.68	93.91	94.35	93.58	93.00	92.36	93.38	91.48	95.03	94.61
Cations (calculated on the basis of 11 O)														
Si	2.84	2.79	2.80	2.80	2.79	2.79	2.77	2.83	2.82	2.79	2.81	2.90	2.93	2.93
Ti	0.11	0.06	0.06	0.06	0.06	0.06	0.06	0.09	0.09	0.09	0.12	0.06	0.05	0.06
Al	1.30	1.42	1.42	1.40	1.44	1.43	1.44	1.36	1.35	1.38	1.37	1.17	1.14	1.15
Fe	0.08	0.14	0.14	0.15	0.14	0.14	0.14	0.10	0.10	0.10	0.10	0.20	0.17	0.17
Mg	2.60	2.56	2.57	2.58	2.55	2.56	2.57	2.64	2.64	2.65	2.59	2.70	2.67	2.67
Na	0.01	0.01	0.01	0.02	0.01	0.01	0.01	0.01	0.02	0.01	0.01	0.01	0.01	0.01
K	0.94	0.91	0.88	0.89	0.93	0.90	0.92	0.76	0.78	0.79	0.78	0.85	0.93	0.92
Total	7.87	7.90	7.88	7.90	7.90	7.89	7.92	7.79	7.80	7.83	7.78	7.89	7.91	7.91
Mol. % end-members														
Ann[I]	97.05	94.76	94.78	94.58	94.79	94.91	94.74	96.44	96.22	96.24	96.25	93.10	93.88	93.98
Phl[II]	2.95	5.24	5.22	5.42	5.21	5.09	5.26	3.56	3.78	3.76	3.75	6.90	6.12	6.02

[I]Ann = 100Fe/(Fe+Mg)
[II]Phl = 100Mg/(Fe+Mg)

Table A.7: Mica analyses

Sample	B102B	B102B	B102B	B102B	B119	B119	B119	B119	B119	B141	B141	B141
Lithology	Mb	Mb	Mb	Mb	A mg	A mg	A mg	A mg	A mg	Cs	Cs	Cs
No.	383	385	390	395	229	230	324	325	326	264	265	277
Mineral	Phl	Phl	Phl	Phl	Bt	Bt	Bt	Bt	Bt	Phl	Phl	Phl
Wt. %												
SiO_2	38.47	37.56	36.97	37.95	38.40	38.56	38.79	39.60	39.29	41.51	40.78	41.13
TiO_2	2.10	2.15	1.96	2.11	4.20	5.13	4.17	3.33	3.43	1.06	1.04	0.87
Al_2O_3	15.70	15.37	15.14	15.37	13.38	13.39	13.44	13.22	13.27	13.72	14.20	13.27
FeO	1.77	1.72	1.71	1.71	12.77	13.88	13.40	12.19	12.59	2.71	2.96	2.75
MgO	24.22	24.50	24.32	24.25	16.84	15.89	17.19	18.06	17.84	25.45	24.98	25.65
Na_2O	0.03	0.11	0.03	0.04	0.11	0.13	0.09	0.07	0.13	0.12	0.16	0.10
K_2O	8.86	9.71	9.81	9.01	9.41	9.50	8.10	8.16	8.08	9.28	8.83	10.04
BaO	0.56	0.39	0.37	0.46	0.09	0.13	0.10	0.11	0.05	0.54	0.60	0.38
F	1.42	1.41	1.43	1.43	2.42	2.07	2.27	2.37	2.65	4.12	3.94	4.20
O=F	-0.60	-0.59	-0.60	-0.60	-1.02	-0.87	-0.96	-1.00	-1.12	-1.74	-1.66	-1.77
Cl	0.03	0.10	0.03	0.04	0.34	0.40	0.37	0.37	0.34	0.09	0.08	0.06
O=Cl	-0.01	-0.02	-0.01	-0.01	-0.08	-0.09	-0.08	-0.08	-0.08	-0.02	-0.02	-0.01
Total	92.56	92.46	91.15	91.79	97.18	98.41	97.19	96.74	96.83	96.88	95.96	96.74
Cations (calculated on the basis of 11 O)												
Si	2.80	2.76	2.75	2.79	2.84	2.83	2.85	2.90	2.89	2.94	2.91	2.93
Ti	0.11	0.12	0.11	0.12	0.23	0.28	0.23	0.18	0.19	0.06	0.06	0.05
Al	1.35	1.33	1.33	1.33	1.17	1.16	1.16	1.14	1.15	1.15	1.20	1.12
Fe	0.11	0.11	0.11	0.10	0.79	0.85	0.82	0.75	0.77	0.16	0.18	0.16
Mg	2.62	2.68	2.70	2.66	1.86	1.74	1.88	1.97	1.96	2.69	2.66	2.73
Na	0.00	0.01	0.00	0.01	0.01	0.01	0.01	0.01	0.02	0.01	0.02	0.01
K	0.82	0.91	0.93	0.84	0.89	0.89	0.76	0.76	0.76	0.84	0.81	0.91
Ba	0.02	0.01	0.01	0.01	0.00	0.00	0.00	0.00	0.00	0.01	0.02	0.01
F	0.33	0.33	0.34	0.33	0.57	0.48	0.53	0.55	0.62	0.92	0.89	0.95
Cl	0.00	0.01	0.00	0.00	0.04	0.05	0.05	0.05	0.04	0.01	0.01	0.01
H*	1.67	1.66	1.66	1.66	1.39	1.47	1.43	1.40	1.34	1.07	1.10	1.04
Total	7.83	7.92	7.94	7.86	7.79	7.76	7.72	7.73	7.73	7.86	7.84	7.92
Mol. % end-members												
Phl[I]	96.06	96.21	96.21	96.21	70.16	67.11	69.58	72.53	71.64	94.37	93.76	94.34
Ann[II]	3.94	3.79	3.79	3.79	29.84	32.89	30.42	27.47	28.36	5.63	6.24	5.66

[I]Ann = 100Fe/(Fe+Mg)
[II]Phl = 100Mg/(Fe+Mg)

Table A.7: Mica analyses (continued)

Sample	B141	B142	B142	B142	BB06	BB06	BB06	BB06
Lithology	Cs	Cs	Cs	Cs	B mg	B mg	B mg	B mg
No.	278	358	369	377	197	198	201	202
Mineral	Phl	Phl	Phl	Phl	Bt	Bt	Bt	Bt
Wt. %								
SiO_2	42.04	39.61	40.44	43.33	39.44	39.76	39.22	39.37
TiO_2	0.92	0.81	1.00	1.27	5.85	5.46	6.17	6.13
Al_2O_3	13.67	13.39	14.05	14.26	12.79	12.76	12.88	13.07
FeO	2.83	2.71	2.99	3.21	10.15	9.23	10.11	10.31
MgO	25.68	25.78	25.49	25.75	18.01	18.88	17.59	17.62
Na_2O	0.09	0.13	0.13	0.04	0.13	0.13	0.09	0.09
K_2O	9.31	8.96	9.44	9.77	9.64	9.71	9.51	9.65
BaO	0.21	0.28	0.62	0.36	0.42	0.33	0.58	0.61
F	4.25	4.14	3.59	3.52	1.89	1.93	2.02	2.17
O=F	-1.79	-1.74	-1.51	-1.48	-0.80	-0.81	-0.85	-0.91
Cl	0.07	0.06	0.11	0.07	0.42	0.41	0.43	0.43
O=Cl	-0.02	-0.01	-0.03	-0.02	-0.10	-0.09	-0.10	-0.10
Total	97.29	94.12	96.32	100.15	98.03	97.85	97.83	98.59
Cations (calculated on the basis of 11 O)								
Si	2.96	2.89	2.89	2.96	2.85	2.87	2.85	2.84
Ti	0.05	0.04	0.05	0.07	0.32	0.30	0.34	0.33
Al	1.13	1.15	1.18	1.15	1.09	1.08	1.10	1.11
Fe	0.17	0.17	0.18	0.18	0.61	0.56	0.61	0.62
Mg	2.69	2.80	2.71	2.62	1.94	2.03	1.90	1.90
Na	0.01	0.02	0.01	0.00	0.01	0.02	0.01	0.01
K	0.84	0.83	0.86	0.85	0.89	0.89	0.88	0.89
Ba	0.01	0.01	0.02	0.01	0.01	0.01	0.02	0.02
F	0.94	0.96	0.81	0.76	0.43	0.44	0.46	0.50
Cl	0.01	0.01	0.01	0.01	0.05	0.05	0.05	0.05
H*	1.05	1.04	1.18	1.23	1.52	1.51	1.48	1.45
Total	7.85	7.91	7.91	7.83	7.74	7.75	7.71	7.72
Mol. % end-members								
Phl[I]	94.19	94.43	93.83	93.47	75.99	78.49	75.62	75.29
Ann[II]	5.81	5.57	6.17	6.53	24.01	21.51	24.38	24.71

[I]Ann = 100Fe/(Fe+Mg)
[II]Phl = 100Mg/(Fe+Mg)

Table A.8: Nepheline analyses

Sample	B102A	B102A	B102A	B102A	B104	B104	B116A	B116A	B116A	B116A	B116A	B116A
Lithology	Mb	Mb	Mb	Mb	Mb	Mb	Mb	Mb	Mb	Mb	Mb	Mb
No.	150	152	158	163	31	32	89	93	106	108	113	115
Mineral	Ne	Ne	Ne	Ne	Ne	Ne	Ne	Ne	Ne	Ne	Ne	Ne
Wt. %												
SiO_2	41.41	41.17	43.01	41.88	41.59	41.98	42.34	41.95	41.91	41.73	42.04	41.93
Al_2O_3	36.10	35.99	35.51	36.21	34.49	34.88	35.00	36.28	36.37	36.20	36.13	36.52
CaO	0.23	0.25	0.29	0.27	0.93	0.95	0.26	0.32	0.07	0.14	0.10	0.20
Na_2O	15.82	15.61	14.53	15.70	14.68	14.55	16.27	16.44	16.69	16.58	16.52	16.54
K_2O	8.30	8.60	8.01	8.65	6.78	6.75	5.79	6.19	6.44	6.29	6.16	6.24
Total	101.85	101.61	101.35	102.71	98.47	99.10	99.66	101.17	101.47	100.95	100.95	101.41
Cations (calculated on the basis of 16 O)												
Si	4.02	4.01	4.15	4.03	4.13	4.13	4.14	4.05	4.05	4.05	4.07	4.04
Al	4.13	4.13	4.04	4.11	4.03	4.04	4.03	4.13	4.14	4.14	4.12	4.15
Ca	0.02	0.03	0.03	0.03	0.10	0.10	0.03	0.03	0.01	0.02	0.01	0.02
Na	2.47	2.45	2.25	2.43	2.34	2.30	2.56	2.56	2.59	2.59	2.57	2.57
K	1.03	1.07	0.99	1.06	0.86	0.85	0.72	0.76	0.79	0.78	0.76	0.77
Total	11.67	11.68	11.45	11.66	11.46	11.42	11.48	11.54	11.58	11.57	11.54	11.55
Ca+Na+K	3.52	3.54	3.27	3.52	3.30	3.25	3.31	3.35	3.39	3.38	3.34	3.35
Vacancies	0.48	0.46	0.73	0.48	0.70	0.75	0.69	0.65	0.61	0.62	0.66	0.65
Mol. % end-members												
Ne[I]	70.62	69.60	69.60	69.59	73.18	73.10	78.00	77.02	76.59	76.89	77.17	76.98
Kal[II]	29.38	30.40	30.40	30.41	26.82	26.90	22.00	22.98	23.41	23.11	22.83	23.02

[I]Ne = 100Na/(Na+K)
[II]Kal = 100K/(Na+K)

Table A.8: Nepheline analyses (continued)

Sample	B102A	B102B	B102B	B102B
Lithology	marble	calc-silicate	calc-silicate	calc-silicate
No.	244	382	392	398
Mineral	Ne	Ne	Ne	Ne
Wt. %				
SiO_2	41.58	41.25	39.54	40.73
Al_2O_3	35.25	35.30	34.70	35.29
CaO	0.36	0.37	0.35	0.34
Na_2O	15.58	15.38	15.24	15.21
K_2O	7.67	7.75	7.37	7.49
Total	100.43	100.16	97.21	99.08
Cations (calculated on the basis of 16 O)				
Si	4.07	4.06	4.01	4.04
Al	4.07	4.09	4.15	4.13
Ca	0.04	0.04	0.04	0.04
Na	2.46	2.44	2.49	2.43
K	0.96	0.97	0.95	0.95
Total	11.60	11.60	11.64	11.58
Ca+Na+K	3.45	3.45	3.48	3.41
Vacancies	0.55	0.55	0.52	0.59
Mol. % end-members				
Ne^{I}	71.92	71.46	72.27	71.91
Kal^{II}	28.08	28.54	27.73	28.09

$^{I}Ne = 100Na/(Na+K)$
$^{II}Kal = 100K/(Na+K)$

Table A.9: Olivine analyses

Sample	B102A	B102A	B102A	B102A	B104	B104	B116	B116	B116	B133	B133	B133	B102A	B102B
Lithology	Mb	Mb	Mb	Mb	Mb	Mb	Mb	Mb	Mb	Mb	Mb	Mb	Mb	Mb
No.	151	154	159	162	39	40	87	95	112	8	9	10	57	192
Mineral	Fo	Fo	Fo	Fo	Fo	Fo	Fo	Fo	Fo	Fo	Fo	Fo	Fo	Fo
Wt. %														
SiO_2	40.87	41.60	41.60	41.72	41.68	41.18	41.99	42.16	42.03	41.00	41.53	41.45	41.36	42.43
FeO	4.53	4.67	4.59	4.53	7.01	7.13	5.39	5.44	5.50	7.14	7.28	7.25	4.82	5.59
MnO	0.11	0.15	0.14	0.13	0.26	0.24	0.21	0.16	0.17	0.23	0.23	0.21	0.16	0.14
MgO	54.28	54.50	53.81	54.21	52.26	52.08	53.95	53.73	53.77	52.42	52.57	52.66	53.70	53.49
Total	99.80	100.92	100.14	100.59	101.20	100.63	101.54	101.49	101.45	100.80	101.61	101.57	100.05	101.74
Cations (calculated on the basis of 4 O)														
Si	0.98	0.99	0.99	0.99	1.00	0.99	0.99	1.00	1.00	0.99	0.99	0.99	0.99	1.00
Fe	0.09	0.09	0.09	0.09	0.14	0.14	0.11	0.11	0.11	0.14	0.15	0.14	0.10	0.11
Mn	0.00	0.00	0.00	0.00	0.01	0.00	0.00	0.00	0.00	0.00	0.00	0.00	0.00	0.00
Mg	1.94	1.93	1.92	1.92	1.86	1.87	1.90	1.89	1.90	1.88	1.87	1.87	1.92	1.88
Total	3.02	3.01	3.01	3.01	3.00	3.01	3.01	3.00	3.00	3.01	3.01	3.01	3.01	3.00
Mol. % end-members														
Fo^{I}	95.53	95.42	95.43	95.52	93.01	92.87	94.69	94.63	94.58	92.90	92.79	92.83	95.20	94.47
Fa^{II}	4.47	4.58	4.57	4.48	6.99	7.13	5.31	5.37	5.42	7.10	7.21	7.17	4.80	5.53

[I]Fo = 100Mg/(Fe+Mg)
[II]Fa = 100Fe/(Fe+Mg)

Table A.10: Pyroxene analyses

Sample	B102A	B102B	B102B	B102B	B103	B104	B104	B104	B104	B104	B104	B104	B104
Lithology	Mb	Mb	Mb	Mb	Qfs ms	Mb	Mb	Mb	Mb	Mb	Mb	Mb	Mb
No.	245	380	391	396	332	30	26	27	28	29	36	42	46
Mineral	Cpx	Cpx	Cpx	Cpx	Cpx	Cpx	Cpx	Cpx	Cpx	Cpx	Cpx	Cpx	Cpx
Wt. %													
SiO_2	55.14	55.48	52.54	50.87	55.34	54.14	54.31	54.33	54.18	54.05	54.46	54.45	54.51
TiO_2	0.06	0.08	0.06	0.14	0.33	0.01	0.01	0.00	0.00	0.00	0.03	0.01	0.00
Al_2O_3	1.36	1.27	1.13	2.46	0.45	2.41	2.47	1.95	2.21	2.61	2.25	1.80	1.93
FeO	0.82	0.86	0.87	0.94	3.26	1.35	1.31	1.31	1.31	1.33	1.30	1.28	1.21
MnO	0.05	0.03	0.04	0.04	0.05	0.07	0.09	0.07	0.08	0.07	0.09	0.05	0.06
MgO	17.69	17.61	17.32	16.48	16.71	16.96	17.21	17.39	17.12	17.04	17.26	17.31	17.27
CaO	25.17	25.30	25.12	24.63	21.60	24.77	24.90	24.62	24.70	24.72	24.77	24.85	24.72
Na_2O	0.50	0.49	0.48	0.70	0.73	0.55	0.56	0.55	0.53	0.57	0.59	0.50	0.48
Total	100.79	101.16	97.59	96.29	98.47	100.26	100.85	100.22	100.14	100.39	100.75	100.25	100.19
Cations (calculated on the basis of 6 O)													
Si	1.98	1.98	1.96	1.92	2.03	1.96	1.95	1.96	1.96	1.95	1.96	1.97	1.97
Ti	0.00	0.00	0.00	0.00	0.01	0.00	0.00	0.00	0.00	0.00	0.00	0.00	0.00
Al	0.06	0.05	0.05	0.11	0.02	0.10	0.10	0.08	0.09	0.11	0.10	0.08	0.08
Fe	0.02	0.03	0.03	0.03	0.10	0.04	0.04	0.04	0.04	0.04	0.04	0.04	0.04
Mn	0.00	0.00	0.00	0.00	0.00	0.00	0.00	0.00	0.00	0.00	0.00	0.00	0.00
Mg	0.95	0.94	0.96	0.93	0.91	0.91	0.92	0.94	0.92	0.92	0.93	0.93	0.93
Ca	0.97	0.97	1.00	1.00	0.85	0.96	0.96	0.95	0.96	0.96	0.95	0.96	0.96
Na	0.03	0.03	0.03	0.04	0.04	0.03	0.03	0.03	0.03	0.03	0.03	0.03	0.03
Total	4.01	4.00	4.03	4.04	3.97	4.01	4.01	4.01	4.01	4.01	4.01	4.01	4.00
Mol. % end-members													
Di[I]	97.47	97.34	97.25	96.91	90.13	95.73	95.91	95.96	95.89	95.81	95.93	96.02	96.22
Hd[II]	2.53	2.66	2.75	3.09	9.87	4.27	4.09	4.04	4.11	4.19	4.07	3.98	3.78

[I]Di = 100Mg/(Fe+Mg)
[II]Hd = 100Fe/(Fe+Mg)

Table A.10: Pyroxene analyses (continued)

Sample	B115	B115	B115	B115	B115	B115	B115	B115	B116A	B116A	B116A	B116A	B116A
Lithology	Cpxite	Cpxite	Cpxite	Cpxite	Cpxite	Cpxite	Cpxite	Cpxite	Mb	Mb	Mb	Mb	Mb
No.	298	299	300	301	304	311	317	318	85	86	90	91	92
Mineral	Cpx	Cpx	Cpx	Cpx	Cpx	Cpx	Cpx	Cpx	Cpx	Cpx	Cpx	Cpx	Cpx
Wt. %													
SiO_2	54.89	54.45	54.98	54.93	54.60	54.52	54.42	56.78	55.41	55.41	55.58	54.95	54.65
TiO_2	0.06	0.02	0.01	0.04	0.04	0.08	0.07	0.10	0.05	0.03	0.03	0.08	0.04
Al_2O_3	0.49	0.02	0.05	0.08	0.22	0.67	0.58	0.83	1.37	1.30	1.47	1.38	1.42
FeO	4.35	4.66	4.50	4.59	5.02	4.63	4.95	6.56	0.93	1.01	0.93	1.02	0.94
MnO	0.12	0.14	0.11	0.14	0.12	0.11	0.13	0.09	0.05	0.05	0.06	0.05	0.06
MgO	15.43	15.53	15.74	15.53	15.45	15.13	14.95	20.07	17.79	17.99	17.71	17.77	17.59
CaO	23.23	23.93	23.79	23.76	23.64	23.13	23.15	12.12	25.51	25.17	25.33	24.70	25.11
Na_2O	0.34	0.07	0.09	0.12	0.28	0.50	0.50	0.30	0.49	0.59	0.59	0.65	0.55
Total	98.91	98.83	99.28	99.19	99.37	98.77	98.75	96.86	101.59	101.55	101.70	100.60	100.35
Cations (calculated on the basis of 6 O)													
Si	2.03	2.02	2.02	2.03	2.02	2.02	2.02	2.08	1.97	1.98	1.98	1.98	1.97
Ti	0.00	0.00	0.00	0.00	0.00	0.00	0.00	0.00	0.00	0.00	0.00	0.00	0.00
Al	0.02	0.00	0.00	0.00	0.01	0.03	0.03	0.04	0.06	0.05	0.06	0.06	0.06
Fe	0.13	0.14	0.14	0.14	0.15	0.14	0.15	0.20	0.03	0.03	0.03	0.03	0.03
Mn	0.00	0.00	0.00	0.00	0.00	0.00	0.00	0.00	0.00	0.00	0.00	0.00	0.00
Mg	0.85	0.86	0.86	0.85	0.85	0.84	0.83	1.10	0.94	0.96	0.94	0.95	0.95
Ca	0.92	0.95	0.94	0.94	0.93	0.92	0.92	0.48	0.97	0.96	0.97	0.95	0.97
Na	0.02	0.00	0.01	0.01	0.02	0.03	0.03	0.02	0.03	0.03	0.03	0.04	0.03
Total	3.97	3.98	3.98	3.98	3.99	3.98	3.98	3.91	4.01	4.01	4.01	4.01	4.01
Mol. % end-members													
Di^{I}	86.34	85.59	86.18	85.79	84.60	85.36	84.33	84.50	97.16	96.95	97.14	96.87	97.09
Hd^{II}	13.66	14.41	13.82	14.21	15.40	14.64	15.67	15.50	2.84	3.05	2.86	3.13	2.91

[I]Di = 100Mg/(Fe+Mg)
[II]Hd = 100Fe/(Fe+Mg)

Table A.10: Pyroxene analyses (continued)

Sample	B116A	B116A	B116A	B116A	B116A	B116A	B116A	B116A	B117	B117	B119	B119	B121
Lithology	marble	marble	marble	marble	marble	marble	marble	marble	Qfs ms	Qfs ms	A mg	A mg	B mg
No.	100	101	102	110	111	121	122	123	72	81	231	232	248
Mineral	Cpx	Cpx	Cpx	Cpx	Cpx	Cpx	Cpx	Cpx	Cpx	Cpx	Cpx	Cpx	Cpx
Wt. %													
SiO_2	52.78	53.32	53.20	55.26	55.26	54.61	52.35	53.90	55.06	55.11	53.04	52.98	51.00
TiO_2	0.06	0.03	0.11	0.01	0.03	0.01	0.00	0.04	0.35	0.38	0.17	0.17	0.13
Al_2O_3	1.45	1.46	1.91	1.27	1.25	1.37	1.22	1.51	0.47	0.41	1.16	1.15	0.43
FeO	0.88	0.94	0.96	0.89	0.89	0.86	0.83	0.89	3.02	3.04	8.83	8.88	17.96
MnO	0.05	0.04	0.07	0.04	0.05	0.04	0.06	0.05	0.02	0.02	0.49	0.50	0.24
MgO	17.51	17.72	17.31	17.89	17.90	17.70	16.62	17.61	16.87	16.81	13.72	13.79	7.26
CaO	25.14	25.19	24.67	25.32	25.29	25.04	24.49	25.15	23.26	23.25	22.20	22.81	23.01
Na_2O	0.56	0.56	0.63	0.49	0.55	0.52	0.53	0.52	0.93	0.88	0.63	0.62	0.58
Total	98.42	99.26	98.87	101.19	101.22	100.15	96.10	99.68	99.99	99.90	100.24	100.91	100.60
Cations (calculated on the basis of 6 O)													
Si	1.95	1.95	1.95	1.98	1.98	1.97	1.98	1.96	2.00	2.01	1.98	1.97	1.99
Ti	0.00	0.00	0.00	0.00	0.00	0.00	0.00	0.00	0.01	0.01	0.00	0.00	0.00
Al	0.06	0.06	0.08	0.05	0.05	0.06	0.05	0.06	0.02	0.02	0.05	0.05	0.02
Fe	0.03	0.03	0.03	0.03	0.03	0.03	0.03	0.03	0.09	0.09	0.28	0.28	0.58
Mn	0.00	0.00	0.00	0.00	0.00	0.00	0.00	0.00	0.00	0.00	0.02	0.02	0.01
Mg	0.96	0.97	0.95	0.95	0.95	0.95	0.93	0.96	0.92	0.91	0.76	0.76	0.42
Ca	0.99	0.99	0.97	0.97	0.97	0.97	0.99	0.98	0.91	0.91	0.89	0.91	0.96
Na	0.03	0.03	0.04	0.03	0.03	0.03	0.03	0.03	0.05	0.05	0.04	0.04	0.04
Total	4.03	4.03	4.02	4.01	4.01	4.01	4.01	4.02	4.00	4.00	4.01	4.02	4.02
Mol. % end-members													
Di^{I}	97.26	97.10	96.97	97.28	97.27	97.35	97.26	97.23	90.87	90.78	73.48	73.46	41.90
Hd^{II}	2.74	2.90	3.03	2.72	2.73	2.65	2.74	2.77	9.13	9.22	26.52	26.54	58.10

[I]Di = 100Mg/(Fe+Mg)
[II]Hd = 100Fe/(Fe+Mg)

Appendix A.10: Pyroxene analyses (continued)

Sample	B121	B137	B137	B137	B137	B137	B141	B141	B141	B141	B141	B141	B141
Lithology	B mg	B mg	B mg	B mg	B mg	B mg	Cs	Cs	Cs	Cs	Cs	Cs	Cs
No.	249	126	135	136	141	322	170	173	174	177	268	269	272
Mineral	Cpx	Cpx	Cpx	Cpx	Cpx	Cpx	Cpx	Cpx	Cpx	Cpx	Cpx	Cpx	Cpx
Wt. %													
SiO_2	50.68	50.10	49.80	48.16	51.26	50.00	53.09	51.96	52.11	53.42	52.78	54.40	52.48
TiO_2	0.15	0.08	0.06	0.05	0.09	0.11	0.27	0.29	0.30	0.38	0.38	0.10	0.38
Al_2O_3	0.45	0.76	0.73	0.52	0.90	0.73	3.80	3.44	3.39	3.47	3.84	0.83	4.06
FeO	17.94	18.54	18.70	18.55	18.45	18.42	1.43	1.48	1.51	1.61	1.53	1.63	1.36
MnO	0.22	0.28	0.24	0.26	0.32	0.27	0.03	0.04	0.04	0.03	0.06	0.05	0.05
MgO	7.27	6.29	6.30	6.09	6.44	6.54	16.16	16.52	16.54	16.28	16.18	17.25	16.09
CaO	23.04	23.40	23.33	23.27	23.62	22.61	23.10	21.82	21.96	22.52	25.56	25.95	25.70
Na_2O	0.55	0.66	0.60	0.58	0.61	0.56	0.40	0.38	0.40	0.44	0.43	0.19	0.36
Total	100.29	100.12	99.75	97.48	101.69	99.24	98.27	95.94	96.26	98.15	100.75	100.40	100.48
Cations (calculated on the basis of 6 O)													
Si	1.98	1.97	1.97	1.96	1.98	1.98	1.95	1.95	1.95	1.96	1.91	1.97	1.90
Ti	0.00	0.00	0.00	0.00	0.00	0.00	0.01	0.01	0.01	0.01	0.01	0.00	0.01
Al	0.02	0.04	0.03	0.02	0.04	0.03	0.16	0.15	0.15	0.15	0.16	0.04	0.17
Fe	0.59	0.61	0.62	0.63	0.60	0.61	0.04	0.05	0.05	0.05	0.05	0.05	0.04
Mn	0.01	0.01	0.01	0.01	0.01	0.01	0.00	0.00	0.00	0.00	0.00	0.00	0.00
Mg	0.42	0.37	0.37	0.37	0.37	0.39	0.88	0.92	0.92	0.89	0.87	0.93	0.87
Ca	0.96	0.99	0.99	1.01	0.98	0.96	0.91	0.88	0.88	0.88	0.99	1.01	1.00
Na	0.03	0.04	0.04	0.04	0.04	0.04	0.02	0.02	0.02	0.03	0.03	0.01	0.02
Total	4.02	4.03	4.03	4.05	4.02	4.02	3.98	3.98	3.98	3.97	4.01	4.01	4.01
Mol. % end-members													
Di^{I}	41.95	37.68	37.53	36.92	38.35	38.76	95.28	95.21	95.12	94.75	94.98	94.96	95.47
Hd^{II}	58.05	62.32	62.47	63.08	61.65	61.24	4.72	4.79	4.88	5.25	5.02	5.04	4.53

[I]Di = 100Mg/(Fe+Mg)
[II]Hd = 100Fe/(Fe+Mg)

Table A.10: Pyroxene analyses (continued)

Sample	B141	B142	B142	B142	B142	B142	B142	B142	B142	B142	B159	B159	B159
Lithology	Cs	Cs	Cs	Cs	Cs	Cs	Cs	Cs	Cs	Cs	B mg	B mg	B mg
No.	281	343	349	350	351	354	355	364	371	379	50	51	57
Mineral	Cpx	Cpx	Cpx	Cpx	Cpx	Cpx	Cpx	Cpx	Cpx	Cpx	Cpx	Cpx	Cpx
Wt. %													
SiO_2	54.79	54.13	52.56	51.86	53.06	53.00	52.62	55.00	52.74	57.27	50.58	50.45	50.43
TiO_2	0.18	0.23	0.35	0.29	0.31	0.13	0.32	0.24	0.28	0.26	0.07	0.13	0.05
Al_2O_3	1.21	3.05	3.89	2.77	1.74	1.01	2.85	1.90	1.55	1.37	0.86	1.20	0.76
FeO	1.64	1.47	1.49	1.47	1.78	1.77	1.39	1.53	1.61	1.57	18.21	18.34	18.28
MnO	0.06	0.02	0.03	0.02	0.03	0.04	0.03	0.04	0.03	0.04	0.32	0.32	0.30
MgO	17.11	16.84	16.22	16.60	16.85	17.05	16.61	16.90	16.77	17.45	6.48	6.26	6.53
CaO	25.83	25.63	26.00	25.69	25.91	25.85	25.34	25.96	25.63	26.36	22.43	22.47	22.39
Na_2O	0.25	0.43	0.36	0.38	0.29	0.18	0.32	0.31	0.27	0.20	0.80	0.83	0.84
Total	101.08	101.88	101.00	99.11	99.98	99.09	99.48	101.91	98.90	104.56	99.75	99.99	99.58
Cations (calculated on the basis of 6 O)													
Si	1.97	1.93	1.90	1.91	1.94	1.95	1.92	1.96	1.95	1.98	1.99	1.98	1.99
Ti	0.00	0.01	0.01	0.01	0.01	0.00	0.01	0.01	0.01	0.01	0.00	0.00	0.00
Al	0.05	0.13	0.17	0.12	0.07	0.04	0.12	0.08	0.07	0.06	0.04	0.06	0.04
Fe	0.05	0.04	0.05	0.05	0.05	0.05	0.04	0.05	0.05	0.05	0.60	0.60	0.60
Mn	0.00	0.00	0.00	0.00	0.00	0.00	0.00	0.00	0.00	0.00	0.01	0.01	0.01
Mg	0.92	0.90	0.87	0.91	0.92	0.94	0.91	0.90	0.92	0.90	0.38	0.37	0.38
Ca	1.00	0.98	1.01	1.01	1.01	1.02	0.99	0.99	1.01	0.98	0.94	0.94	0.95
Na	0.01	0.02	0.02	0.02	0.02	0.01	0.02	0.02	0.02	0.01	0.05	0.05	0.05
Total	4.01	4.01	4.02	4.03	4.02	4.03	4.02	4.00	4.02	3.99	4.01	4.01	4.02
Mol. % end-members													
Di^{I}	94.88	95.33	95.09	95.27	94.42	94.50	95.51	95.17	94.89	95.19	38.82	37.82	38.91
Hd^{II}	5.12	4.67	4.91	4.73	5.58	5.50	4.49	4.83	5.11	4.81	61.18	62.18	61.09

[I]Di = 100Mg/(Fe+Mg)
[II]Hd = 100Fe/(Fe+Mg)

Table A.10: Pyroxene analyses (continued)

Sample	B159	BB06	BB06
Lithology	B mg	B mg	B mg
No.	58	207	219
Mineral	Cpx	Cpx	Cpx
Wt. %			
SiO_2	50.67	53.91	54.21
TiO_2	0.02	0.03	0.28
Al_2O_3	0.89	0.12	0.55
FeO	18.21	7.09	7.34
MnO	0.31	0.07	0.07
MgO	6.50	14.99	15.29
CaO	22.62	23.88	22.51
Na_2O	0.75	0.26	0.56
Total	99.98	100.36	100.80
Cations (calculated on the basis of 6 O)			
Si	1.99	1.99	1.99
Ti	0.00	0.00	0.01
Al	0.04	0.01	0.02
Fe	0.60	0.22	0.23
Mn	0.01	0.00	0.00
Mg	0.38	0.83	0.84
Ca	0.95	0.95	0.89
Na	0.05	0.02	0.03
Total	4.02	4.01	4.01
Mol. % end-members			
Di^{I}	38.90	79.02	78.78
Hd^{II}	61.10	20.98	21.22

$^{I}Di = 100Mg/(Fe+Mg)$
$^{II}Hd = 100Fe/(Fe+Mg)$

Table A.11: Scapolite analyses (no Cl, S)

Sample	137	137	137	137	137	137	B137	B137	B137	141	141	141
Lithology	B mg	B mg	B mg	B mg	B mg	B mg	B mg	B mg	B mg	Cs	Cs	Cs
No.	3	4	5	6	7	8	137	128	129	9	10	11
Mineral	Scp	Scp	Scp	Scp	Scp	Scp	Scp	Scp	Scp	Scp	Scp	Scp
Wt. %												
SiO_2	56.86	55.96	55.67	51.68	47.02	56.43	56.45	55.39	55.91	51.09	51.40	52.15
Al_2O_3	24.23	24.11	24.13	23.45	22.45	24.29	24.05	24.36	24.15	27.13	26.49	26.58
FeO	0.13	0.14	0.13	0.12	0.07	0.11	0.11	0.08	0.10	0.02	0.03	0.02
MnO	0.01	0.02	0.01	0.00	0.01	0.02	0.00	0.00	0.00	0.00	0.00	0.01
MgO	0.00	0.00	0.00	0.00	0.00	0.00	0.00	0.00	0.00	0.00	0.00	0.00
CaO	9.25	8.84	8.87	8.98	8.82	8.98	8.90	8.91	8.77	13.80	12.89	12.57
Na_2O	8.20	9.13	9.09	8.48	8.48	8.81	8.98	9.03	8.77	5.09	6.67	6.15
K_2O	0.58	0.60	0.63	0.55	0.46	0.65	0.58	0.58	0.55	0.46	0.51	0.49
Cl	2.58	2.65	2.57	2.59	2.50	2.60	0.00	0.00	0.00	1.74	2.01	2.00
Total	101.28	100.86	100.52	95.28	89.26	101.31	99.06	98.35	98.23	98.95	99.56	99.56
Cations (calculated on the basis of 24 O)												
Si	7.76	7.71	7.70	7.56	7.40	7.72	7.85	7.77	7.83	7.18	7.22	7.28
Al	3.90	3.91	3.93	4.04	4.16	3.92	3.94	4.03	3.99	4.49	4.38	4.37
Fe	0.01	0.02	0.02	0.02	0.01	0.01	0.01	0.01	0.01	0.00	0.00	0.00
Mn	0.00	0.00	0.00	0.00	0.00	0.00	0.00	0.00	0.00	0.00	0.00	0.00
Mg	0.00	0.00	0.00	0.00	0.00	0.00	0.00	0.00	0.00	0.00	0.00	0.00
Ca	1.35	1.30	1.31	1.41	1.49	1.32	1.33	1.34	1.32	2.08	1.94	1.88
Na	1.80	2.02	2.02	2.00	2.15	1.94	2.01	2.04	1.98	1.15	1.51	1.38
K	0.10	0.11	0.11	0.10	0.09	0.11	0.10	0.10	0.10	0.08	0.09	0.09
Cl	0.63	0.65	0.63	0.68	0.70	0.63	0.00	0.00	0.00	0.44	0.50	0.50
Total	14.93	15.07	15.09	15.13	15.29	15.03	15.24	15.29	15.21	14.98	15.14	15.01
XEqAn*	0.30	0.30	0.31	0.35	0.39	0.31	0.31	0.34	0.33	0.50	0.46	0.46
Mol. % End-members												
Me[1]	41.59	38.00	38.11	40.12	39.89	39.05	38.57	38.45	38.82	62.72	54.81	56.13

*XEqAn = (Al-3)/3

[1]Me = 100(Ca+Mg+Fe+Mn)/(Na+K+Ca+Mg+Fe+Mn)

Table A.12: Scapolite analyses

Sample	B115	B115	B115	B115	B137	B137	B141	B141	B141	B141	B141	B141	B141
Lithology	Cpxite	Cpxite	Cpxite	Cpxite	B mg	B mg	Cs	Cs	Cs	Cs	Cs	Cs	Cs
No.	305	306	313	314	319	323	258	259	260	261	262	263	266
Mineral	Scp	Scp	Scp	Scp	Scp	Scp	Scp	Scp	Scp	Scp	Scp	Scp	Scp
Wt. %													
SiO_2	60.01	59.90	59.01	59.22	54.97	53.70	49.57	50.32	49.62	50.22	51.21	51.96	51.00
Al_2O_3	21.01	20.82	21.20	21.38	23.77	21.58	26.84	26.52	27.08	26.59	25.83	25.49	25.89
FeO	0.09	0.12	0.08	0.07	0.13	0.09	0.03	0.11	0.06	0.03	0.07	0.07	0.05
MgO	0.01	0.09	0.01	0.00	0.00	0.00	0.00	0.00	0.00	0.00	0.00	0.00	0.00
MnO	0.00	0.00	0.00	0.00	0.01	0.00	0.01	0.03	0.04	0.00	0.01	0.01	0.00
CaO	4.27	4.07	4.59	4.53	8.43	7.58	14.01	13.56	14.23	13.46	12.10	11.65	12.70
Na_2O	5.67	5.65	6.26	6.53	7.83	7.77	4.66	4.84	4.40	4.71	5.70	5.90	5.42
K_2O	0.79	0.83	1.02	1.06	0.58	0.54	0.54	0.63	0.60	0.59	0.58	0.59	0.60
SO_3	0.05	0.06	0.06	0.07	0.14	0.14	0.00	0.02	0.00	0.02	0.04	0.00	0.03
Cl	3.55	3.62	3.57	3.56	2.63	2.59	1.81	1.87	1.72	1.93	2.18	2.24	2.02
O=Cl	-0.80	-0.82	-0.81	-0.80	-0.59	-0.58	-0.41	-0.42	-0.39	-0.44	-0.49	-0.51	-0.46
Total	94.72	94.39	95.03	95.64	97.93	93.45	97.07	97.48	97.40	97.13	97.25	97.45	97.28
Cations (calculated on the basis of 24 O)													
Si	8.32	8.33	8.22	8.20	7.65	7.81	7.05	7.12	7.04	7.12	7.24	7.32	7.22
Al	3.43	3.41	3.48	3.49	3.90	3.70	4.50	4.42	4.53	4.44	4.30	4.23	4.32
Fe	0.01	0.01	0.01	0.01	0.01	0.01	0.00	0.01	0.01	0.00	0.01	0.01	0.01
Mn	0.00	0.00	0.00	0.00	0.00	0.00	0.00	0.00	0.00	0.00	0.00	0.00	0.00
Mg	0.00	0.02	0.00	0.00	0.00	0.00	0.00	0.00	0.00	0.00	0.00	0.00	0.00
Ca	0.63	0.61	0.68	0.67	1.26	1.18	2.13	2.06	2.16	2.04	1.83	1.76	1.93
Na	1.27	1.26	1.40	1.46	1.75	1.82	1.07	1.10	1.00	1.07	1.30	1.34	1.23
K	0.14	0.15	0.18	0.19	0.10	0.10	0.10	0.11	0.11	0.11	0.11	0.11	0.11
S	0.01	0.01	0.01	0.01	0.01	0.02	0.00	0.00	0.00	0.00	0.00	0.00	0.00
C*	0.16	0.14	0.15	0.16	0.37	0.35	0.56	0.55	0.59	0.54	0.48	0.46	0.51
Cl	0.83	0.85	0.84	0.84	0.62	0.64	0.44	0.45	0.41	0.46	0.52	0.54	0.48
Total	14.81	14.80	14.97	15.02	15.67	15.62	15.85	15.82	15.85	15.79	15.78	15.75	15.80
X_{Cl}**	0.83	0.85	0.84	0.84	0.62	0.64	0.44	0.45	0.41	0.46	0.52	0.54	0.48
XEqAn***	0.14	0.14	0.16	0.16	0.30	0.23	0.50	0.47	0.51	0.48	0.43	0.41	0.44
Mol. % End-members													
Me[l]	31.55	31.14	30.51	29.28	40.69	38.34	64.78	63.05	66.13	63.40	56.80	55.08	58.99

*Calculated assuming 1 (S+C+Cl) apfu. **X_{Cl} = Cl/(Cl+CO3+SO4). ***XEqAn = (Al-3)/3

[l]Me = 100(Ca+Mg+Fe+Mn)/(Na+K+Ca+Mg+Fe+Mn)

Table A.12: Scapolite analyses (continued)

Sample	B141	B141	B141	B141	B141	B142	B142	B142
Lithology	Cs	Cs	Cs	Cs	Cs	Cs	Cs	Cs
No.	275	276	280	282	284	357	360	370
Mineral	Scp	Scp	Scp	Scp	Scp	Scp	Scp	Scp
Wt. %								
SiO_2	53.89	51.29	51.11	50.32	48.26	49.56	46.54	48.87
Al_2O_3	24.61	25.19	25.61	26.39	22.82	24.20	26.53	26.18
FeO	0.08	0.06	0.04	0.00	0.50	0.05	0.00	0.00
MgO	0.00	0.00	0.33	0.01	5.93	0.00	0.00	0.00
MnO	0.00	0.00	0.00	0.01	0.14	0.00	0.00	0.00
CaO	9.78	11.70	11.67	13.42	10.58	10.58	14.64	13.73
Na_2O	6.53	5.78	5.24	5.22	3.24	6.24	4.70	5.07
K_2O	0.45	0.52	0.55	0.53	0.54	0.58	0.60	0.54
SO_3	0.03	0.00	0.01	0.00	0.00	0.01	0.00	0.00
Cl	2.72	2.23	1.97	1.90	1.39	2.55	1.69	1.85
O=Cl	-0.61	-0.50	-0.44	-0.43	-0.31	-0.57	-0.38	-0.42
Total	97.51	96.27	96.10	97.39	93.10	93.19	97.11	95.83
Cations (calculated on the basis of 24 O)								
Si	7.52	7.31	7.28	7.13	7.11	7.30	6.87	7.05
Al	4.05	4.23	4.30	4.40	3.96	4.20	4.61	4.45
Fe	0.01	0.01	0.00	0.00	0.06	0.01	0.00	0.00
Mn	0.00	0.00	0.00	0.00	0.02	0.00	0.00	0.00
Mg	0.00	0.00	0.07	0.00	1.30	0.00	0.00	0.00
Ca	1.46	1.79	1.78	2.04	1.67	1.67	2.31	2.12
Na	1.47	1.32	1.20	1.19	0.77	1.48	1.12	1.18
K	0.08	0.09	0.10	0.10	0.10	0.11	0.11	0.10
S	0.00	0.00	0.00	0.00	0.00	0.00	0.00	0.00
C*	0.35	0.46	0.52	0.54	0.65	0.36	0.58	0.55
Cl	0.64	0.54	0.48	0.46	0.35	0.64	0.42	0.45
Total	15.58	15.75	15.74	15.86	15.99	15.76	16.02	15.91
XCl**	0.64	0.54	0.48	0.46	0.35	0.64	0.42	0.45
XEqAn***	0.35	0.41	0.43	0.47	0.32	0.40	0.54	0.48
Mol. % End-members								
Me[l]	48.74	55.80	58.80	61.32	77.82	51.36	65.33	62.45

*Calculated assuming 1 (S+C+Cl) apfu. **X_{Cl} = Cl/(Cl+CO3+SO4). ***XEqAn = (Al-3)/3

[l]Me = 100(Ca+Mg+Fe+Mn)/(Na+K+Ca+Mg+Fe+Mn)

Appendix A.13: Spinel analyses			
Sample	B133	B133	B133
Lithology	marble	marble	marble
No.	19	20	25
Mineral	Spl	Spl	Spl
Wt. %			
SiO_2	0.00	0.00	0.00
TiO_2	0.01	0.00	0.04
Al_2O_3	67.87	66.76	66.55
Cr_2O_3	0.01	0.00	0.00
FeO	10.64	11.89	11.95
MnO	0.16	0.17	0.16
MgO	21.92	21.62	21.44
CaO	0.14	0.03	0.10
Na_2O	0.05	0.06	0.06
K_2O	0.02	0.02	0.03
Total	100.80	100.55	100.33
Cations (calculated on the basis of 4 O)			
Si	0.00	0.00	0.00
Ti	0.00	0.00	0.00
Al	1.98	1.96	1.96
Cr	0.00	0.00	0.00
Fe	0.22	0.25	0.25
Mn	0.00	0.00	0.00
Mg	0.81	0.80	0.80
Ca	0.00	0.00	0.00
Na	0.00	0.00	0.00
K	0.00	0.00	0.00
Total	3.01	3.02	3.02

Table A.13: Titanite analyses (no F)

Sample	B137	B137	B159
Lithology	B mg	B mg	B mg
No.	139	178	54
Mineral	Ttn	Ttn	Ttn
Wt. %			
SiO_2	30.37	29.71	30.31
TiO_2	33.70	34.15	35.32
Al_2O_3	2.74	2.14	1.60
Cr_2O_3	0.16	0.13	0.10
FeO	1.40	1.39	1.55
CaO	29.11	24.34	28.30
Total	97.58	91.99	97.29
Cations (calculated on the basis of 5 O)			
Si	1.02	1.05	1.02
Ti	0.85	0.90	0.90
Al	0.11	0.09	0.06
Cr	0.00	0.00	0.00
Fe	0.04	0.04	0.04
Ca	1.05	0.92	1.02
Total	3.07	3.00	3.05

Table A.14: Titanite analyses

Sample	B121	B121	B115	B115	B142	B142
Lithology	B mg	B mg	cpxenite	cpxenite	cpxenite	cpxenite
Group	2	2	2	2	2	2
No.	254	255	302	303	373	374
Mineral	Ttn	Ttn	Ttn	Ttn	Ttn	Ttn
Wt. %						
SiO_2	29.51	29.92	30.54	30.72	31.85	32.06
TiO_2	36.31	36.86	34.96	35.42	30.46	34.92
Al_2O_3	2.02	2.08	2.24	2.21	3.86	3.25
Cr_2O_3	0.18	0.16	0.12	0.14	0.12	0.08
FeO	1.06	0.96	0.49	0.49	0.40	0.23
CaO	27.86	28.22	26.73	26.22	26.45	29.14
F	0.79	0.80	0.79	0.94	0.83	0.86
O=F	-0.33	-0.34	-0.33	-0.39	-0.35	-0.36
Total	97.38	98.66	95.54	95.74	93.61	100.19
Cations (calculated on the basis of 5 O)						
Si	0.99	0.99	1.03	1.03	1.09	1.03
Ti	0.91	0.92	0.89	0.90	0.78	0.85
Al	0.08	0.08	0.09	0.09	0.16	0.12
Cr	0.00	0.00	0.00	0.00	0.00	0.00
Fe	0.03	0.03	0.01	0.01	0.01	0.01
Ca	1.00	1.00	0.97	0.94	0.97	1.01
F	0.08	0.08	0.08	0.10	0.09	0.09
Total	3.10	3.10	3.08	3.08	3.10	3.10

APPENDIX C: SAMPLE LOCATION MAP

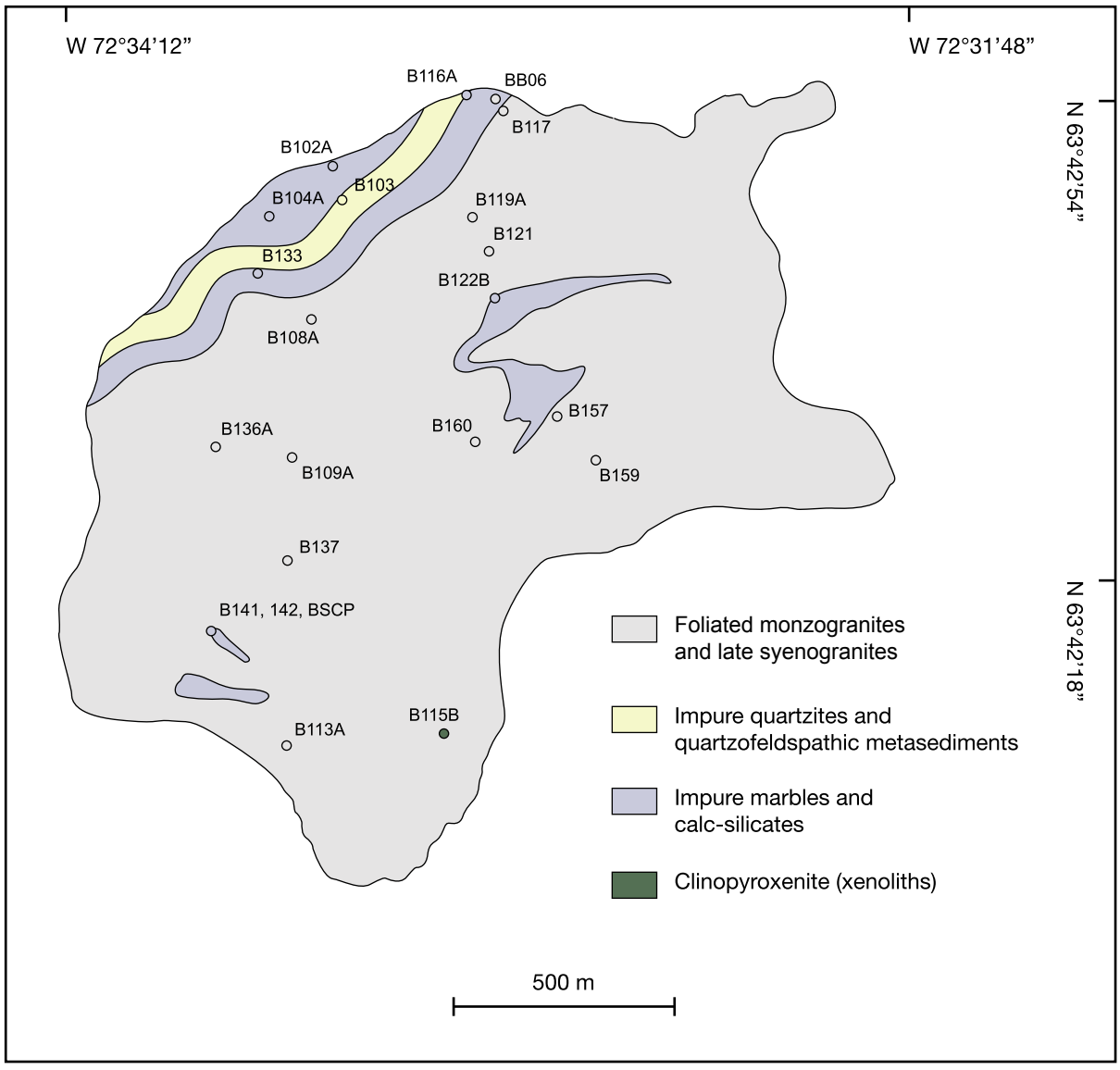

APPENDIX D: REGIONAL GEOLOGY MAPS

Two Geological Survey of Canada Open File Maps covering the southwestern Baffin Island study area are provided on the accompanying CDROM:

St-Onge, M.R., Sanborn-Barrie, M., and Young, M. 2007. Geology, Mingo Lake, Baffin Island, Nunavut. Geological Survey of Canada Open File Map 5433, 1:250,000 scale.

St-Onge, M.R., Sanborn-Barrie, M., and Young, M. 2007. Geology, Foxe Peninsula, Baffin Island, Nunavut. Geological Survey of Canada Open File Map 5434, 1:250,000 scale.